CAPTURING, ANALYZING AND COLLECTING ADHERENT CELLS USING MICROARRAY TECHNOLOGIES

Philip Charles Gach

A dissertation submitted to the faculty of the University of North Carolina at Chapel Hill in partial fulfillment of the requirements for the degree of Doctor of Philosophy in the Department of Chemistry

Chapel Hill
2012

Approved by:

Nancy L. Allbritton

Royce W. Murray

Steven A. Soper

Richard Superfine

Anne M. Taylor

ABSTRACT

PHILIP C. GACH: Capturing, Analyzing and Collecting Adherent Cells Using Microarray Technologies
(Under the direction of Nancy L. Allbritton)

Effective separation of a particular cell of interest from a heterogeneous cell population is crucial to many areas of biomedical research including microscopy, clinical diagnostics and stem cell studies. Examples of such studies include the analysis of single cells, isolation of transfected cells and cell transformation studies. Biological technologies can have skewed results if cells outside of the type of interest are present. Additionally, in many instances the targeted cells are of low abundance with respect to the heterogeneous population. For these reasons, it is important to have a technique capable of identifying the desired cells, separating these cells from unwanted cells and collecting the marked cells for further analysis.

Two biotools, referred to as micropallets and microrafts, have recently been introduced for sorting adherent cells. These devices comprise arrays of microelements weakly attached to a substrate. Following culture of adherent cells on the elements, individual microstructures are selectively detached from the array while still carrying the cells. These technologies have shown success in sorting single cells from small heterogeneous cell populations with high post sorting viabilities. However, previous device designs employed gravity-based collection methods and small microelement arrays which substantially reduced the collection yields, purities and sample sizes.

In this dissertation new approaches are described for capturing, examining and isolating individual cells by micropallet and microraft technologies. Initially a new approach was developed to isolate released microstructures from the array employing magnetism. Microstructures were embedded with uniformly dispersed magnetic nanoparticles which allowed collection by an external magnet immediately following release. Application of a magnetic field permitted microstructure collection with high yield, precision and purity. This improved collection efficiency enabled isolation of very rare cell types. Large arrays constituting over 10^6 micropallets were developed along with imaging analysis software to identify and sort low abundance target cells. This system was employed to isolate breast cancer stem cells from a heterogeneous cell population and circulating tumor cells directly from peripheral blood. Additionally, an array-based cell colony replication strategy was established which allowed highly efficient colony splitting and sampling.

ACKNOWLEDGEMENTS

There are several people I thank for providing assistance and support during the duration of my graduate studies. I would like to use this opportunity to express gratitude to my advisor Nancy Allbritton, for offering me a position in her lab. I have greatly appreciated Nancy's guidance and encouragement over the past 5 years. I also thank Chris Sims for his technical assistance in the lab. I am also grateful to my preliminary and dissertation committee members, Royce Murray, Steve Soper, Richard Superfine, Anne Taylor, Michael Ramsey and Klaus Hahn for providing precious advice on my research.

I extend my gratitude to the wonderful collaborators and technical staff who assisted on many of my projects. Richard Superfine, Briana Carsons, Wallace Ambrose, Mark Walters and Michael Chua aided in the development and characterization of the magnetic polymers formulated in Chapter 2 and Chapter 3. Adrienne Cox, Jim Fiordalisi and Barry Udis are acknowledged for their assistance with experiment design and FACS in Chapter 5. Jen Jen Yeh, Gabby Herrera and Rebecca Werlau are thanked for their helpful discussions and providing blood samples used in Chapter 6. I am thankful to Jim Bear, Sam King, Michael Ramsey and JP Alarie for their assistance with IA32 cell assays and microstructure characterization. I acknowledge the National Institutes of Health for supporting my research, grants EB007612 and EB012549.

I would like to thank the members of the Allbritton lab, past and present, for all their assistance during my graduate career. Special thanks to Wei Xu for training me in

the art of microfabrication, tissue culture and many of the other techniques required to in my research. I am grateful to the other members of the microfabrication group: Jonny Clark and Michael Hughes for assistance with fabrication; Yuli Wang for advice on fabrication, Hamed Shadpour and Nick Dobes for receiving the majority of my random questions; Pete Attayek for developing and optimizing the automated array screening software; Michelle Kovarik for career guidance; Asad Ahmad, Joe Balowski, David Detwiler, Rahul Dhopeshwarkar, Annadele Herman, Hsuan Lai, Doug Ornoff, Frank Pai, Colleen Phillips, Gina Salazar, Pavak Shah and Jocelyn Wang. I would also like to thank the members on the other side of the lab; Jazz Dickinson, Dechen Jiang, Sumith Kottegoda, Emilie Mainz, Adam Melvin, Ryan Phillips, Scott Phillips, Angie Proctor, Abby Turner, Kelong Wang, Greg Woss and Shan Yang. I am appreciative to you all for the assistance provided with manuscript preparations, presentation development and keeping everything in the lab working. It's been great having you all around to complain with about failed experiments, enjoy team building activities outside of the lab and engage in some of the most enlightening conversations to ever take place around a lunchroom table.

Lastly, I would like to acknowledge my family and friends. I am grateful to my parents and brother for their loving support. To my friends, you have made Chapel Hill a wonderful and memorable place to live. I also thank Dennis Peters, my undergraduate mentor, for introducing me to scientific research and for all his encouragement.

TABLE OF CONTENTS

LIST OF TABLES

LIST OF FIGURES

LIST OF ABBREVIATIONS AND SYMBOLS

γFe_2O_3 – iron(III)oxide nanoparticle

PCR – polymerase chain reaction

MACS – magnetic-activated cell sorting

FACS – fluorescence-activated cell sorting

LCM – laser capture microdissection

LPC – laser pressure catapulting

CTC – circulating tumor cell

SU-8 – Formaldehyde, polymer with (chloromethyl)oxirane and 4,4'-(1-methylethylidene)bis[phenol]

1002F – phenol, 4,4′-(1-methylethylidene)bis-, polymer with 2,2′-[(1-methylethylidene) bis(4,1-phenyleneoxymethylene]bis[oxirane]

PEG – polyethylene glycol

PDMS – polydimethylsiloxane

Nd – neodymium

YAG – yttrium aluminum garnet

MEMS – microelectromechanical systems

μ – micro

Sm_2Co_{17} – samarium cobalt

PMMA – polymethylmethacrylate

EHEC – ethyl(hydroxyethyl)cellulose

CE – 3,4-epoxycyclohexylmethyl-3´4´-epoxycyclohexanecarboxylate

SWNT – single-wall carbon nanotubes

3T3 – mouse fibroblast cell line

HeLa – human cervical cancer cell line

RBL – rat basophilic leukemic cell line

GBL – γ-butyralactone

1002F developer – 1-methoxy-2-propanol

DMEM – Dulbecco's modified Eagle's medium

FBS – fetal bovine serum

PBS – phosphate buffered saline

pH – potential hydrogen

EDTA – ethylenediaminetetraacetic acid

XTT – sodium 3´-[1-(phenylaminocarbonyl)- 3,4-tetrazolium]-bis (4-methoxy-6-nitro) benzene sulfonic acid hydrate

m – milli

m – meter

L – liter

^{o} – degrees

C – celsius

CO_2 – carbon dioxide

g – gram

min – minute

% – percent

SEM – scanning electron microscopy

k – kilo

V – volts

A – amps

TEM – transmission electron microscopy

M - molar

x – times

n – nano

s – second

DC – direct current

UV – ultra violet

n – number

Fcϵ - fragment crystallizable-epsilon receptors

IgE – immunoglobulin E

F_g – gravitational force

F_m – magnetic force

m – mass

g – acceleration due to gravity

V – volume

$\Delta\chi$ – difference in magnetic susceptibilities

N – newton

T – tesla

< – less than

> – greater than

± – plus or minus

Fe – iron

OH^- – hydroxide

Fe_3O_4 – magnetite or iron(III) oxide

γFe_2O_3 – maghemite or iron(II) oxide

γ – gamma

HOOC(OA) – oleic acid

H_2O – dihydrogen monoxide or water

Ni – nickel

AIBN – 2,2'-azobisisobutyionitrile

DNA – deoxyribonucleic acid

h – hour

PS-AA – poly(styrene-*co*-acrylic acid)

v/v – volume/volume

ATR – attenuated total reflectance

FTIR – Fourier transform infrared spectroscopy

c – centi

rmp – revolutions per minute

vol – volume

in – inch

Hg – mercury

wt – weight

Au – gold

min – minute

GFP – green fluorescent protein

eGFP – enhanced green fluorescent protein

C2C12 – mouse myoblast cell line

CMV – cytomegalovirus

CCD – charge-coupled device

DIC – differential interference contrast

L – length

W – width

H – height

W – watt

J – joule

G – gauge

B – magnitude of the magnetic field intensity

B_p – pole strength

r – radius

$\geq$ – greater than or equal to

$\leq$ – less than or equal to

^{2} – squared

^{3} – cubed

CD – cluster of differentiation

diam – diameter

3D – three-dimensional

CMOS – complementary metal-oxide-semiconductor

FITC – Fluorescein isothiocyanate

DAPI – 4',6-diamidino-2-phenylindole

Texas Red – sulforhodamine 101 acid chloride

ABS – Acrylonitrile butadiene styrene

N.A. – numerical aperature

F_{epi} – light gathering power for epi-illumination

M – magnification

M – million or mega

GUI – graphical user interface

Em – emission

Ex – excitation

S – signal

N – noise

FDA – Food and Drug Administration

MCF-7 – human breast cancer cell line

ECM – extracellular matrix

EpCAM – epithelial cell adhesion molecule

CAN – cerium(IV) ammonium nitrate

EDC – N-(3-dimethylaminopropyl)-N´-ethylcarbodiimide hydrochloride

PAA – polyacrylic acid

PDX – patient-derived xenograft

sh – short hairpin

RNA - ribonucleic acid

Cy – cyanine

IA32 – mouse embryonic fibroblast cell line

A549 – human alveolar adenocarcinoma cell line

HT1080 – human fibrosarcoma cell line

NaCl – sodium chloride

$KHPO_4$ – mono potassium phosphate

KH_2PO_4 – potassium dihydrogen phosphate

KCl – potassium chloride

BSA – bovine serum albumin

RIPA – radioimmunoprecipitation assay

PVDF – polyvinylidene fluoride

HRP – horseradish peroxidase

GAPDH – glyceraldehyde 3-phosphate dehydrogenase

– number

= – equals

RNAi – ribonucleic acid interference

Chapter 1: Introduction to Single Cell Sorting: Applications and Technologies

1.1 Cell Heterogeneity

An adult human body is composed of trillions of mammalian cells and harbors numerous other cells such as bacteria and yeast. Mammalian cells that construct our bodies have been classified into hundreds of discrete cell types.[1,2] Like the organisms they comprise, individual cells are not developmentally static but rather undergo numerous changes during their lifespans. How cells have developed to their current lineage and how environmental effects control their fate are crucial questions in biology and medicine. Distinguishing various cells is critical to our ability to examine and genetically modify cells. This task is complicated as cellular processes of genetically equivalent cells and even the same cell change over time, resulting in cellular heterogeneity.[3-10] The behavior of these cells varies drastically as a function of numerous factors with their surroundings playing a dominant role in fate determination. The complex interactions of cellular environment, function, and behavior have spurred the development of many new tools for analyzing and exploiting these fundamental units of life.

1.2 Analysis of Single Cells

Characterization of cellular phenotype and behavior is critical to identification and understanding of cells.[11,12] This information is important to research in the fields of cell biology, biomedical sciences and systems biology. Examination of human cells has allowed detection of disease such as cancer, neurodisorders and genetic disorders.[13]

Further analyses of these cells provide information regarding possible therapies and treatments. A plethora of information about disease may be obtained by observing cell interactions and changes in their *in vivo* environment. Investigating cells *in vivo*, in their native surroundings, produces the most biologically relevant systems for monitoring cells. However, reliance on these systems for disease research limits assay throughput and increases costs. Several approaches aim to remove cells from their *in vivo* microenvironment and culture cells in an *in vitro* system. These methods include human cell culture in a Petri dish, microtiter plate, microfluidic system or animal model. No matter the mode of culture and isolation, the information these cells provide depends on the method of analysis.

Traditional biochemical assays analyze bulk populations of cells. Standard cell assays, such as, western blotting, electrophoresis, PCR, mass spectrometry and immunofluorescence imaging, pool the lysates or data from thousands to millions of cells for analysis. While averaging data over a large group of cells is sufficient for many applications, this strategy masks critical information provided by individual or small subsets of cells. Several approaches to analyzing cells on a cell-to-cell basis have produced interesting information and results not documented by ensemble assays.[14,15] Many of the technologies for analyzing bulk populations of cells have been adapted to analyze single cells, including microscopy,[16,17] mass spectrometry,[18] PCR,[19,20] gel electrophoresis,[21,22] chromatography[23,24] and capillary electrophoresis.[25] Flow cytometry has obtained substantial commercial success for its ability to efficiently analyze millions of individual cells at great speeds (>100,000 cells/s).[26,27] Flow cytometry allows analysis of cells by multiple parameters: size, granularity and up to 16 fluorescence properties

making it useful for a wide variety of applications.[28,29] Unfortunately, there is generally a trade-off in the information that can be obtained by these various single cell analysis techniques. For example, PCR, MS and capillary electrophoresis offer a wealth of information; however, they are destructive techniques and therefore not capable probing cellular responses over time. Likewise, flow-based technologies such as flow cytometry are typically not compatible with multi-time-point analysis and discrimination of intracellular spatial organization requires sophisticated imaging analysis.[30] Acquisition of this information has been efficiently acquired by immobilizing cells during analysis.

Imaging cytometry analyzes immobilized cells by microscopy techniques including brightfield and fluorescence microscopy.[31] Imaging cytometry techniques affording efficient cell analysis include laser scanning cytometry[32-34] and automated microscopy also referred to as high content screening or cellomics.[35] Microscopy-based cell imaging is valuable in that the spatial location of fluorescent tags attached specifically to target proteins, surface receptors, and other biomolecules may be evaluated. Monitoring subcellular components as they exist naturally in cells allows interrogation strategies not feasible by whole cell analysis. Furthermore, examining adherent cells cultured on a substrate allows repeated examination of individual cells over time. This permits observation of cellular responses to environmental stimuli resulting from external factors such as drug additions and cell-cell interactions. The main limitation of these systems is the lower throughput compared with flow cytometry, due to imaging time and data processing speed.

The strengths of imaging cytometry for studying cellular interactions and function have led to the development of numerous microfabricated systems designed to control the

immobilization and microenvironment of cells.[36,37] These devices allow researchers to arrange individual cells in well-ordered arrays. Fixing cells in predefined locations offers numerous advantages over standard culture with cells at random locations, including controlled cell-to-cell interactions, simplified image processing and traceability of cells. Tracking cells over time is especially useful for studying time dependent cell responses and for system integration with automated tasks. Various strategies have been applied to create cell arrays by employing physical, chemical, optical, or electrical forces.[38] Physically trapping cells with microstructures is perhaps the simplest means for arraying cells as this method does not require any external equipment. Several microstructure geometries exist for trapping cells including wells,[39,40] pores,[41] wiers,[42] and pallets.[43] Following cell trapping numerous assays and further manipulation have been achieved on these cells.

1.3 Cell Sorting

In order to perform many types of cellular analysis, it is essential to have methods to isolate and culture specified target cells. Effective cell culture often requires isolation of target cells from the surrounding heterogeneous cellular population. Non-target cells can affect the growth of target cells and reduce accuracy of cellular analysis.[12] For these reasons it is important to have a technique capable of identifying the cell of interest, separating the cell from unwanted cells and collecting the cell for further studies. A number of available technologies can provide isolation of target cells from a cell mixture. These systems operate on a variety of instrumental attributes including: serial vs parallel analysis, destructive vs live cell analyses, and flow-based vs stationary systems. Techniques for sorting cells include magnetic-activated cell sorting (MACS),[44]

fluorescence-activated cell sorting (FACS),[26,28,45] microfluidic-based cell sorting,[46] limiting dilution,[12,47] laser capture microdissection (LCM),[48] laser pressure catapulting (LPC),[49] and microarray technologies.[44,50]

1.4 Flow-Based Cell Sorting

Many cell sorting strategies have been developed for isolating non-adherent cells from a heterogeneous population. Non-adherent cells, typically found in our bloodstream, include erythrocytes (red blood cells), leukocytes (white blood cells) and thrombocytes (platelets).[51] In addition to common blood cells, tumorigenic cells or bacteria are occasionally present in the bloodstream of patients. The number of tumor cells, commonly referred to as circulating tumor cells (CTCs), in a patient has recently been correlated with tumor progression in response to anti-cancer therapies.[52-54] Ease of cell collection from patients and the wealth of information these cells possess have led to the development of many technologies for isolating and analyzing non-adherent blood cells.[51,55]

Adherent mammalian cells may also be removed from their growth surfaces and temporarily suspended in a non-adherent state. These cells are typically stripped from their culture substrate by enzymatic digestion or mechanical shearing. These approaches have successfully generated suspensions of viable adherent cells. However, removal of adherent cells from their growth surfaces is accompanied by changed cell morphology, reduced cellular surface markers, altered cell physiology and decreased viability.[56,57] Strategies for sorting suspended adherent cells and non-adherent cells include: column chromatography, sedimentation, filtering, MACS, FACS, dielectrophoresis and

microfluidics. MACS and FACS have achieved perhaps the most commercial success due to their efficiency at cell sorting.

Cell sorting methods employing magnetism, referred to as MACS, utilize the cell-specific antibodies to bind magnetic beads to the cells of interest (positive selection) or unwanted cells (negative selection).[44] Typically avidin labeled-cells are captured on biotinylated magnetic beads and injected into a column or microfluidic channel. A magnetic field is then applied to attract the cells with attached magnetic beads within the device. Non-attached cells pass freely through the column or channel at this point. Target cells are then eluted to side channels or upon removal of the external magnet.[58-60] Though these sorting strategies offer extremely high throughputs they are reliant on specific surface antibodies to bind cells to magnetic beads. This results in limited cell sorting parameters and poor purity caused by non-specific antibody binding.

Integration of cell sorting capabilities with flow cytometry instrumentation allows sensitive and multiparameter analysis of cells followed by isolation of the target cells.[27] Cell sorting can be achieved through fluidic switching[61] or isolation of individual droplets formed from a fluid stream,[62] but the majority of cell isolation strategies are derived from the latter approach. Instrumentation employing the isolation of cells within individual droplets has been commercialized and is referred to as fluorescence-activated cell sorters (FACS). FACS instruments have successfully isolated viable mammalian cells by numerous sorting parameters and with relatively high throughput (>10,000 cells/s). However, FACS systems are not effective at sorting small sample sizes (<50,000 cells) or isolating rare target cells, frequencies below 0.01%.[63,64] Additionally, suspending adherent cells for sorting causes cell stress and reduced cell viability as noted above.[57]

1.5 Adherent Cell Sorting

FACS and MACS allow high-throughput and efficient sorting of suspended cells. However, there are many applications where sorting is necessary while cells remain adhered to a substrate, such as when cell identification depends on microscopy-based methods.[50] This can be the case for cells that that can be identified by differences in their growth rates, morphology or biomarker localization.

Traditional approaches to enriching adherent cells selectively target cells based on their ability to proliferate in the presence of specific growth inhibitors or by their selective affinity for culture substrates.[12,65] Techniques for further isolation of pure cell strains from a heterogeneous culture rely on plating a dilute cell suspension and selectively choosing the small colonies of interest by employing cloning rings or limiting dilution methods.[12,66] Isolation of cell colonies by cloning rings requires initial attachment of dispersed adherent cells to a substrate followed by growth of the individual cells into discrete colonies. A collar, or the cloning ring, applied around target colonies provides an isolating barrier allowing selective trypsinization and collection of the cells within the cloning ring.[47,67] With the limiting dilution technique, cell suspensions are added to multiwell plates to achieve wells containing single cells. Following cell culture, a few of the thousands of wells will possess a clonal population.[12] These methods have long been favored by the biology community because of their minimal instrumentation requirements. However, while instrumentation costs are low, there are expenses associated with prolonged cell maintenance in expensive growth media. In addition, these techniques require significant amounts of labor, time, and reagents, all of which make these sorting strategies impractical for many applications.

Alternative approaches for achieving positive selection of adherent cells employ lasers to separate target cells from the heterogeneous cell population.[68] The two primary methods for isolating adherent cells, use a laser to either capture the target cell onto a membrane or cut around a cell adhered to a membrane, commonly referred to as laser capture microdissection and laser cutting microdissection, respectively.[69] In laser capture microdissection, a thermoplastic membrane covering the cells is selectively fused to the target cells by a focused laser.[70] When the membrane is cooled to room temperature these cells become attached. Upon removal of the membrane the embedded cells are isolated from the remaining cells. Conversely, in laser cutting microdissection the laser is used to cut the film to which the cells are adhered.[49,71,72] The dislodged film with the attached cell is then collected by a variety of techniques including a pressure catapulting approach, gravity collection or collection with a fine-needle. The primary application of laser microdissection has been isolating cells from tissue samples for genetic and proteomic analysis.[73,74] Recent papers have demonstrated the utility of these technologies for isolating and subsequently culturing viable cells. Though genetic analysis has demonstrated cells are not disturbed by these technologies, published protocols to date have only sorted small cell colonies. Additionally, undefined positioning of cultured cells during sorting makes tracking cells over prolonged periods difficult and results in low sorting throughputs.

1.6 Releasable Microarray Technology and Research Goals

Microfabricated and microprinted arrays afford researchers highly controlled positioning of biomolecules and cells, as described in Section 1.3. While these technologies are well developed for analyzing cells; isolation of individual target cells is

generally achieved by low-throughput and unreliable procedures. Techniques for removing cells from the microarray include micromanipulation,[75,76] laser capture microdissection[77] and optofluidics.[78] The Allbritton laboratory previously introduced two technologies for culturing adherent cells on arrays of microelements which could be selectively detached from the array while still carrying the attached cells, referred to as 'micropallets' and 'microrafts'.[79-82] To date these arrays constitute 10^3 – 10^4 microelements fabricated on a substrate with a physical barrier serving to isolate cells on the surfaces of individual microstructures. Microfabrication permits tailoring of the geometry,[83-85] material[86] and functionalization[87-90] of these microdevices to meet the requirement of cell attachment and growth. Consequently, a wide variety of cell types have been cultured and isolated by these devices including; immortalized cell lines,[80] primary cells[87] and stem cells.[91]

Micropallets are developed by exploiting standard photolithography methods to fabricate photoresponsive polymers (SU8 and 1002F photoresists) onto a glass substrate.[92] A physical barrier comprised of air[43,93] or PEG[94] is then generated between the microstructures. Following functionalization of the micropallets, cells are cultured on the tops of the elements. SU8 and 1002F photoresists have poor adhesion to glass and consequently the microdevices may be removed with minimal forces. The generation of a cavitation bubble produced by a pulsed Nd:YAG laser focused at the glass substrate:micropallet interface is employed to selectively release target micropallets from the array.[95-97] Microrafts accomplish analogous results, however, employ alternative fabrication and release mechanisms.[82] A PDMS multiwell plate serves to replace the glass substrate and virtual air wall enclosing micropallets. Trapping of a polymer within

the microwells by a dewetting phenomenon generates isolated microrafts.[98] Additionally, individual microrafts are dislodged from the PDMS frame by mechanical actuation with a microneedle. Detached microstructures are then collected by a pipette tip[79] or via gravitational collection onto a collection dish. [81,82] Unfortunately, these collection approaches are plagued by loss of microstructures and contamination by undesired cells.

The goal of this graduate dissertation was to develop new strategies for capturing, analyzing and collecting cells by microarray technologies. Micropallets were embedded with magnetic nanoparticles to allow collection of released micropallets by an external magnet as described in Chapter 2. A new strategy for uniformly dispersing the magnetic nanoparticles throughout photoresists was developed to retain transparency of the polymers to allow cell imaging. Related fabrication and collection approaches were then employed to magnetically collect microrafts manufactured from a new selection of transparent magnetic polymers in Chapter 3. Localization of the external magnetic fields and regions of microstructure magnetism provided novel strategies for controlling micropallet collection as described in Chapter 4. Magnetic actuation of the microstructures afforded high collection efficiencies while eliminating foreign cell contamination. These attributes made sorting rare cells by large arrays of micropallets feasible as detailed in Chapter 5. Large arrays of micropallets were further utilized to isolate CTCs directly from whole blood in Chapter 6. Chapter 7 details a strategy for array-based replication of cell colonies to allow selection using destructive assays on colony fragments.

1.6 References

1. Vickaryous M, Hall B. Human cell type diversity, evolution, development, and classification with special reference to cells derived from the neural crest. *Biological Reviews*. 2006;81(3):425-455.

2. Alberts B, Bray D, Lewis J, Raff M, Roberts K, Watson JD. Molecular Biology of the Cell, 2nd Edn. New York: Garland Publishing, Inc.; 1989.

3. Ferrell JE, Machleder EM. The biochemical basis of an all-or-none cell fate switch in Xenopus oocytes. *Science*. 1998;280:895-896.

4. Taniguchi Y, Choi P, Li G, et al. Quantifying E-coli Proteome and Transcriptome with Single-Molecule Sensitivity in Single Cells. *Science*. 2010;329(5991):533-538.

5. Brehm-Stecher B, Johnson E. Single-cell microbiology: Tools, technologies, and applications. *Microbiology and Molecular Biology Reviews*. 2004;68(3):538-+.

6. Han A, Yang L, Frazier A. Quantification of the heterogeneity in breast cancer cell lines using whole-cell impedance spectroscopy. *Clinical Cancer Research*. 2007;13(1):139-143.

7. Sims CE, Allbritton NL. Analysis of single mammalian cells on-chip. *Lab on a Chip*. 2007;7:423-440.

8. Graf T, Stadtfeld M. Heterogeneity of Embryonic and Adult Stem Cells. *Cell Stem Cell*. 2008;3(5):480-483.

9. Klein C, Blankenstein T, Schmidt-Kittler O, et al. Genetic heterogeneity of single disseminated tumour cells in minimal residual cancer. *Lancet*. 2002;360(9334):683-689.

10. Dexter D, Leith J. Tumor heterogeneity and drug-resistance. *Journal of Clinical Oncology*. 1986;4(2):244-257.

11. Lindstrom S, Andersson-Svahn H. Overview of single-cell analyses: microdevices and applications. *Lab on a Chip*. 2010;10(24):3363-3372.

12. Freshney RI. Culture of Animal Cells, 6th Ed.: John Wiley & Sons, Inc.; 2010.

13. Walling M, Shepard J. Cellular heterogeneity and live cell arrays. *Chemical Society Reviews*. 2011;40(7):4049-4076.

14. Sims CE, Allbritton NL. Single-cell kinase assays: opening a window onto cell behavior. *Current Opinion in Biotechnology*. 2003;14:1-6.

15. Kovarik M, Allbritton N. Measuring enzyme activity in single cells. *Trends in Biotechnology*. 2011;29(5):222-230.

16. Jongkind J, Ploem J, Reuser A, Galjaard H. Enzyme assays at single cell level using a new type of microfluorimeter. *Histochemistry*. 1974;40(3):221-229.

17. Reuser A, Jongkind J, Galjaard H. Methods for analysis of acid alpha-1,4-glucosidase activity in single (hybrid) cells. *Journal of Histochemistry & Cytochemistry*. 1976;24(4):578-586.

18. Abramson F, McCaman M, McCaman R. Femtomole level of analysis of bioenic-amines and amino-acids using functional group mass-spectrometry. *Analytical Biochemistry*. 1974;57(2):482-499.

19. Taniguchi K, Kajiyama T, Kambara H. Quantitative analysis of gene expression in a single cell by qPCR. *Nature Methods*. 2009;6(7):503-U550.

20. Warren L, Bryder D, Weissman I, Quake S. Transcription factor profiling in individual hematopoietic progenitors by digital RT-PCR. *Proceedings of the National Academy of Sciences of the United States of America*. 2006;103(47):17807-17812.

21. Rydberg B, Johanson KJ. Estimation of DNA strand breaks in single mammalian cells; DNA Repair Mechanisms. New York: Academic Press; 1978:456 - 468.

22. Osborne N. Do snail neurons contain more than one neurotrasmitter. *Nature*. 1977;270(5638):622-623.

23. Oates M, Cooper B, Jorgenson J. Quantitative amino-acid-analysis of individual snail neurons by open tubular liquid-chromatography. *Analytical Chemistry*. 1990;62(15):1573-1577.

24. Osborne N, Szczepan.AC, Neuhoff V. Amines and amino-acids in identified neurons of helix-pomatia. *International Journal of Neuroscience*. 1973;5(3):125-131.

25. Kennedy R, Oates M, Cooper B, Nickerson B, Jorgenson J. Microcolumn separations and the analysis of single cells. *Science*. 1989;246(4926):57-63.

26. Givan AL. Flow Cytometry First Principles (ed 2nd). New York: Wiley-Liss; 2001.

27. Ibrahim S, van den Engh G, Kumar A, Galaev I, Mattiasson B. Flow cytometry and cell sorting. *Cell Separation: Fundamentals, Analytical and Preparative Methods*. 2007;106:19-39.

28. Shapiro HM. Practical Flow Cytometry (ed 4th). New York: Wiley-Liss; 2003.

29. Bonetta L. Flow cytometry smaller and better. *Nature Methods*. 2005;2(10):785.

30. Goda K, Ayazi A, Gossett DR, et al. High-throughput single-microparticle imaging flow analyzer. *Proceedings of the National Academy of Sciences of the United States of America*. 2012.

31. Chieco P, Jonker A, Van Noorden CJF. Image Cytometry. New York: Springer-Verlag; 2001.

32. Kamentsky LA. Laser scanning cytometry. *Methods in Cell Biology*. 2001;63:51-87.

33. Kamentsky L. Laser scanning cytometry. *Methods in Cell Biology, Vol 63*. 2001;63:51-87.

34. Darzynkiewicz Z, Bedner E, Li X, Gorczyca W, Melamed M. Laser-scanning cytometry: A new instrumentation with many applications. *Experimental Cell Research*. 1999;249(1):1-12.

35. Starkuviene V, Pepperkok R. The potential of high-content high-throughput microscopy in drug discovery. *British Journal of Pharmacology*. 2007;152(1):62-71.

36. Zare R, Kim S, Yarmush M, Duncan J, Gray M. Microfluidic Platforms for Single-Cell Analysis. *Annual Review of Biomedical Engineering, Vol 12*. 2010;12:187-201.

37. Yarmush M, King K. Living-Cell Microarrays. *Annual Review of Biomedical Engineering*. 2009;11:235-257.

38. Di Carlo D, Lee L. Dynamic single-cell analysis for quantitative biology. *Analytical Chemistry*. 2006;78(23):7918-7925.

39. Revzin A, Tompkins RG, Toner M. Surface engineering with poly(ethylene glycol) photolithography to create high-density cell arrays on glass. *Langmuir*. 2003;19:9855-9862.

40. Lindstrom S, Andersson-Svahn H. Miniaturization of biological assays - overview on microwell devices for single-cell analyses. *Biochimica Biophys Acta*. 2011;1810:308-316.

41. Vona G, Sabile A, Louha M, et al. Isolation by size of epithelial tumor cells - A new method for the immunomorphological and molecular characterization of circulating tumor cells. *American Journal of Pathology*. 2000;156(1):57-63.

42. Di Carlo D, Aghdam N, Lee L. Single-cell enzyme concentrations, kinetics, and inhibition analysis using high-density hydrodynamic cell isolation arrays. *Analytical Chemistry*. 2006;78(14):4925-4930.

43. Wang Y, Sims CE, Marc P, Bachman M, Li GP, Allbritton NL. Micropatterning of living cells on a heterogeneously wetted surface. *Langmuir*. 2006;22:8257-8262.

44. Patel D. Separating Cells. New York: Springer-Verlag; 2001.

45. Schildkraut ER, Hercher M, Shapiro HM, et al. A system for storage and retrieval of individual cells following flow cytometry. *J Histochemistry and Cytochemistry*. 1979;27(1):289-292.

46. Chen P, Feng X, Du W, Liu B. Microfluidic chips for cell sorting. *Frontiers in Bioscience-Landmark*. 2008;13:2464-2483.

47. Kirkland DJ. Chemical transformation of Chinese hamster cells. I. A comparison of some properties of transformed cells. *British Journal of Cancer*. 1976;34:134-144.

48. EmmertBuck M, Bonner R, Smith P, et al. Laser capture microdissection. *Science*. 1996;274(5289):998-1001.

49. Schutze K, Lahr G. Identification of expressed genes by laser-mediated manipulation of single cells. *Nature Biotechnology*. 1998;16(8):737-742.

50. Sims C, Bachman M, Li G, Allbritton N. Choosing one from the many: Selection and sorting strategies for single adherent cells. *Analytical and Bioanalytical Chemistry*. 2007;387(1):5-8.

51. Toner M, Irimia D. Blood-on-a-chip. *Annual Review of Biomedical Engineering*. 2005;7:77-103.

52. Cohen S, Punt C, Iannotti N, et al. Relationship of circulating tumor cells to tumor response, progression-free survival, and overall survival in patients with

metastatic colorectal cancer. *Journal of Clinical Oncology*. 2008;26(19):3213-3221.

53. Cristofanilli M, Budd G, Ellis M, et al. Circulating tumor cells, disease progression, and survival in metastatic breast cancer. *New England Journal of Medicine*. 2004;351(8):781-791.

54. Paterlini-Brechot P, Benali N. Circulating tumor cells (CTC) detection: Clinical impact and future directions. *Cancer Letters*. 2007;253(2):180-204.

55. Lauks I. Microfabricated biosensors and microanalytical systems for blood analysis. *Accounts of Chemical Research*. 1998;31(5):317-324.

56. Ingber DE. Tensegrity: the architectural basis of cellular mechanotransduction. *Annual Review of Physiology*. 1997;59:575-599.

57. Seidl J, Knuechel R, Kunz-Schughart LA. Evaluation of membrane physiology following fluorescence activated or magnetic cell separation. *Cytometry*. 1999;36(2):102-111.

58. Miltenyi S, Muller W, Weichel W, Radbruch A. High-gradient magnetic cell-separation with MACS. *Cytometry*. 1990;11(2):231-238.

59. Xia N, Hunt T, Mayers B, et al. Combined microfluidic-micromagnetic separation of living cells in continuous flow. *Biomedical Microdevices*. 2006;8(4):299-308.

60. Pregibon D, Toner M, Doyle P. Magnetically and biologically active bead-patterned hydrogels. *Langmuir*. 2006;22(11):5122-5128.

61. Kamentsk LA, Melamed M. Spectrophotometric cell sorter. *Science*. 1967;156(3780):1364-&.

62. Herzenberg L, Sweet R. Fluorescence-activated cell sorting. *Scientific American*. 1976;234(3):108-117.

63. Scriba TJ, Purbhoo M, Day CL, et al. Ultrasensitive detection and phenotyping of CD4+ T cells with optimized HLA class II tetramer staining. *J Immunology*. 2005;175(10):6334-6343.

64. Xu W, Sims CE, Allbritton NL. Microcup arrays for the efficient isolation and cloning of cells. *Analytical Chemistry*. 2010;82:3161-3167.

65. Rando TA, Blau HM. Primary mouse myoblast purification, characterization, and transplantation for cell-mediated gene therapy. *J Cell Biology*. 1994;125(6):1275-1287.

66. Puck T, Marcus P, Cieciura S. Clonal growth of mammalian cells in vitro - growth characteristics of colonies from single HeLa cells with and without a feeder layer. *Journal of Experimental Medicine*. 1956;103(2):273-&.

67. McFarland DC. Preparation of pure cell cultures by cloning: Methods in Cell Science; 2000:63 - 66.

68. Berns MW, Greulich KO. Laser Manipulation of Cells and Tissues, 1st Ed.: Academic Press; 2007.

69. Murray G. An overview of laser microdissection technologies. *Acta Histochemica*. 2007;109(3):171-176.

70. Emmert-Buck MR, Bonner RF, Smith PD, et al. Laser capture microdissection. *Science*. 1996;274:998-1001.

71. Bohm M, Wieland I, Schutze K, Rubben H. Microbeam MOMeNT - Non-contact laser microdissection of membrane-mounted native tissue. *American Journal of Pathology*. 1997;151(1):63-67.

72. Schutze K, Posl H, Lahr G. Laser micromanipulation systems as universal tools in cellular and molecular biology and in medicine. *Cell and Molecular Biology (Noisy-le-grand)*. 1998;44(5):735-746.

73. Burgemeister R. New aspects of laser microdissection in research and routine. *Journal of Histochemistry and Cytochemistry*. 2005;53:409-412.

74. Ladanyi A, Sipos F, Szoke D, Galamb O, Molnar B, Tulassay Z. Laser microdissection in translational and clinical research. *Cytometry Part A*. 2006;69A(9):947-960.

75. Tokilmitsu Y, Kishi H, Kondo S, et al. Single lymphocyte analysis with a microwell array chip. *Cytometry Part A*. 2007;71A(12):1003-1010.

76. Love JC, Ronan JL, Grotenbreg GM, van der Veen AG, Ploegh HL. A microengraving method for rapid selection of single cells producing antigen-specific antibodies. *Nature Biotechnology*. 2006;24(6):703-707.

77. Revzin A, Sekine K, Sin A, Tompkins R, Toner M. Development of a microfabricated cytometry platform for characterization and sorting of individual leukocytes. *Lab on a Chip*. 2005;5(1):30-37.

78. Kovac J, Voldman J. Intuitive, image-based cell sorting using optofluidic cell sorting. *Analytical Chemistry*. 2007;79(24):9321-9330.

79. Salazar GT, Wang YL, Young G, et al. Micropallet arrays for the separation of single, adherent cells. *Analytical Chemistry*. 2007;79(2):682-687.

80. Wang Y, Young G, Aoto P, et al. Broadening cell selection criteria with micropallet arrays of adherent cells. *Cytometry A*. 2007;71:866-874.

81. Wang Y, Young G, Bachman M, Sims CE, Li GP, Allbritton NL. Collection and expansion of single cells and colonies released from a micropallet array. *Analytical Chemistry*. 2007;79:2359-2366.

82. Wang Y, Phillips C, Xu W, et al. Micromolded arrays for separation of adherent cells. *Lab on a Chip*. 2010;10(21):2917-2924.

83. Pai JH, Xu W, Sims CE, Allbritton NL. Microtable arrays for culture and isolation of cell colonies. *Analytical Bioanalytical Chemistry*. 2010;398(6):2595-2604.

84. Wei X, Sims C, Allbritton N. Microcup Arrays for the Efficient Isolation and Cloning of Cells. *Analytical Chemistry*. 2010;82(8):3161-3167.

85. Xu W, Herman A, Phillips C, Pai JH, Sims CE, Allbritton NL. Selection and separation of viable cells based on a cell-lethal assay. *Analytical Chemistry*. 2011;83(1):278-283.

86. Pai J, Wang Y, Salazar G, et al. Photoresist with low fluorescence for bioanalytical applications. *Analytical Chemistry*. 2007;79(22):8774-8780.

87. Detwiler DA, Dobes NC, Sims CE, Kornegay JN, Allbritton NL. Polystyrene-coated micropallets for culture and separation of primary muscle cells. *Analytical Bioanalytical Chemistry*. 2012;402:1083-1091.

88. Gunn N, Bachman M, Li G, Nelson E. Fabrication and biological evaluation of uniform extracellular matrix coatings on discontinuous photolithography generated micropallet arrays. *Journal of Biomedical Materials Research Part A*. 2010;95A(2):401-412.

89. Shadpour H, Sims CE, Allbritton NL. Enrichment and expansion of cells using antibody-coated micropallet arrays. *Cytometry A*. 2009;75A:609-618.

90. Xu W, Luikart A, Sims C, Allbritton N. Contact printing of arrayed microstructures. *Analytical and Bioanalytical Chemistry*. 2010;397(8):3377-3385.

91. Shadpour H, Sims CE, Thresher RJ, Allbritton NL. Sorting and expansion of murine embryonic stem cell colonies using micropallet arrays. *Cytometry A*. 2009;75(2):121-129.

92. Lorenz H, Despont M, Fahrni N, LaBianca N, Renaud P, Vettiger M. SU-8: a low-cost negative resist for MEMS. *Journal of Micromechancis and Microengineering*. 1997;7:121-124.

93. Wang Y, Bachman M, Sims CE, Li GP, Allbritton NL. Stability of virtual air walls on micropallet arrays. *Analytical Chemistry*. 2007;79:7104-7109.

94. Wang Y, Salazar G, Pai J, Shadpour H, Sims C, Allbritton N. Micropallet arrays with poly(ethylene glycol) walls. *Lab on a Chip*. 2008;8(5):734-740.

95. Ma H, Mismar W, Wang Y, et al. Impact of release dynamics of laser-irradiated polymer micropallets on the viability of selected adherent cells. *J Royal Society Interface*. 2011;doi: 10.1098/rsif.2011.0691.

96. Quinto-Su PA, Salazar GT, Sims CE, Allbritton NL, Venugopalan V. Mechanism of pulsed laser microbeam release of SU-8 2100 polymer micropallets for the collection and separation of adherent cells. *Analytical Chemistry*. 2008;80:4675-4679.

97. Salazar GT, Wang YL, Sims CE, Bachman M, Li GP, Allbritton NL. Characterization of the laser-based release of micropallets from arrays. *Journal of Biomedical Optics*. 2008;13(3).

98. Jackman R, Duffy D, Ostuni E, Willmore N, Whitesides G. Fabricating large arrays of microwells with arbitrary dimensions and filling them using discontinuous dewetting. *Analytical Chemistry*. 1998;70(11):2280-2287.

Chapter 2: Transparent Magnetic Photoresists for Bioanalytical Applications

2.1 Introduction

Materials consisting of both polymers and inorganic particles have been of interest for several decades. These materials possess the ease of processing of polymer substrates along with the integrated benefits of the inorganic phase such as magnetism, conductivity, or luminescence. The use of magnetic particles as a polymer filler has garnered much attention recently due to their utility in biotechnology including cell separations, diagnostics and therapeutic treatments.[1-4] Nanocomposites consisting of a photoresist organic phase and magnetic inorganic phase have found utility in the field of microelectromechanical systems (MEMS) development. These materials would be of great use in developing devices such as micro actuators, sensors, relays and magneto-optical devices based on the Faraday effect. Introduction of magnetic particles into a photosensitive epoxy has been accomplished in recent studies. Damean et al. mixed 100 nm nickel particles at concentrations up to 13% in SU-8, an epoxide-based photoresist, for the purpose of fabricating magnetically actuated microcantilevers.[5] 1-10 μm ferrite particles were introduced into SU-8 to develop microactuators by Hartley and colleagues.[6] Atomic force microscopy probes have been developed by Ingrosso and coworkers by adding maghemite dissolved in toluene to a photoresist.[7] Feldmann and Büttgenbach achieved mixtures of SU-8 with up to 90% ferrites and rare-earth alloys of size 1-10 μm for developing magnetic MEMS.[8] Magnetic rods consisting of 1.8 μm beads have been mixed into SU-8 by Alargova et al.[9] Dutoit and collaborators blended 10

μm Sm_2Co_{17} particles into SU-8.[10] SU-8 with magnetite nanoparticles has also been prepared previously.[11,12] These composite materials possessed either large micrometer-sized structures or aggregrated nanoparticles as the magnetic component. These formulations were useful when manufacturing MEMS that did not require uniform magnetism or optical transparency over the entire device. A photoresist with a uniform distribution of magnetic nanoparticles would enable high quality light microscopy of the surfaces as well as uniform forces to be applied across the device during application of a magnetic field.

Nanoparticle self-aggregation in polymers has been minimized in materials such as polydimethylsiloxane (PDMS),[13,14] polymethylmethacrylate (PMMA),[15,16] polystyrene,[17] polyimide,[18,19] ethyl(hydroxyethyl)cellulose (EHEC)[20] or 3,4-epoxycyclohexylmethyl-3´4´-epoxycyclohexanecarboxylate (CE) but not in an epoxide-based photoresist.[21] The composites were made by capping the nanoparticles with an organic phase or through use of a solvent-based dispersion technique. Peluse et al. integrated magnetic nanoparticles into polystyrene through thermal decomposition of iron mercaptide.[17] Solvent-based dispersion typically involved mixing dilutions of the nanoparticles and polymer separately dissolved in an organic solution, such as chloroform, benzene or toluene, and then evaporating the bulk of the solvent. This method has shown success in dispersing maghemite nanoparticles into PDMS[22] or gold, Diamantane, and single-wall carbon nanotubes (SWNT) into SU-8.[13]

In this study, 10 nm maghemite particles were uniformly distributed into the epoxide-based photoresists SU-8[23,24] and 1002F[25]. To achieve this, oleic acid-capped maghemite nanoparticles were dissolved in toluene and mixed with the photoresist

monomer in toluene. Photoresists with nanoparticle concentrations ranging from 0.01 to 1% maghemite were prepared and nanoparticle distribution aggregation was measured. The UV and visible absorption of the magnetic photoresists was also assessed. Furthermore, microstructures of varying dimensions were formed to determine the achievable resolution and aspect ratios. The ability of cells to attach to and grow on the magnetic photoresists was quantified by culturing 3T3, HeLa and RBL cells on the surfaces. The quality of brightfield and fluorescence microscopy images obtained when illuminating through and collecting light transiting the photoresists was evaluated. The utility of these magnetic structures was demonstrated by using the resist to form micropallet arrays for cell separation and demonstrating collection of released micropallets with cells using a magnetic field.[26,27]

2.2 Materials and Methods

2.2.1 Reagents. The following materials were obtained from the Aldrich Chemical Company (St. Louis, MO): iron(III) chloride tetrahydrate, iron(III) chloride anhydrous, iron(III) nitrate nonahydrate, toluene (reagent grade), triarylsulfonium hexafluorophosphate salts, mixed, 50% in propylene carbonate, γ-butyralactone (GBL, 99+%), 1-methoxy-2-propanol (1002F developer, 98.5%). EPON resin 1002F (phenol, 4,4'-(1-methylethylidene)bis-, polymer with 2,2'-[(1-methylethylidene) bis(4,1-phenyleneoxymethylene]bis-[oxirane]) was obtained from Miller-Stephenson (Sylmar, CA) and (heptadecafluoro-1,1,2,2-tetrahydrodecyl)trichlorosilane was purchased from Gelest Inc (Morrisville, PA). Dulbecco's modified Eagle's medium (DMEM), fetal bovine serum (FBS), 1X phosphate buffered saline (PBS), pH 7.4, 0.05% trypsin with EDTA solution and penicillin/streptomycin were received from Invitrogen (Carlsbad,

CA). Cell proliferation kit II (XTT: (sodium 3´-[1-(phenylaminocarbonyl)- 3,4-tetrazolium]-bis (4-methoxy-6-nitro) benzene sulfonic acid hydrate) was obtained from MD biosciences Inc. (St. Paul, MN). Sylgard 184 silicone elastomer kit (PDMS) was received from Dow Corning (Midland, MI). Fibronectin extracted and purified from human plasma was obtained from Chemicon International Inc. (Temecula, CA). Rat basophilic leukemic (RBL) and wild-type HeLa cells were purchased from the American Type Culture Collection (ATCC, Manassas, VA). All other chemicals were procured from Fisher Scientific (Pittsburgh, PA).

2.2.2 Magnetic photoresist development. Magnetite nanoparticles were fabricated through the coprecipitation of iron salts in an alkaline medium.[28] The particles were then oxidized to form maghemite nanoparticles by heating in an acidic solution of iron nitrate.[29] The aqueous ferrofluid was then extracted into oleic acid. Excess oleic acid was removed by washing with ethanol. The nanoparticles were then dissolved in toluene. A 1:5 mixture of 1002F photoresist in toluene was slowly added to a 1:5 dispersion of maghemite nanoparticles in toluene under sonication (Branson 250 sonifier, Danbury, CT). The toluene was then evaporated (Büchi R200 rotovapor, Flawil, Switzerland).

2.2.3 Measurement of photoresist absorption. 100 μm-thick films of 1002F photoresist with various concentrations of magnetic nanoparticles were spin-coated onto plasma-cleaned 25 mm-diameter cover glass (Fisher Scientific). Films were then processed identically to that used for pallet fabrication below. Sixteen absorbance measurements were made at various sections of four different films using a SpectraMax M5 (Molecular Devices Corporation, Sunnyvale, CA) with an uncoated cover glass used

as a blank. The standard deviation for the transmittance readings was under 5% of the measured value for every data point.

2.2.4 Cell culture. HeLa, 3T3 or RBL cells were cultured in DMEM supplemented with FBS (10%), L-glutamine (584 mg L^{-1}), penicillin (100 units mL^{-1}) and streptomycin (100 µg ml^{-1}) in a 37^{o}C incubator with a 5% CO_2 atmosphere. Before use, cell media was replaced with PBS. Conditioned media was developed by growing subconfluent cultures of HeLa, RBL or 3T3 cells in DMEM supplemented with FBS (10%), L-glutamine (584 mg L^{-1}), penicillin (100 units mL^{-1}) and streptomycin (100 µg ml^{-1}) for 48 hours. The supernatant was centrifuged (3,000Xg, 20 min), stored at -20^{o}C and thawed immediately prior to use.

2.2.5 Measurement of cell metabolism. The metabolism of cells growing on photoresists was assessed using the XTT assays as described previously [15]. Adherent HeLa, RBL or 3T3 cells in a logarithmic growth phase were detached from culture plates with 0.05% trypsin and plated on glass, 100 µm-thick 1002F films or 100 µm-thick 1002F films containing 1% magnetic nanoparticles at a density of 5,000 cells/mL (100 µL) and cultured for 24, 48 or 96 hours. XTT assays were then performed on cells as per the manufacturer's instructions (Roche Applied Science, Indianapolis, IN). During a four hour incubation period, active mitochondria from cells will metabolize 2,3-bis(2-methoxy-4-nitro-5-sulfophenly)-5-[(phenylamino) carbonyl]-2H-tetrazolium hydroxide (XTT) to form a water-soluble formazan derivative which is highly absorbent at 480 nm. The contents of four separate chambers were then transferred to a sterile 96 well plate and the absorbance at 480 nm and 650 nm was measured (SpectraMax M5, Molecular Devices Corporation, Sunnyvale, CA).

2.2.6 Scanning electron microscopy (SEM). The presence of sharp side walls for magnetic microstructures was verified through imaging with SEM (Hitachi S-4700 cold cathode field emission). The SEM was operated in normal working mode with both upper and lower secondary electron detectors used for imaging, an accelerating voltage of 1 kV, and an emission current of 13 µA.

2.2.7 Transmission electron microscopy (TEM) of cells. 100-µm films of SU8 or 1002F photoresists containing nanoparticles were fabricated and coated with fibronectin. HeLa cells at (5,000 cells/mL, 500 µL) were cultured on the surfaces in a 5% CO_2 incubator at 37^{o}C for 48 hours. Cells were washed with 1X PBS buffer 5 times then fixed in Karnovsky's fixative (2.5% glutaraldehyde, 3% paraformaldehyde and 0.1% calcium chloride in 0.1 M sodium cacodylate, pH 7.4) and washed three times with 0.1 M sodium cacodylate buffer. Cells were then placed in 0.05 M osmium tetraoxide in 0.1 M cacodylate buffer for 2 hours followed by 5 changes of distilled water. Cells were then dehydrated by sequential washings in 25%, 50%, 75% and 95% ethanol for 5 minutes each followed by 5 changes of 100% ethanol through infinite dilution for 10 minutes each. Following dehydration, cells were set in a prepared 50:50 mixture of Polybed 812 resin and 100% ethanol overnight followed by 2 changes of 100% Polybed 812 resin for 8 hours and then polymerization at 65^{o}C overnight. Sections of the samples were cut using an ultra microtone, plated on copper grids, and post fixed with uranyl acetate for 15 minutes and lead citrate for 5 minutes followed by three rinses of distilled water. Sections were then observed using a TEM (JEOL 100CX II).

2.2.8 Fabrication of micropallet arrays and PDMS chambers. Magnetic films and pallets were made following protocols reported in prior publications with a few

adjustments.[25,27] Briefly, an oven at 95^{o}C was used for all pre-baking and post-baking steps in place of a hotplate. Magnetic photoresists containing 1% magnetic nanoparticles require approximately 10x higher UV illumination intensities during fabrication relative to that of native 1002F pallets. During long exposure times an aluminum block was placed beneath the glass slide to dissipate heat.

Following pallet fabrication, a PDMS ring was attached to the surface of the pallet array with PDMS. Virtual air walls were then developed through chemical vapor deposition of a hydrophobic perfluoroalkylsilane layer on the silicone oxide surface as described previously.[27] Prior to loading with cells, pallet arrays and films were sterilized through rinsing with 95% ethanol and dried in a tissue culture hood. Excess ethanol was removed with five PBS rinses. Top surfaces of the pallets on the array were then coated with 1 mL of 25 μg/mL fibronectin in PBS for four hours at room temperature. Following surface coating the array was rinsed five times with 1X PBS. 1X PBS was replaced with cell culture media and suspensions of HeLa, 3T3 or RBL cells were added to the array to yield <1 cell per pallet (1mL of 30,000 cells for 50x50x50 μm^3 pallets and 1mL of 15,000 cells for 100x100x50 μm^3 pallets). Cells were allowed to settle and adhere onto single pallets. Six hours later, cells were imaged and pallets released and collected in 1X PBS. After cell/pallet collection, the PBS was replaced with conditioned medium.

Released pallets were collected onto a substrate attached to the pallet array by a PDMS ring and an O-ring. For these studies the collection substrate was composed of a multiwell PDMS plate as described previously.[26] A silicon O-ring (24 mm outer diameter, McMaster-Carr, Los Angeles, CA) was attached to the collection substrate

using PDMS to provide a fluid chamber for culture media. Prior to use for cell collection, the collection chamber was autoclaved, rinsed with ethanol and washed with PBS ten times. Following sterilization, the PDMS multiwell plate was treated with 25 μg/mL fibronectin in 1X PBS for six hours at room temperature.

2.2.9 Laser-based pallet release. Individual micropallets were released with single or multiple pulses (5 ns, 532 nm Nd:YAG Polaris II laser, New Wave Research, Fremont, CA) focused at the interface of the pallet and substrate using a 20x objective as described previously.[16] Pulse energies were measured with an energy meter (J4-09 probe, Molectron EPM 1000). Threshold energies for pallet release were calculated by plotting the probability of pallet release as a function of the pulse energy and fitting the curve to a Gaussian error function.[16]

2.2.10 Magnetic field characterization. Characterization of the neodymium magnet used in all collection experiments was performed with a DC magnetometer (AlphaLab Inc). The magnetic field strength and magnetic field gradients of the permanent magnet was profiled as a function of distance from the probe.

2.3 Results and Discussion

2.3.1 Development of magnetic photoresists. Superparamagnetic maghemite nanoparticles were used for manufacturing magnetic microstructures because of their small size, controllable magnetism and biological compatibility.[30] Ten-nm magnetite nanoparticles were fabricated through the Massate method and then oxidized to maghemite to provide stability in an oxygen environment.[28,29] Oleic acid was added to the nanoparticles which then formed a stable ferrofluid in toluene at concentrations below 5% (Figure 2.1).[31] When this ferrofluid was mixed into SU-8 or 1002F negative

photoresist, large colloids formed due to the nanoparticle's preference for self-adhesion (Figure 2.2). To prevent this aggregation, both the photoresist and ferrofluid were diluted into toluene prior to mixing. A mixture of SU8 or 1002F photoresist in toluene was slowly added to the maghemite nanoparticles under sonication. The mixture was then heated to evaporate the toluene. Films of varying thicknesses were then fabricated from the magnetic photoresists. To fully cure, photoresists with maghemite nanoparticles required 2 to 10 times higher UV illumination intensities than that of the native photoresists. The uniformity of the nanoparticle distribution in the photoresist was assessed by transmission electron microscopy (TEM) of films fabricated from photoresists with 1% maghemite particles. The TEM images confirmed the lack of colloid formation during the fabrication process with retention of the small nanoparticle size (10±5 nm, n=77) (Figure 2.3A,B). The maghemite nanoparticles were stably suspended in 1002F or SU8 at concentrations up to 1% with minimal aggregation for over six months.

2.3.2 Absorbance of magnetic photoresists. Many biomedical applications require a transparent photoresist for visualization of structures such as cells or other features above or below the photoresist or for measurement of light-based signals such as absorbance or fluorescence. To determine whether the photoresist with maghemite particles was transparent, the transmittance of 1002F films possessing varying concentrations of maghemite particles was measured (Figure 2.3C). The transmittance in the shorter wavelengths decreased as the concentration of magnetic nanoparticles was increased. The decreased UV transparency was the most likely reason for the increased illumination intensities required to fully cure the polymeric photoresist. An 80% light

transmittance was observed for resists with 0.1-1% particles at 458-572 nm, respectively. Thus transparency was excellent at the longer visible wavelengths frequently used for biomedical assays and imaging. SU8 films with nanoparticles yielded similar transmittance curves to that of 1002F films with identical nanoparticle concentrations (data not shown).

2.3.3 Cell growth on magnetic photoresists. Photoresists are commonly used as substrates for cell culture on devices targeted towards biomedical research.[32-34] The metabolism of cell cultures grown on photoresists with and without maghemite nanoparticles and on a standard tissue culture surface was compared for three cell lines (HeLa, RBL and 3T3) (Figure 2.4). Identical numbers of cells were plated on each of the surfaces for these measurements. Cell cultures grown on glass slides possessed a slightly greater metabolic rate than those grown on the photoresists. This may be due to either a faster growth rate or greater mitochondrial activity of the cells on glass. Cell cultures grown on native 1002F or magnetic 1002F possessed similar metabolic rates (two sided t-test on 96 hr values, [HeLa] $t(6)=0.831$, $p=0.4$, [RBL] $t(6)=0.425$, $p=0.7$, [3T3] $t(6)=1.866$, $p=0.1$). These results demonstrated that the maghemite nanoparticles possessed minimal effects on the short term growth of cells. The small decrease in the metabolic activity of cell cultures grown on photoresists relative to that on glass may be due to the greater hydrophobicity of 1002F and consequently reduced cell adhesion to 1002F compared to that on glass.[25]

There is much controversy as to the influence of cellular nanoparticle uptake on the health and well being of cells and tissues.[35-38] Thus presence of maghemite nanoparticles within cells grown on the nanoparticle-containing surfaces would be an

undesired consequence. To determine whether particles accumulated in cells in contact with the surfaces, HeLa cells were cultured on 100-μm thick films of SU8 and 1002F with and without 1% dispersed maghemite particles. Following fixation and staining, sections of the cells were imaged by TEM. HeLa cells cultured on the photoresist with nanoparticles (but not those on standard 1002F) possessed large aggregates of the magnetic nanoparticles within the cytoplasm (Figure 2.5A). To understand how cells might come into contact with the nanoparticles, vertical sections of photoresist with 1% maghemite nanoparticles were examined by TEM. Nanoparticles were observed to be at high density near the surface of the photoresist (Figure 2.5B). Evaporation of solvent during the baking process may have transported the particles to the surface of the photoresist. It was likely that these surface nanoparticles were those taken up by the cells. To reduce the high density of nanoparticles on the photoresist surface, two approaches were tested. The first strategy was to apply a 2-μm layer of 1002F without nanoparticles over the magnetic photoresist to provide a barrier between the cells and the magnetic photoresist surface. HeLa cells cultured on this barrier surface above the magnetic photoresist did not possess identifiable nanoparticles within their cytoplasm as demonstrated by TEM (Figure 2.5C). Alternatively, the surface of the magnetic photoresist was roughened for 30 minutes, as described previously, to remove the photoresist near the surface of the films and thus the high density region of nanoparticles.[39] Vertical slices of the roughened magnetic photoresists (1% maghemite) were obtained and imaged with TEM. The high density layer of nanoparticles was fully removed by the roughening process (Figure 2.5D). When HeLa cells cultured on these films were examined by TEM, the cells did not possess identifiable cytoplasmic

nanoparticles (data not shown). Thus both strategies, a barrier coating or surface nanoparticle removal, eliminated nanoparticle uptake by the cells.

2.3.4 Imaging cells on magnetic photoresists. A uniform dispersion of magnetic nanoparticles in polymers is required for high quality cell imaging by optical microscopy. To compare the image quality of cells on photoresists containing aggregated and uniformly distributed nanoparticles, RBL cells were cultured on: glass, 5 and 50 μm thick films of 1002F or SU8, 5 and 50 μm thick films of 1002F or SU8 containing 1% dispersed maghemite nanoparticles and 5 and 50 μm thick films of 1002F or SU8 containing 1% aggregated maghemite nanoparticles. RBL cells, which possess Fcε receptors, were incubated with AlexaFluor 647-labeled IgE. Cells cultured on the various substrates were then imaged by brightfield and fluorescence microscopy. Cells cultured on glass, 1002F, SU8, or 1002F/SU-8 (5 and 50 μm films) with uniformly distributed maghemite nanoparticles were clearly visualized by brightfield microscopy (Figure 2.6A and B). When cells were cultured on 1002F or SU8 photoresists (5-μm films) containing aggregated maghemite nanoparticles and examined by brightfield microscopy, portions of the cells were obscured by the particle aggregates and thus not visualized (Figure 2.6C). When cells on these surfaces were imaged by fluorescence microscopy, a halo of scattered light surrounded the cells and much of the cell's interior appeared jagged and irregular (Figure 2.7). Cells cultured on thicker films of photoresists (50-μm films) containing aggregated nanoparticles were not identifiable (Figure 2.7). Uniformity in the distribution of magnetic nanoparticles throughout the photoresists is a critical to obtain quality images of cells with either brightfield or fluorescence microscopy.

2.3.5 Formation of microstructures with the magnetic photoresist. For widespread utility, a photoresist must be capable of forming microstructures with good aspect ratios and micron-sized resolution. To evaluate whether microstructures could be formed, a test pattern possessing structures ranging in size from 2 to 20 μm was used to form microstructures from photoresists with 1% dispersed maghemite particles. Square and circular microstructures with dimensions of 3 to 20 μm possessed sharp side walls when formed from either 1002F or SU-8 photoresist with 1% maghemite nanoparticles (Figure 2.8A-C). Microstructures with thicknesses between 5 and 100 μm were also successfully fabricated. An aspect ratio of 4:1 was achieved with both of the magnetic photoresists (Figure 2.8B and C). This is comparable to the aspect ratio of 4:1 achieved with native 1002F photoresist and 5:1 with SU-8 under similar fabrication conditions.[25] Successful formation of microstructures with various dimensions demonstrates the feasibility of further micro device development with the magnetic photoresists.

2.3.6 Magnetic manipulation of microstructures. The utility of magnetic microstructures lies in their ability to be manipulated by an external magnetic field. Magnetic cantilevers, micro actuators, microstir bars and micropallets are a few examples of structures in which a high magnetic response would be desirable in a microstructure.[5,40,41] The ability to manipulate micro structures formed from a magnetic photoresist was analyzed by fabricating micropallets from 1002F with 1% maghemite particles and using an external magnetic field to collect the structures released from a surface. To determine whether pallet collection using a magnetic force might be possible, the gravitational force (F_g, Equation 1) and magnetic force (F_m, Equation 2) on a micropallet was estimated.

$$F_g = mg \qquad (1)$$

$$F_m = \frac{V \cdot \Delta\chi}{\mu_o}(B \cdot \nabla)B \qquad (2)$$

m is the mass of a pallet, g is the acceleration due to gravity, V is the volume of magnetic particles (m^3), $\Delta\chi$ is the difference in the magnetic susceptibilities between the of nanoparticle and the surrounding medium, B is the magnetic field strength and μ_o is the permeability of vacuum. The effects of viscous drag were neglected in these equations. As an example, 100x100x100 μm^3 pallet with 1% magnetic nanoparticles experiences a gravitational force of 12 nN. Under a typical magnetic field strength of 50 mT (generated by a small permanent magnet), the magnetic force on the pallet would be 40 nN. This suggests that the microstructures can easily be collected against the force of gravity.

To demonstrate the ability to collect microstructures, the collection of individual micropallets from an array was used. Micropallet technology utilizes an array of 10^3-10^6 releasable platforms, each large enough to fit a single cell or a colony of cells. After selective identification, the pallet of interest can be detached from the substrate with a laser pulse and collected. The efficiency of micropallet collection following release from an array was measured as a function of pallet size, magnetic nanoparticle content, magnetic field strength and magnetic field gradient. The magnetic field strength was altered by varying the distance of the micropallet array from a permanent magnet. Arrays composed of either 50x50x50 μm^3 or 100x100x100 μm^3 pallets fabricated from 1002F containing 0 to 1% magnetic nanoparticles were utilized. A PDMS ring ranging in thickness from 0.5 mm to 21 mm was placed around the array and then filled with PBS. A glass coverslip (0.017 mm thick) with attached magnet was placed in contact with the PBS. The number of pallets collected on the glass coverslip surface adjacent to the

magnet following laser-based pallet release from the array was measured. Pallets with 1% maghemite were readily collected when the magnetic strength field in the array plane was 449 to 43 mT corresponding to a coverslip distance of 1 to 15 mm above the array (Table 2.1, Figure 2.8D-F). In contrast pallets of photoresist without nanoparticles could not be collected on the coverslip when the coverslip was placed 1 to 15 mm above the array. In this instance the released pallet settled back onto the array surface. Notably micropallets with as little as 0.1% maghemite could be collected with 100% efficiency for magnetic strength fields in the array plane of 449 to 204 mT corresponding to coverslip distances of 1 to 5 mm. Pallets with 0.01% maghemite particles could also be collected although at reduced efficiency. Not surprisingly collection efficiency was independent of pallet size since the pallet and nanoparticle mass scaled proportionally as pallet size increased.

In addition to collecting magnetic devices vertically, magnetic manipulation may be an efficient method for collection of microstructures in a horizontal direction. The feasibility of a horizontal collection method was tested by placing a Nd magnet axially against an array of 50x50x50 μm^3 square pallets developed from 1002F and containing a concentration of 1% maghemite. Pallets were released (triplicate data sets were n=10) at various distances from the magnet (2 to 20 mm) and the percentage of released pallets collected on a PDMS surface adjacent to the magnet was assessed. A 100% collection efficiency was observed for magnetic pallets released at distances of 2 to 12 mm from magnet, representing a magnetic field strength of 390 to 60 mT. A Nd magnet-separation of 14 mm (47 mT) from the magnet produced a pallet collection efficiency of 77 ± 12 % and pallets released at a distance of 16 mm (38 mT) from the external magnet had a probability of collection of 3 ± 12 %. No magnetic pallets greater than 18 mm (30 mT)

from the external magnet were collected. These results demonstrate that the magnetic microstructures can be collected with very high efficiency using magnetic forces parallel or perpendicular to the force of gravity. Prior collection methods for the micropallets yielded maximal collection efficiencies ranging between 10 to 63% of the released pallets.[26]

2.3.7 Separating cells using magnetic pallet arrays. Previously, arrays of micropallets have been demonstrated to be ideal platforms for culture and then separation of cells.[26] To determine whether the magnetic micropallet arrays might also be used to separate cells, HeLa, RBL or 3T3 cells were cultured on these arrays at a density of <1 cell/pallet. The arrays were fabricated from pallets (50 μm side, 30 μm height) composed of 1002F with 0.1 or 1% maghemite nanoparticles. Pallets were collected using the vertical format with a Nd magnet placed over a multiwell collection plate under conditions that yield a 100% pallet collection efficiency. Following collection, the cells were placed in an incubator for 100 hours and the number of cells that formed a colony was counted. The percentage of collected single HeLa, RBL or 3T3 cells that survived collection and expanded into a colony was 90 ± 7%, 87 ± 10% and 87 ± 9%, respectively for magnetic pallets with 0.1% magnetic nanoparticles. Similarly, colony formation of released HeLa, RBL or 3T3 cells was 88 ± 6%, 92 ± 6% and 85 ± 4%, respectively for magnetic pallets containing 1% maghemite. The survival of cells collected with magnetic pallets was consistent with the values recorded for cells successfully collected with non-magnetic pallets.[26] However in these prior reports a maximum of 63% of released non-magnetic micropallets could be collected. The combined high collection efficiency and high survival rate of cells on magnetic pallets makes this magnetic arrays

attractive for applications in which all identified cells must be collected i.e. isolation of rare cells from a population.

2.4 Conclusions

Transparent magnetic photoresists have been developed, characterized and their utility a bioanalytical application demonstrated. Ten-nm maghemite nanoparticles were successfully distributed into 1002F and SU8 photoresists with minimal aggregation at concentrations up to 1%. These photoresists retained their transparency at long wavelengths. The magnetic photoresists have been used to successfully create microstructures with sizes ranging from 3 to 100 μm. Uptake of nanoparticles by cells cultured on the photoresists was eliminated by capping with a native photoresist or by removal of the photoresist top layer which possessed concentrated nanoparticles. The metabolic activity of cells cultured on the magnetic photoresist was similar to that of cells grown on native photoresist. Manipulation of the magnetic microstructures by an external field was demonstrated by collection of micropallets with and without cells. These polymeric magnetic materials should find wide use in the fabrication of structures for BioMEMS applications such as magnetic cell arrays, micro actuators, magnetic cantilevers, magnetic AFM probes, stir bars, sensors, relays and magneto-optical devices.[42]

2.5 Tables and Figures

% Fe_2O_3	Pallet/Magnet Separation (mm)	B Field at Pallet Array (mT)	Collection Probability (%) 50x50x50 μm^3	Collection Probability (%) 100x100x100 μm^3
0	0.5	502 ± 5	10 ± 5	0 ± 0
0.01	0.5	502 ± 5	93 ± 8	55 ± 15
	1	449 ± 4	3 ± 3	0 ± 0
0.10	1	449 ± 4	100 ± 0	100 ± 0
	5	204 ± 11	100 ± 0	100 ± 0
	9	94 ± 4	23 ± 8	17 ± 8
1.00	1	449 ± 4	100 ± 0	100 ± 0
	5	204 ± 11	100 ± 0	100 ± 0
	9	94 ± 4	100 ± 0	100 ± 0
	12	60 ± 2	100 ± 0	100 ± 0
	15	43 ± 3	100 ± 0	100 ± 0
	18	30 ± 2	65 ± 13	73 ± 25
	21	21 ± 2	3 ± 3	8 ± 6
Triplicate experiments (n=20 pallets per experiment).				

Table 2.1 Vertical collection of magnetic micropallets.

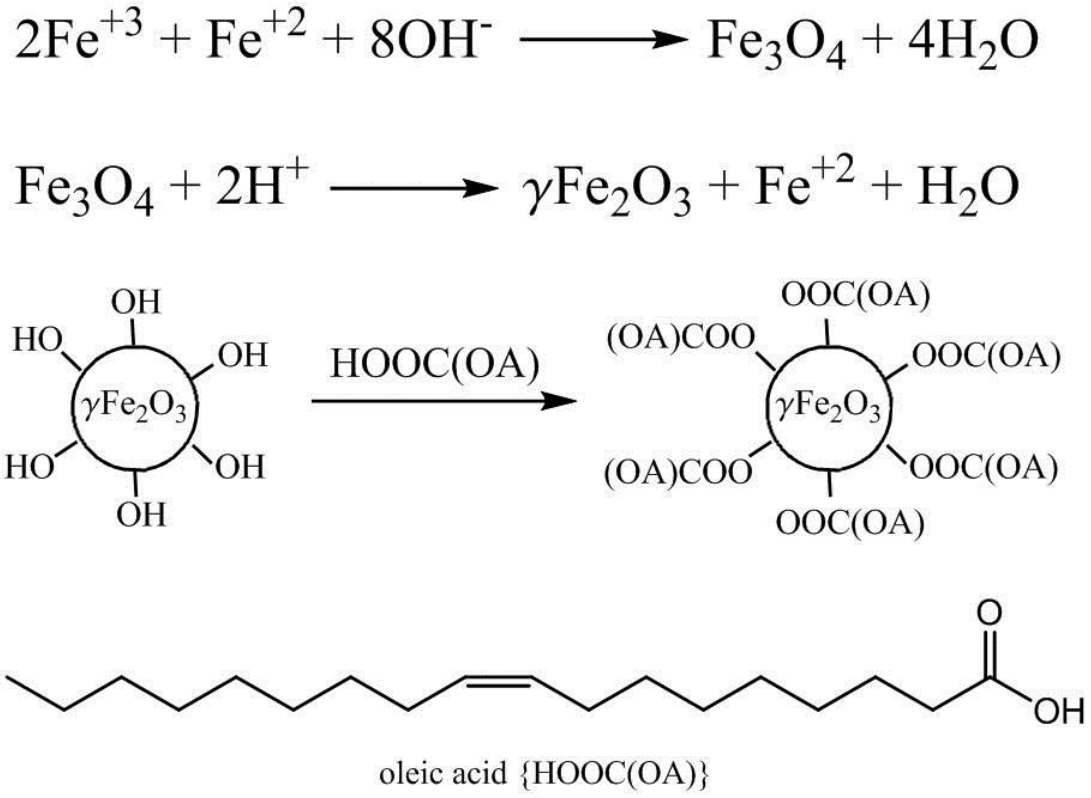

Figure 2.1 Schematic of the fabrication process of oleic acid-coated maghemite nanoparticles.

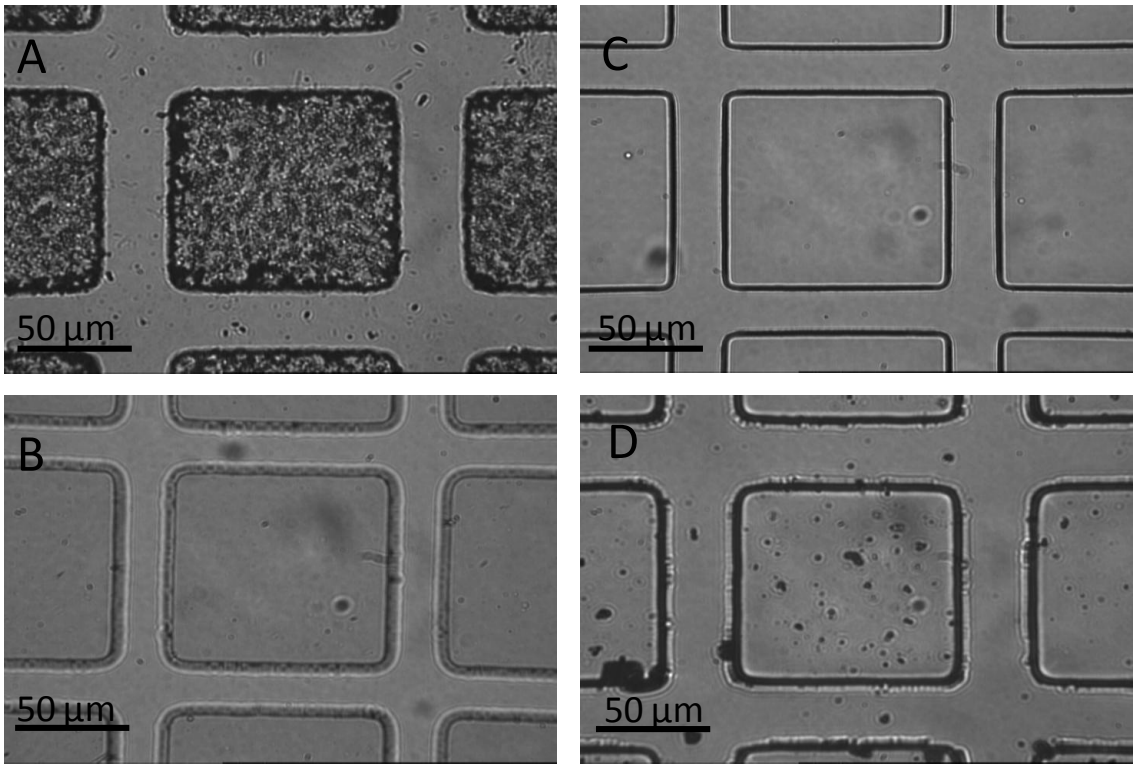

Figure 2.2 Transmitted light microscopy of microstructures (100-µm squares with a 30-µm height) made with 1002F photoresist containing 1% maghemite nanoparticles directly mixed into 1002F (A) and 1% maghemite nanoparticles incorporated into 1002F through toluene dilutions (B). Micropallets were also fabricated with 1% maghemite nanoparticles uniformly incorporated into SU8 (C). 1% 100 nm Ni particles in 1002F photoresist (D). Scale bars are each 50 µm.

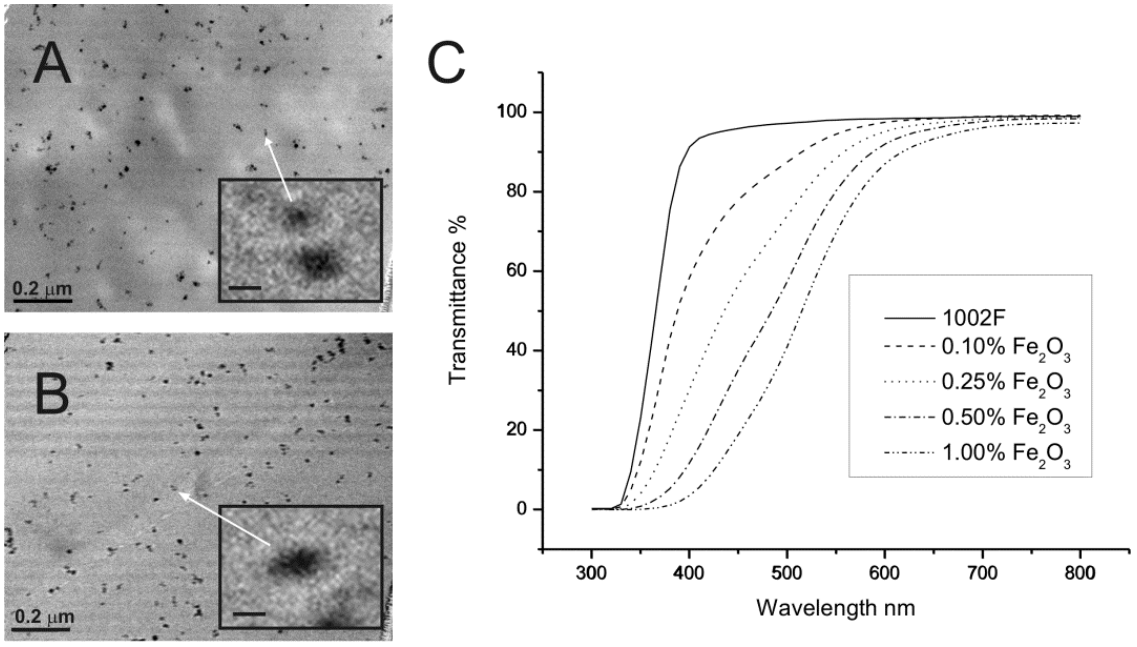

Figure 2.3 Photoresists with dispersed maghemite nanoparticles. TEM images of 1% maghemite nanoparticles in 1002F (A) or SU-8 photoresists (B) (scale bar is 200 nm). Insert shows an expanded view of a single nanoparticle (scale bar is 10 nm). Transmittance of 100 μm thick films of 1002F with various concentrations of magnetic nanoparticles (C).

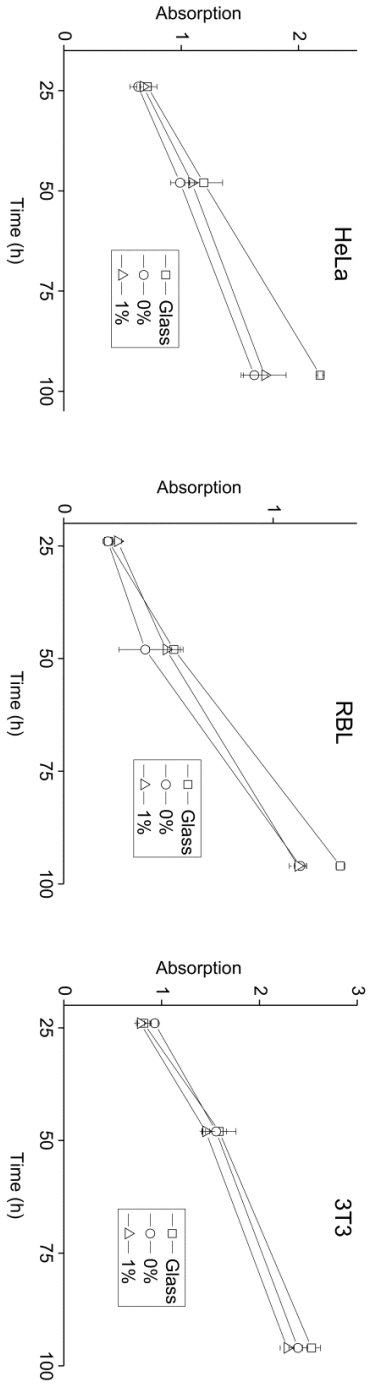

Figure 2.4 Measurement of metabolism by colorimetric assay of cells grown on photoresist. HeLa, RBL or 3T3 cells were cultured on glass (squares), 1002F photoresist (circles), or 1002F photoresist with 1% maghemite nanoparticles (triangles) for varying times. Shown on the "y" axis is the absorbance of the orange formazon product produced by metabolically active cells. Error bars represent the standard deviation of four measurements.

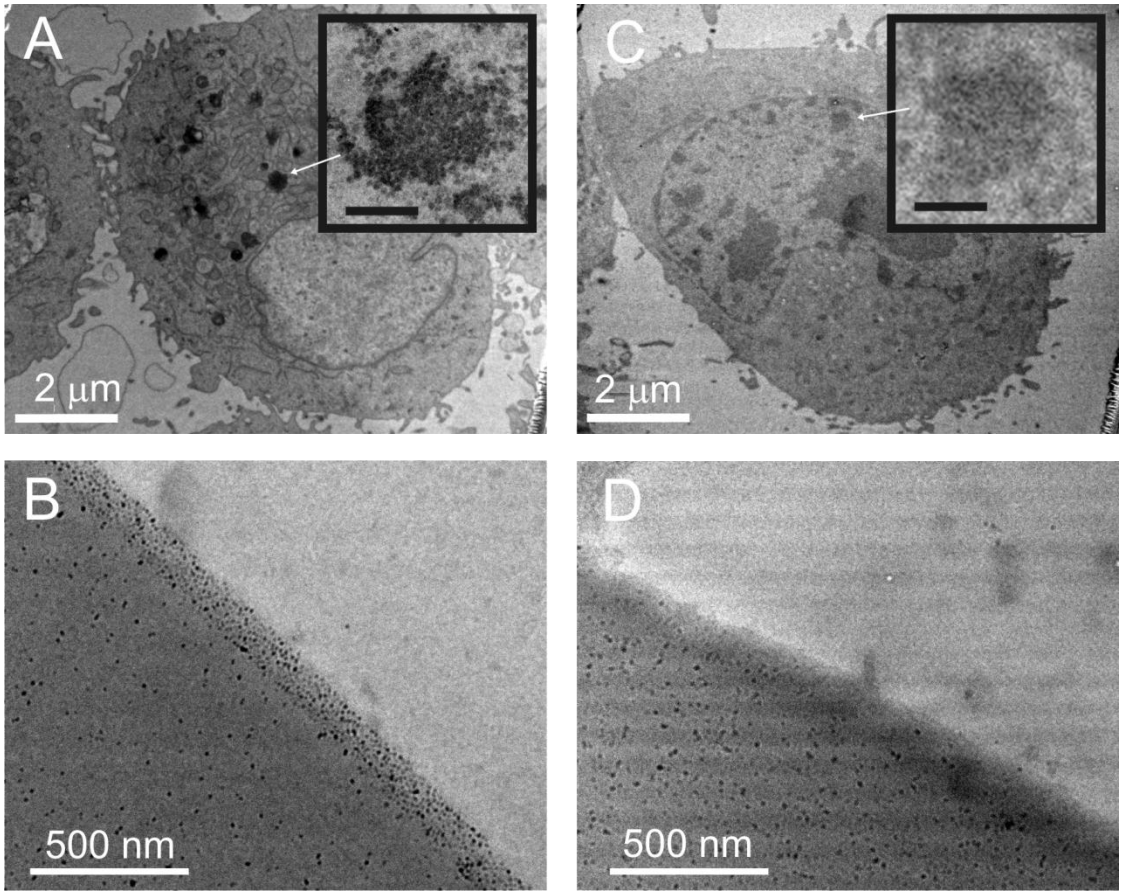

Figure 2.5 Uptake of maghemite nanoparticles by cells. TEM images of HeLa cells cultured on 1% magnetic 1002F without (A) and with a 2 μm-thick protective film of native 1002F over the magnetic photoresist (C). Arrows show clusters of nanoparticles within the cells. Inserts show enlarged images of the magnetic nanoparticles (A) and cellular organelles without nanoparticles (C) (scale bars are 150 nm). TEM images of 1002F photoresist containing 1% maghemite nanoparticles before (B) and after surface roughening (D).

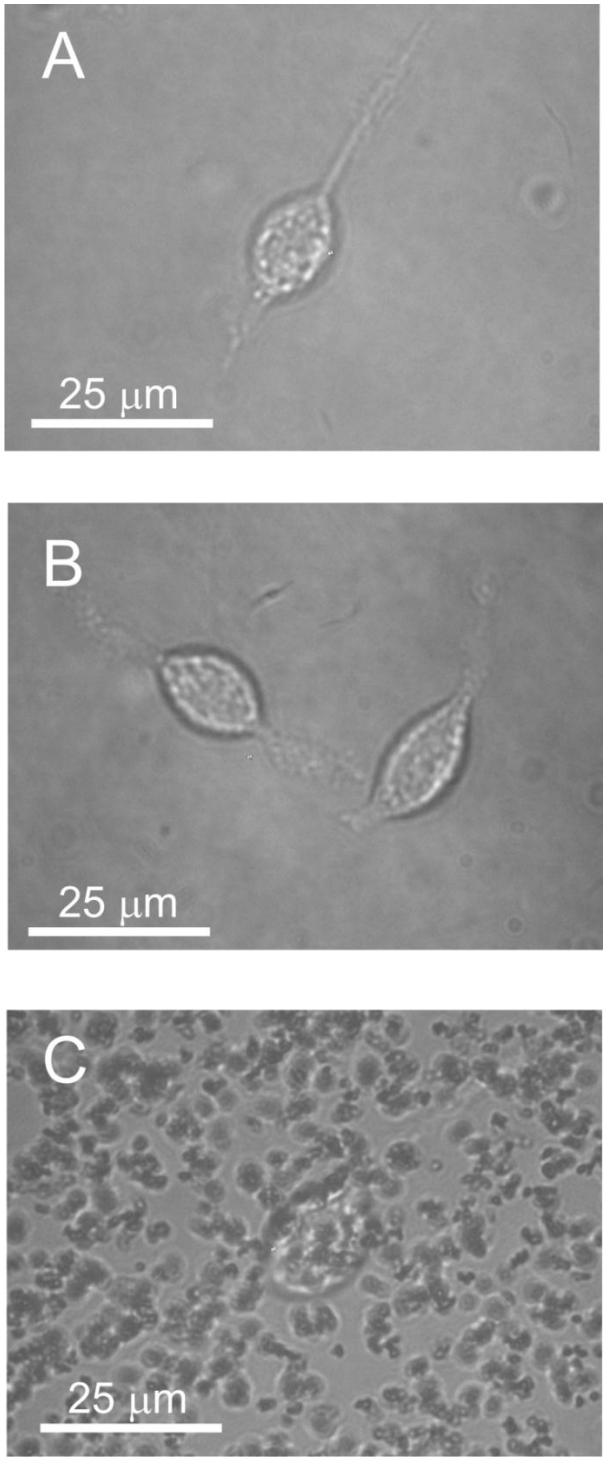

Figure 2.6 Brightfield images of photoresists with attached RBL cells. The 5-μm thick films were comprised of 1002F (A), 1002F with 1% maghemite particles uniformly dispersed (B), and 1002F with 1% maghemite particles aggregated (C).

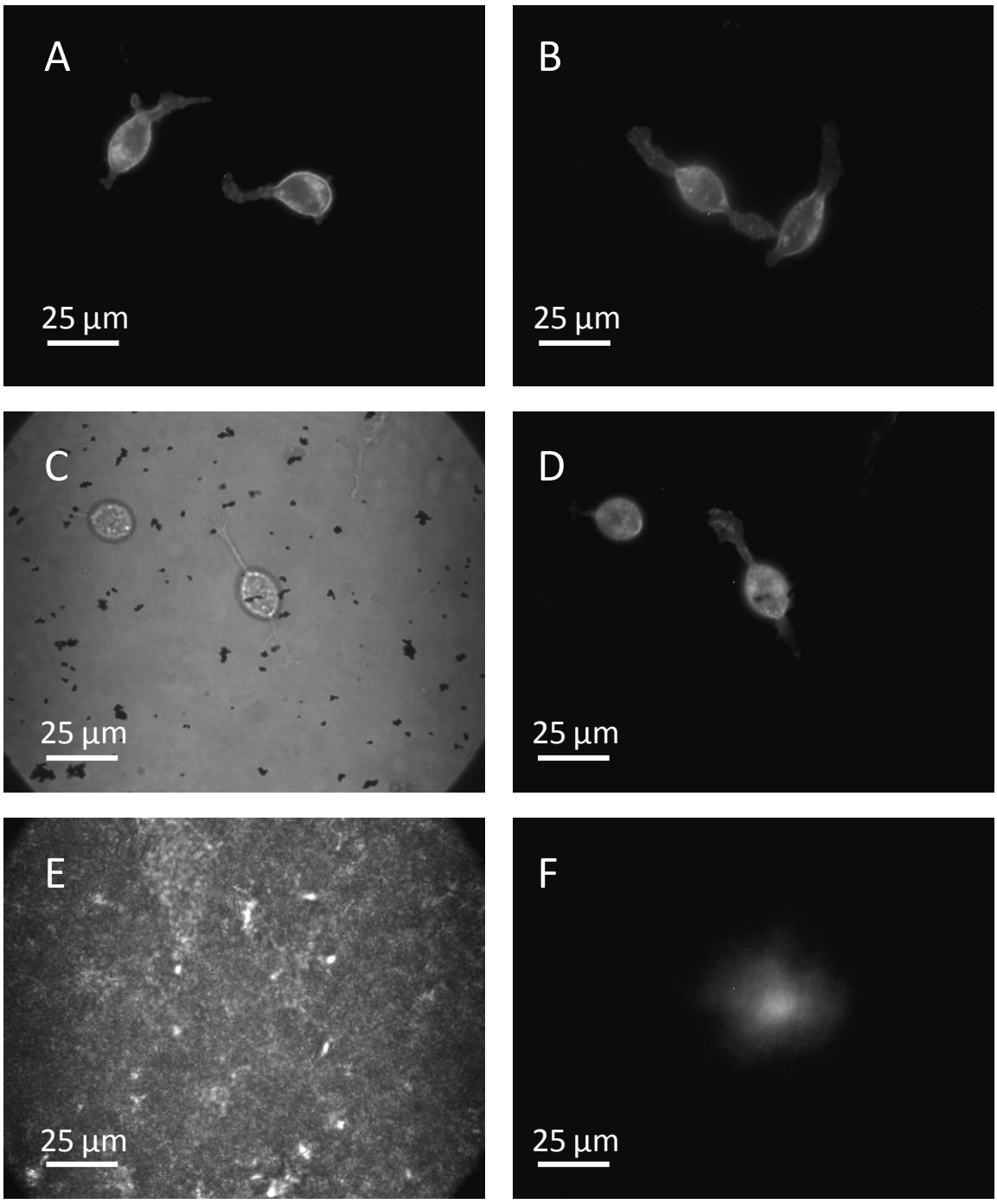

Figure 2.7 Fluorescence images of RBL cells stained with Alexa Fluor 647-labeled IgE cultured on glass (A) or a 5-µm thick film of SU8 containing 1% uniformly distributed maghemite nanoparticles (B). Transmitted light and corresponding fluorescence images of RBL cells cultured on a 5-µm thick film of 1002F containing 1% aggregated nickel nanoparticles (C-D) or 50-µm thick film of 1002F containing 1% aggregated maghemite nanoparticles (E-F).

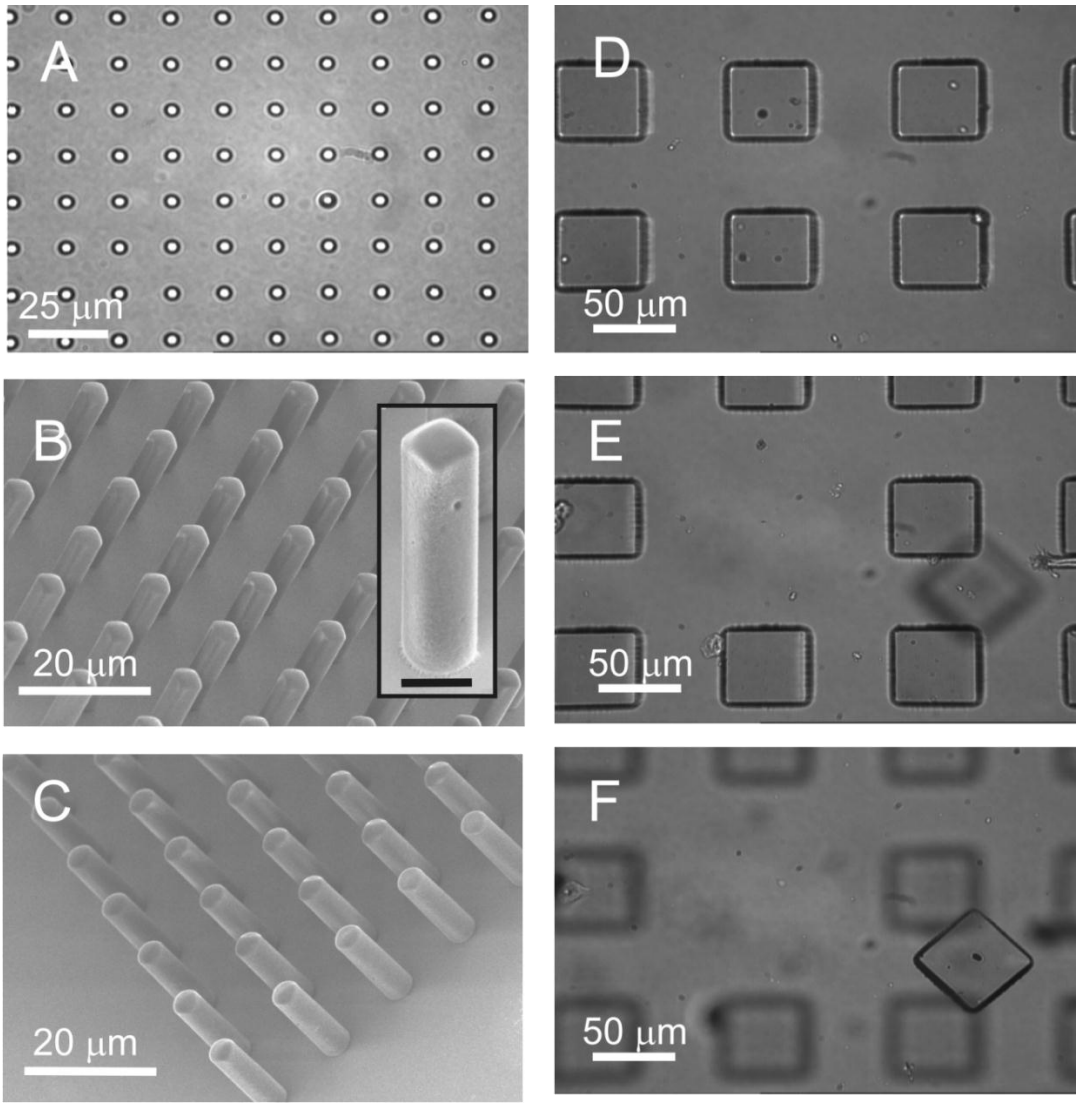

Figure 2.8 Microstructures from magnetic photoresists. Brightfield image of 3 μm circular structures composed of SU8 with 1% maghemite nanoparticles (A). SEM images of rectangular structures formed from 1002F photoresist containing 1% maghemite nanoparticles (B) and cylindrical structures formed from SU-8 photoresist containing 1% maghemite nanoparticles (C). The microstructures in B and C were fabricated from masks with 3 μm-sized openings and film heights of 12 μm. Insert shows an expanded view of a single rectangular structure (scale bar is 5 μm). Brightfield image of an array prior to laser-based release of a pallet (D). The pallets were 100x100x30 μm^3 in size and composed of 1002F with 1% maghemite nanoparticles. At the array surface the magnetic field was 502 mT. (E) Image of the same array after pallet release. The objective focal plane is located at in the plane of the array. (F) Image of the released pallet. The objective focal plane is located on the glass slide 0.5 mm above the array.

2.6 References

1. Duguet E, Vasseur S, Mornet S Devoisselle JM. Magnetic nanoparticles and their applications in medicine. *Nanomedicine (London, England)*. 2006;1(2):157-168.

2. Kumano S, Murakami T, Kim T, Hori M, Okada A, Sugiura T, et al. Using superparamagnetic iron oxide-enhanced MRI to differentiate metastatic hepatic tumors and nonsolid benign lesions. *AJR American J Roentgenology*. 2003;181:1335-1339.

3. Amirfazli A. Magnetic nanoparticles hit the target. *Nature Nanotechnology*. 2007;2:467-468.

4. Prasad NK, Rathinasamy K, Panda D, Bahadur D. Mechanism of cell death induced by magnetic hyperthermia with nanoparticles of γ–$Mn_{\chi}Fe_{2-\chi}O_3$ synthesized by a single step process. *J Material Chemistry*. 2007;17:5042-5051.

5. Damean N, Parviz BA, Lee JN, Odom T, Whitesides GM. Composite ferromagnetic photoresist for the fabrication of microelectromechanical systems. *J Micromechanics and Microengineering*. 2005;15:29-34.

6. Hartley AC, Miles RE, Corda J, Dimitrakopoulos N. Large throw magnetic microactuator. *Mechatronics*. 2008;18:459-465.

7. Ingrosso C, Martin C, Llobera A, Perez Murano F, Innocenti C, Sangregorio C, et al. Magnetic nanocrystals modified epoxy photoresist for microfabrication of AFM probes. *Procedia Chemistry*. 2009;1:580-584.

8. Feldmann M, Büttgenbach S. Novel microrobots and micromotors using Lorentz force driven linear microactuators based on polymer magnets. *IEEE Transactions Magnetism*. 2007;43:3891-3895.

9. Alargova RG, Paunov VN, Velev OD. Formation of polymer microrods in shear flow by emulsification solvent attraction mechanism. *Langmiur*. 2006;22:765-774.

10. Dutoit BM, Besse PA, Blanchard H, Guérin L, Popovic RS. High performance micromachined Sm_2Co_{17} polymer bonded magnets. *Sensors and Actuators A Physical*. 1999;77:178-182.

11. Wiche G, Goettert J, Song Y, Hormes J, Kumar CSSR. Functional micro devices using 'nanoparticle-photoresist' composites. *International Journal of Computational Engineering Science.* 2003;4:525-528.

12. Suter M, Graf S, Ergeneman O, Schmid S, Camenzid A, Nelson BJ, Hierold C. Superparamagnetic photosensitive polymer nanocomposite for microactuators. *Transducers IEEE*. 2009:869-872.

13. Chiamori HC, Brown EV, Adhiprakasha ET, Straalsund JB, Melosh NA, Pruitt BL. Suspension of nanoparticles in SU-8 and characterization of nanocomposite polymers. *Microelectronics Journal.* 2008;39(2):228-236.

14. Yamanishi Y, Sakuma S, Arai F. Production and application of high-accuracy polymer-based magnetically driven microtool. *J Robotics and Mechatronics.* 2008;20:274-279.

15. Li S, Qin J, Fornara A, Toprak M, Muhammed M, Kim DK. Synthesis and magnetic properties of bulk transparent PMMA/Fe-oxide nanocomposites. *Nanotechnology*. 2009;20:185607.

16. Gass J, Poddar P, Almand J, Srinath S, Srikanth H. Superparamagnetic polymer nanocomposites with uniform Fe_3O_4 nanoparticle dispersions. *Advance Functional Materials.* 2005;16:71-75.

17. Peluso A, Pagliarulo V, Carotenuto G, Pepe GP, Davino D, Visone C, et al. Synthesis and characterization of polymer embedded iron oxide nanocomposites. *Microwave and Optical Technology Letters*. 2009;51:2774-2777.

18. Lagorce LK, Allen MG. Magnetic and mechanical properties of micromachined strontium ferrite/polyimide composites. *J Microelectromechanical Systems*. 1997;6:307-312.

19. Rojanapornpun O, Kwok CY. Fabrication of integrated micromachined polymer magnet. *Proceedings of SPIE* 2004;4592:347-354.

20. Hayashi K, Fujikawa R, Sakamoto W, Inoue M, Yogo T. Synthesis of highly transparent lithium ferrite nanoparticle/polymer hybrid self-standing films exhibiting faraday rotation in the visible region. *J Physical Chemistry C.* 2008;112:14255-14251.

21. Sangermano M, Priola A, Kortaberria G, Jimeno A, Garcia I, Mondragon I, Rizza G. Photopolymerization of epoxy coatings containing iron-oxide nanoparticles. *Macromolecular Materials Engineering*. 2007;292:956-961.

22. Evans BA, Shields AR, Lloyd Carrol R, Washburn S, Falvo MR, Superfine R. Magnetically actuated nanorod arrays as biomimetic cilia. *Nano Letters*. 2007;7:1428-1438.

23. Shaw JM, Gelorme JD, LaBianca NC, Conley WE, Holmes SJ. Negative photoresist for optical lithography. *IBM J Research and Development*. 1997;41:81-94.

24. Gelmorme JD, Cox RJ, Gutierrez SA. Photoresist Composition and Printed Circuit Boards and Packages Made Therewith. (IBM). US Patent No. 4882245, 1989.

25. Pai J-H, Wang, Y, Salazar GTA, Sims, CE, Bachman M, Li GP, Allbritton NL. Photoresist with low fluorescence for bioanalytical applications. *Analytical Chemistry*. 2007;79:8774-8780.

26. Wang Y, Young G, Bachman M, Sims CE, Li GP, Allbritton NL. Collection and expansion of single cells and colonies released from a micropallet array. *Analytical Chemistry*. 2007;79:2359-2366

27. Wang Y, Sims CE, Marc P, Bachman M, Li GP, Allbritton NL. Micropatterning of living cells on a heterogeneously wetted surface. *Langmuir*. 2006;22:8257-8262.

28. Massart R. Preparation of aqueous magnetic liquids in alkaline and acidic media. *IEEE Transactions Magnetism*. 1981;17:1247-1248.

29. Bee A, Massart R, Neveu S. Synthesis of very fine maghemite particles. *J Magnetism and Magnetic Materials*. 1995;149:6-9.

30. Pamme N. Magnetism and microfluidics. *Lab on a Chip*. 2006;6:24-38.

31. van Ewijk GA, Vroege GJ, Philipse AP. Convenient preparation methods for magnetic colloids. *J Magnetism and Magnetic Materials*. 1999;201:31-33.

32. Heuschkel MO, Guerin L, Buisson B, Bertrand D, Renaud P. Buried microchannels in photopolymer for delivering of solutions to neurons in a network. *Sensors and Actuators B Chemistry*. 1998;48:356-361.

33. Kotzar G, Freas M, Abel P, Fleishman A, Roy S, Zorman C, et al. Evaluation of MEMS materials of construction for implantable medical devices. *Biomaterials*. 2002;23:2737-2750.

34. Voskerician G, Shive MS, Shawgo RS, Recum HV, Anderson JM, Cima MJ, Langer R. Biocompatibility and biofouling of MEMS drug delivery devices. *Biomaterials*. 2003;24:1959-1967.

35. Häfeli UO, Riffle JS, Harris-Shekhawat L, Carmichael-Baranauskas A, Mark F, Dailey JP, Bardenstein D. Cell uptake and in vitro toxicity of magnetic nanoparticles suitable for drug delivery. *Molecular Pharmacology*. 2009; 6:1417-1428.

36. Gupta AK, Naregalkar RR, Vaidya VD, Gupta M. Recent advances on surface engineering of magnetic iron oxide nanoparticles and their biomedical applications. *Nanomedicine (London, England)*. 2007;2(1):23-39.

37. Jain TK, Reddy MK, Morales MA, Leslie-Pelecky DL, Labhasetwar V. Biodistribution, clearance, and biocompatibility of iron oxide magnetic nanoparticles in rats. *Molecular Pharmacology*. 2008;5:316-327.

38. Gupta A, Gupta M. Cytotoxicity suppression and cellular uptake enhancement of surface modified magnetic nanoparticles. *Biomaterials*. 2005;26:3995-4021.

39. Shadpour H, Sims CE, Thresher RJ, Allbritton NL. Sorting and expansion of murine embryonic stem cell colonies using micropallet arrays. *Cytometry* 2009;75A:121-129.

40. Lu LH, Ryu KS, Liu C. A magnetic microstirrer and array for microfluidic mixing. *J Microelectromechanical Systems*. 2002;11(3):462-469.

41. Cugat O, Delamare J, Reyne G. Magnetic micro-actuators and systems (MAGMAS). *IEEE Transactions Magnetism*. 2003;39(5):3607-3612.

42. This chapter reproduced with permission from Gach P, Sims C, and Allbritton N. Transparent magnetic photoresists for bioanalytical applications. *Biomaterials*. 2010;31:8810-8817. Copyright 2010 Elsevier.

Chapter 3: Isolation and Manipulation of Living Adherent Cells by Micromolded Magnetic Rafts

3.1 Introduction

The ability to efficiently isolate cells or colonies from a mixed population for further expansion or analysis is a process common to many areas of biomedical research and biotechnology.[1] Examples of such endeavors include cloning of stem cells or genetically engineered cells for the development of cell lines and creation of animal models, and isolation of tumor cells for genetic analysis.[2,3] Admixing of cells with different characteristics from those of interest can lead to skewed or inaccurate results in such biological studies. In many cases, the cells of interest will be in low abundance among the population. For this reason, it is important to have a technique capable of identifying single cells with the desired characteristic, separating those cells from the unwanted cells, and then collecting the cells with high purity for further expansion or analysis. Commonly used techniques for performing these types of cell isolation procedures include limiting dilution, colony picking and fluorescence-activated cell sorting (FACS).[4-8] A number of new technologies for single-cell isolation have been developed in recent years, but have yet to be widely adopted including laser micro-dissection or laser ablation,[9,10] optical tweezers,[11] dielectrophoresis,[12] and microarray technologies.[13,14]

The use of magnetism as an external physical force for isolating cells is particularly attractive due to its simplicity, effectiveness and ease of manipulation.[14]

Magnetic cell separation (MACS®) developed by Miltenyi Biotec and the related techniques such as magnetic columns, flow channels, arrays and tweezers rely on magnetic particles bound to the surface of the cells or taken up by the cells to provide magnetic domains encompassing the cell for selective manipulation by an external magnet.[15-21] Magnetic microdevices or microstructures have been fabricated as microtools for precise positioning of cells,[22] or as mobile structures termed "microtransporters", "microcarriers" or "microplates" for manipulation of cells.[23-25] These microstructures, either fabricated from magnetic materials or doped with magnetic nanoparticles, have not yet been shown to be useful for isolating individual cells from a mixed population. Recently, an array of magnetic microstructures was developed in combination with our previous microarray technology for cell sorting by embedding magnetic nanoparticles within the micropallet array elements.[26,27] The transparent microstructures served as sites for attaching adherent cells. After screening the entire array, the cells of interest could be selectively detached from the array using a pulsed laser and collected against gravity with an external magnet to produce very pure populations of collected cells.[26,27]

While the micropallet array is an efficient approach for cell sorting, the platform is expensive and complicated as it requires a photolithographically defined array created in a cleanroom environment and a laser integrated into a high quality microscope. An inexpensive and robust platform, termed a "microraft array", was recently developed by our group for the efficient isolation of viable, single cells or colonies from a mixed population.[14] A simple dip-coating process was used to fabricate an array composed of a large number of micron-scale elements (the microrafts) on a polydimethylsiloxane

(PDMS) template. Within the array, the microrafts serve as releasable culture sites for individual cells or colonies. After identification of target cells or colonies, microrafts possessing cells of interest can be released with a needle inserted through the PDMS template. Following release, the microraft is allowed to drop from the inverted array onto a collection vessel, such as a Petri dish *via* gravity. This method has been successful in sorting cells with extremely high collection efficiency (100%) and post-sorting single-cell proliferation capability (95%); however, loosely adherent cells on the array can become detached during the release and collection procedure reducing the purity of isolated cells. Impurity of the isolated cells is undesirable for many applications, such as the creation of stably transfected cell lines. Re-sorting can be generally used to improve purity, but results in cell loss and requires additional time and effort. To overcome this problem, magnetism was evaluated as a means to collect the released microrafts and their adherent cells or colonies to achieve high purity of the collected cells. In the current article, the microraft array platform was enhanced by doping the microraft material with magnetic nanoparticles. The dispersion of nanoparticles inside the polymer matrix of the microrafts and the resultant optical properties were examined. The fabrication of magnetic microraft arrays *via* the dip-coating process was tested. An array of two-layer microrafts composed of a magnetic base and a non-magnetic surface was fabricated to provide an optimal, nanoparticle-free culture surface. Imaging of cells by brightfield, fluorescence and confocal microscopy was demonstrated. Finally, isolation and magnetic manipulation of single, viable cells from the array was demonstrated and the purity of isolated cells was determined.

3.2 Materials and Methods

3.2.1 Materials. The following materials were obtained from the Aldrich Chemical Company (St. Louis, MO): iron(II) chloride tetrahydrate (99%), iron(III) chloride anhydrous (98%), iron(III) nitrate nonahydrate (99+%), 28% ammonium hydroxide solution, oleic acid (90%), toluene (reagent grade), triarylsulfonium hexafluorophosphate salts, mixed, 50% in propylene carbonate, 99+% pure γ-butyralactone (GBL), 1-methoxy-2-propanol (1002F developer, 98.5%), glutaraldehyde, rhodamine B, 2,2'-azobisisobutyionitrile (AIBN, 98%), styrene (≥99%) and acrylic acid (99.5%). EPON resin SU-8 and EPON resin 1002F (phenol, 4,4'-(1-methylethylidene)bis-, polymer with 2,2'-[(1-methylethylidene) bis(4,1-phenyleneoxymethylene]bis-[oxirane]) were obtained from Miller-Stephenson (Sylmar, CA). Dulbecco's Modified Eagle Medium (DMEM), fetal bovine serum (FBS), 1× phosphate buffered saline (PBS) pH 7.4, 0.05% trypsin with EDTA solution, penicillin/streptomycin, CellTracker™ Red CMTPX, CellMask™ Orange plasma membrane stain and Hoechst dye No. 33342 were obtained from Invitrogen (Carlsbad, CA). Draq-5 DNA dye was from Biostatus (Leicestershire, UK). Poly(dimethylsiloxane) (PDMS, Sylgard 184 silicone elastomer kit) was purchased from Dow Corning (Midland, MI). Collagen I from rat tail tendon and Falcon™ Petri dishes were purchased from BD Biosciences (San Jose, CA). Polycarbonate plates (12" x 12" x 0.25") were purchased from McMaster-Carr (Los Angeles, CA). Wild-type HeLa cells were obtained from the American Type Culture Collection (ATCC, Manassas, VA). All other chemicals were procured from Fisher Scientific (Pittsburgh, PA).

3.2.2 Magnetic polystyrene development. Nanoparticles of Fe_3O_4 were synthesized by the co-precipitation of iron salts in deionized water through the addition of ammonium hydroxide.[28] The nanoparticles were magnetically decanted and the fluid was replaced with fresh deionized water and iron nitrate. Mixing for 1 h at 80 ^oC in the presence of iron nitrate oxidized the nanoparticles to γFe_2O_3.[29] Magnetically decanting the nanoparticles and replacing the liquid with deionized water produced a magnetic ferrofluid. The nanoparticles were extracted with oleic acid to produce hydrophobic γFe_2O_3 nanoparticles. The magnetic phase was magnetically decanted and excess oleic acid removed by three washes in ethanol. The oleic acid-coated γFe_2O_3 nanoparticles were then dissolved in toluene (5 g of γFe_2O_3/1L toluene). Poly(styrene-*co*-acrylic acid) (PS-AA) was prepared by copolymerization of styrene and acrylic acid in GBL, as described previously.[13] Briefly 95 g styrene, 5 g acrylic acid, 0.1 g 2,2'-azobisisobutyronitrile (AIBN) and 100 g GBL were mixed in a flask and heated in a 60 ^oC water bath for 72 h to complete copolymerization. A 1:5 v/v mixture of PS-AA in toluene was slowly added to the γFe_2O_3 ferrofluid. The toluene was then evaporated (Büchi R200 rotovapor, Flawil, Switzerland) until a thick gel remained. GBL was added to this magnetic polystyrene gel until the desired viscosity for efficient dip coating was achieved.

3.2.3 Measurement of magnetic polystyrene absorbance. Films of PS-AA (50 µm-thick) with various concentrations of magnetic nanoparticles were spin-coated onto plasma-cleaned 45 × 50 mm #1.5 cover glass (Fisher Scientific). Films were then heated in a 95 ^oC oven for 2 h to evaporate excess solvent. Fifteen absorbance measurements were made at various sections of the films using a SpectraMax M5 (Molecular Devices

Corporation, Sunnyvale, CA) with an uncoated cover glass used as a blank. The standard deviation for the transmittance readings was under 5% of the measured value for every data point.

3.2.4 Attenuated total reflectance Fourier transform infrared spectroscopy (ART-FTIC). ATR-FTIR spectra of 200 μm thick films of polystyrene, PS-AA or PS-AA containing 1% γFe_2O_3 were measured using a Thermo Electron Nicolet 8700 FTIR spectrometer. Measurements were made with an ATR (attenuated total internal reflection) module with a germanium crystal (resolution of 4.00 cm^{-1}).

3.2.5 Fabrication of PDMS molds. A mold or template composed of PDMS was formed using soft lithography with an SU-8 master. SU-8 masters were fabricated by typical photolithography, as described previously.[13] SU-8 masters were composed of 100 × 100 μm squares, 40 μm thick with 20 μm gaps. Following development, the SU-8 masters were made non-sticky to PDMS by spin coating 1% vol. octyltrichlorosilane in propylene monomethyl ether acetate at 2000 rpm for 30 s, followed by baking at 120 ^oC on a hotplate for 10 min. PDMS prepolymer (10:1 mixture of base to curing-agent) was poured over the SU-8 master and degassed (house vacuum) to remove trapped air bubbles. Following degassing the sample was spin-coated at 500 rpm for 30 s and baked at 100 ^oC for 30 min to give a 200 μm layer of PDMS over the SU-8 master. The PDMS was then gently peeled from the SU-8 master to produce the PDMS mold containing an array composed of 44,000 wells (100 × 100 μm).

3.2.6 Fabrication of magnetic microrafts. Releasable magnetic microstructures were molded within PDMS microwells. For arrays composed of single-layer microrafts, PS-AA, 1002F or SU8 containing 1% γFe_2O_3 by weight was applied over the PDMS

mold. Trapped air bubbles within the microwells were removed though degassing under vacuum (Oerlikon Leyboid pump). The PDMS mold or template was then attached to a rotary DC motor and lowered into a solution of the magnetic polymer. Slowly raising the PDMS mold produced a convex solution of polymer isolated in each microwell as the template dewetted. Placing the PDMS mold in a 95 ^{o}C oven for 2 h evaporated the bulk of the GBL resulting in concave microstructures within the microwells. Further evaporation of the GBL was achieved by a 1 h bake at 120 ^{o}C in a vacuum oven (-30 in. Hg). A magnetic microraft developed with PS-AA containing 1% γFe_2O_3 dissolved in 75% GBL had a final γFe_2O_3 concentration of 4% by weight following evaporation of the GBL. For simplicity, the initial concentration of γFe_2O_3 in the PS-AA was used to define the magnetic loading throughout this report. Multi-layer microrafts were constructed through repeated dip coating and drying of the array in various polymers dissolved in GBL.

Following fabrication of the microraft arrays, the PDMS template was attached to a polycarbonate cassette, with the array facing toward the inside of the cassette. Slight stretching of the PDMS template during attachment to the cassette reduced sagging. While still attached to the cassette, a second polycarbonate structure to create a square inner chamber surrounding the array (25.4 mm × 25.4 mm × 10 mm height – Figure 3.6) was glued to the top of the mold using PDMS with a 70 ^{o}C bake for 1 h.

3.2.7 Scanning electron microscopy (SEM) of microrafts. Microrafts with and without cells were imaged by SEM (Hitachi S-4700 cold cathode field emission). Prior to imaging, cells were rinsed with PBS then fixed in a solution of 2.5 wt% gluteraldehyde in PBS for 30 min followed by dehydration with sequential 10 min washings of 25%, 50%

75%, 95% and 100% ethanol. Bare microrafts or microrafts with fixed cells were coated with a 5 nm layer of Au. Samples were then imaged by SEM operated in normal working mode with electrons imaged on upper and lower secondary electron detectors with an accelerating voltage of 1kV and emission current of 13 nA.

3.2.8 Transmission electron microscopy (TEM) of microrafts. Nanoparticle distribution within the polymer and microraft construction was analyzed though examination of ultrathin sections of microrafts using TEM. SU8 photoresist was poured over the microrafts while on the PDMS mold, UV exposed and allowed to polymerize in a 65 ^{o}C oven for 8 h. After the sample was brought to room temperature, the SU8 with adhered microrafts was gently peeled from the PDMS mold. Cross-sections (80 nm thick) through the microrafts were cut with an ultra microtone. Sections were then plated on copper grids and imaged with TEM (JEOL 100CX II).

3.2.9 Release and collection of magnetic microrafts. Microrafts were released with the array in one of two orientations – inverted or upright. Microrafts on an inverted array were released by means of a microneedle (anodized steel, 150 μm base diameter and 17.5 μm tip diameter [Fine Science Tools, Foster City, CA]) positioned above the array and inserted through the PDMS template to dislodge the microraft which then settled on the collection dish, as previously reported.[14] Release was followed by purification with an external magnet. Microrafts were also released from an upright array with the microneedle positioned below the array and above the objective of an inverted microscope (Figure 3.10A). The microneedle was attached to a "U" brace on an XYZ micromanipulator. The visual field was kept clear of equipment except the microneedle by incorporating a 90^{o} bend in the microneedle. Individual microrafts were released by

raising the needle to puncture the PDMS template and dislodge the selected microraft. Following release, the microneedle was lowered to its original position so that the array could be translated with the microscope stage in preparation for the next release. An external magnet positioned above the collection substrate enabled immediate collection following microraft release (Figure 3.9). The magnet was kept over the collection plate to retain microrafts in the collection chamber against gravity and as the array and collection plates were separated.

3.2.10 Cell culture on magnetic microrafts. To expedite the attachment of cells to the microraft surface, the array was oxidized in a plasma cleaner (Harrick Plasma, Ithaca, NY) for 1 min. The microraft array and cassette holder were sterilized with 75% ethanol and allowed to dry in a tissue culture hood. Arrays were rinsed ×3 with sterile deionized H_2O, and then 1 mL collagen in deionized H_2O (100 μg mL $^{-1}$) was added to the array and incubated for 1 h including a 20 min degassing by vacuum to remove trapped air bubbles within the wells. Alternatively, plasma treatment and collagen coating can be omitted, but it took an extended period of time (>6 h) for cells to attach to the microraft surface. The arrays were rinsed ×3 with deionized H_2O followed by the addition of DMEM supplemented with FBS (10%), L-glutamine (584 mg L $^{-1}$), penicillin (100 units mL $^{-1}$), and streptomycin (100 μg mL $^{-1}$). A suspension of 15,000 cells was then added to the microraft array and allowed to settle and adhere to the microrafts over 2 h in a 37 ^{o}C incubator with a 5% CO_2 atmosphere. Cells used in these studies included wild-type HeLa cells, a human ovarian carcinoma cell line, HeLa cells stably transfected with enhanced green fluorescent protein (eGFP) fused to the nuclear H1-histone protein (a kind gift of Eva Lee, UC Irvine), and C2C12 cells, a murine myoblast cell line.

Prior to cell selection, the arrays were washed ×2 with DMEM and then the chamber surrounding the array was filled with DMEM. A sterile polystyrene Petri dish was then mated to the microraft cassette to create a sealed chamber filled with cell culture media. Following the release procedure, the Petri dish containing the isolated microrafts/cells was removed from the cassette, immediately filled with 3 mL media, and was returned to a tissue culture incubator for continued culture of the cells.

3.2.11 Cell transfection. C2C12 cells were transfected with a CMV driven eGFP expression plasmid by a calcium phosphate-mediated transfection procedure using a ProFection® mammalian transfection kit (Promega Corp. Madison, WI) per manufacturer protocol. Cells were used 72 h after the transfection procedure.

3.2.12 Imaging of cells on magnetic microrafts. HeLa cells grown on microrafts and the expanded colonies were imaged by both brightfield and fluorescence microscopy using a cooled charge-coupled device (CCD) camera (Photometrics CoolSNAP HQ^2, Tucson, AZ) mounted to an inverted epifluorescence microscope (NIKON TE200-U, Melville, NY). Additionally, fluorescence microscopy was used to visualize HeLa cells co-labeled with Hoechst 33342 DNA dye and the cytoplasmic stain CellTracker™ Red CMTPX. Fluorescently labeled C2C12 cells were imaged by differential interference contrast (DIC) and confocal microscopy with an inverted laser scanning microscope (Zeiss 510, Thornwood, NY). After transient transfection with eGFP, C2C12 cells were plated on microraft arrays and stained with CellMask™ orange plasma membrane stain and Draq5 DNA dye following manufacturer protocols. Fluorescence images were provided in pseudocolors representative of the fluorophore's excitation maximum wavelength.

3.3 Results

3.3.1 Characterization of transparent magnetic polystyrene. A nanocomposite of uniformly distributed magnetic nanoparticles in a polystyrene:acrylic acid (PS-AA) co-polymer was developed to provide a magnetic and biocompatible material that could be molded into microstructures for cell culture and cell isolation. A ferrofluid containing superparamagnetic γFe_2O_3 nanoparticles and PS-AA in GBL was prepared as described above. Evaporation of the toluene left a composite of γFe_2O_3 nanoparticles up to 1 wt% uniformly dispersed throughout a PS-AA matrix. This nanocomposite was then dissolved in GBL to provide a stable viscous media. The uniformity of the nanoparticle distribution in microrafts was confirmed by imaging films of the polymer under brightfield and with TEM. Films (100 μm thick) of the nanocomposite were transparent and slightly yellow when viewed using brightfield microscopy. TEM demonstrated well separated γFe_2O_3 nanoparticles (9 ± 4 nm, $n = 97$) throughout the polymer with no aggregates above 30 nm (Figure 3.1A-B).

Brightfield and fluorescence imaging are commonly employed for the detection of cells or other biological specimens. The compatibility of the polystyrene nanocomposite for these uses was assessed by measuring the background absorbance and fluorescence of 50-μm thick films with various concentrations of γFe_2O_3 spin-coated onto glass slides. Increases in the concentration of γFe_2O_3 from 0.01 to 1% showed corresponding increases in absorbance at shorter wavelengths. A nanocomposite containing 1% γFe_2O_3 reached 80% transmittance at a wavelength of 521 nm, whereas 0.1% γFe_2O_3 reached 80% transmittance at 425 nm (Figure 3.1C). The fluorescence of the magnetic films was comparable to that of native PS-AA (data not shown).

Substrates for cell culture should provide good cellular adhesion and support long-term cell growth. Since AA possesses carboxylic acid groups, the surface of PS-AA will present a negative surface charge which should promote cell attachment without the need for surface oxidation or an extracellular matrix coating.[13,30] Fourier transform infrared spectroscopy (FTIR) in the attenuated total reflectance (ATR) mode was used to assess the presence of carboxylic acid groups in the PS-AA copolymer. The absorption peak at 1704 cm^{-1}, characteristic of the carboxylic acid C=O stretch, was observed in films of both PS-AA and magnetic PS-AA, but not native polystyrene, demonstrating the retention of the polymer's negative charge with and without magnetic nanoparticle incorporation (Figure 3.2). HeLa cells plated on 1% γFe_2O_3 PS-AA showed adhesion 6 hours after cell addition and well-formed colonies were present after 8 days in culture. These results demonstrated that PS-AA with 1% γFe_2O_3 was an excellent substrate for cell growth.

3.3.2 Single-layer magnetic rafts. Soft lithography has been used to develop a variety of microdevices for biomedical applications. Previously, microrafts on a PDMS substrate were developed to array and then isolate cells. In that work, a dip-coating process was used to fabricate microstuctures from biocompatible polymers (SU-8, Epon 1002F epoxy resin, Epon 1009F epoxy resin, polystyrene or PS-AA) within an array of PDMS wells. The wells acted as a template to create the molded structures.[13] In the current work, magnetic microrafts were created by dip-coating various polymers (SU-8, 1002F and PS-AA) containing 0.01-1 wt% uniformly distributed γFe_2O_3 nanoparticles dissolved in 70 wt% GBL on a PDMS template consisting of an array of 100 × 100 μm microwells isolated by walls 40 μm tall and 20 μm thick. The doped polymers showed

successful dewetting on the PDMS as was required to construct the individual microrafts (Figure 3.3A, 3.4A-B). Microrafts composed of PS-AA containing 1% γFe_2O_3 were isolated within the PDMS wells and possessed a slightly concave upper surface as monitored by SEM (Figure 3.3B).

The transparency of the magnetic polymers was retained during microraft fabrication (Figure 3.3A). It has previously been shown that magnetic nanoparticles can accumulate at the air interface of a polymer during photolithographic processing of magnetic photoresists.[26] Horizontal slices through the magnetic microrafts were imaged by TEM to determine whether a similar process might occur during raft fabrication. All microrafts composed of 1% γFe_2O_3 in 1002F showed evenly distributed nanoparticles throughout the polymer with the exception of a 20 nm layer of nanoparticles accumulated at the surface and base of the microrafts (Figure 3.4C-D). These results confirmed the previous finding that nanoparticles are enriched at the surfaces of the 1002F nanocomposite.[26] In contrast, microrafts developed with 1% γFe_2O_3 in PS-AA possessed uniformly distributed nanoparticles throughout the polymer without noticeable accumulation of nanoparticles at the microraft surface or base (Figure 3.3C-D). It is likely that γFe_2O_3 nanoparticles were trapped within the viscous PS-AA matrix during GBL evaporation, whereas the particles in the 1002F monomer were mobile until the resist was exposed to UV light. Since the magnetic PS-AA more closely mimics the oxidized polystyrene surfaces for conventional tissue culture relative to the 1002F surface, the fabrication of microrafts with magnetic PS-AA was the focus of the remainder of this work.

3.3.3 Two-layer magnetic rafts. The application of layers of materials onto the surface of microdevices permits tailoring of surface properties for specific device functions. For example, a layer of native 1002F polymer applied over a magnetic 1002F surface was previously shown to provide a protecting layer to prevent nanoparticle uptake by cells.[26] Two-layer microrafts were constructed using sequential dip coating of the PDMS mold. Microrafts were initially formed by dip coating the mold into PS-AA containing 1% γFe_2O_3. A layer of PS-AA was then overlaid onto the magnetic microrafts using a second dip coating step (Figure 3.5A). Following, evaporation of solvent, a uniform layer of PS-AA was coated on the magnetic microraft (Figure 3.5B). The polymer remained isolated within the PDMS wells and the microrafts retained smooth side walls as confirmed by SEM (Figure 3.5C). The central thickness of the 1% γFe_2O_3-PS-AA and PS-AA layers were 10 and 8 μm, respectively as measured by TEM (Figure 3.5D). While the viscosities of the solutions used for the first and second layers were identical, the PS-AA layer was thinner since the effective depth of the well was decreased during the second dip coating step. The thickness of the microraft layers could be adjusted by controlling the concentration of polymer dissolved in GBL during dip coating. For example, addition of PS-AA dissolved in 80 wt% GBL resulted in a second layer thickness of 3 μm (data not shown).

3.3.4 Cell culture on magnetic rafts. Effective devices for culturing and isolating individual cells and cell colonies must be capable of providing both good cellular adhesion and supporting long-term growth on the substrate. PS-AA has previously been shown to be a biologically compatible substrate.[13] This substrate can also be coated with extracellular matrices, such as fibronectin and collagen, to further improve cell adherence

and growth. HeLa cells plated on magnetic PS-AA microrafts coated with collagen adhered to and spread across the surface of the microrafts within 2 h of plating as observed by brightfield microscopy and SEM (Figure 3.7A-B). However, plasma treatment or the addition of an extracellular matrix (ECM) also modified the surface of the PDMS walls which reduced their barrier function in keeping the cells localized to individual microrafts. Thus, HeLa cells cultured on arrays treated by oxidation or ECM adsorption were observed to spread across the PDMS wall to adjacent microrafts after three days in culture. On the other hand, native PS-AA and magnetic PS-AA allow cellular adhesion within 6 h of plating without surface modification (Figure 3.7C). Colonies of HeLa cells grown on these surfaces remained isolated on the microraft surface and within the confines of the PDMS walls for up to six days.

Many biological assays rely on fluorescent markers to identify the cells of interest. The ability to perform fluorescence imaging on two-layer magnetic rafts was demonstrated by examining cells loaded with fluorescence dyes using both epifluorescence and confocal microscopy. Cells plated on two-layer magnetic microrafts were stained with a nuclear dye (Hoechst 33342, excitation/ emission 350/461 nm) and a cytoplasmic dye (CellTracker Red, excitation/ emission 570/602 nm). Imaging by brightfield and fluorescence microscopy demonstrated the visualization of cellular detail on two-layer microrafts (Figure 3.8). The ability to perform fluorescence confocal imaging of cells on two-layer microrafts was demonstrated using C2C12 cells transfected with a fluorescent protein and co-labeled with nuclear and membrane dyes. C2C12 cells transiently transfected with eGFP (excitation/emission 492/517 nm) were plated on unmodified two-layer microrafts then stained with CellMask^{TM} orange plasma membrane

dye (excitation/emission 554/567 nm) and a DNA dye (Draq-5, excitation/emission 646/697 nm). Confocal images showed clear compartmentalization of the dyes without distortion despite imaging through the microrafts (Figure 3.7D-F).

3.3.5 Release and collection of magnetic microrafts. The utility of magnetic microrafts relies upon the ability to selectively release and manipulate them with an external magnet. Using a magnetic collection approach can also provide a method for purifying collected cells from non-target cells that may be shed from the array during the collection procedure. Single-layer magnetic microrafts were released in inverted and upright orientations. The efficiency of collection of released magnetic microstructures under varying magnetic field strengths and different concentrations of γFe_2O_3 was examined (Table 2.1). Using the upright approach as an example, the microrafts were released and immediately collected onto a glass surface by an external magnet when the magnetic force experienced by the microrafts was sufficient to overcome gravitational force, as shown in Figure 3.9. In triplicate experiments, 20 microrafts were released and then magnetically collected in this manner. Microrafts containing 1% γFe_2O_3 were collected with 100% efficiency (n=60) at magnet displacements up to 20 mm, corresponding to a magnetic field of 22 mT at the glass surface. Increasing the distance between the glass surface and the collection plate to 24 mm (18 mT) reduced the collection efficiency to 28% ± 17%. Decreasing the concentration of γFe_2O_3 to 0.1% required reducing the distance between the collection plate and glass slide to 6 mm (166 mT) in order to achieve a collection efficiency of 100% ± 0%. Microrafts containing 0.01% γFe_2O_3 were not successfully collected when magnet separations down to 1 mm (449 mT) were attempted. Two-layer microrafts composed of 1% magnetic PS-AA

bottoms and PS-AA tops produced collection probabilities of 100% at distances up to 16 mm (35 mT) and 73 ± 12% at 20 mm (22 mT).

3.3.6 Magnetic purification of collected microrafts using an inverted array. Along with providing direct collection of microrafts, magnetism can provide a method for purifying the cells from contaminating cells and debris during gravity based collection following release from inverted microrafts. Microrafts were released and allowed to settle into a collection plate, as described previously.[14] The microraft array was replaced with a glass slide attached to a polycarbonate cassette, while a magnet was held under the collected microrafts to aid in their retention. The magnet was then removed and placed over the collection glass. Gentle agitation of the lower glass substrate suspended the magnetic microrafts and allowed the magnet to retain them against gravity on the collection plate. In triplicate experiments, 20 microrafts were released and then magnetically purified in this manner (Table 2.1). Microrafts containing 1% γFe_2O_3 were collected with 100% efficiency (n=60) at magnet displacements up to 20 mm, corresponding to a magnetic field of 22 mT, at the glass substrate. Increasing the height of the collection substrate to 24 mm (18 mT) lowers the collection probability to 20% ± 25%. Decreasing the concentration of γFe_2O_3 in the microrafts to 0.1% results in collection efficiencies of 100% ± 0%, 53% ± 26% and 17% ± 8% with magnet separations of 6, 8 and 10 mm (166, 113 and 79 mT), respectively. Microrafts containing 0.01% γFe_2O_3 were not successfully collected when magnet separations down to 1 mm (449 mT) were attempted. Multi-layer microrafts composed of 1% magnetic PS-AA bottoms and PS-AA tops produced collection probabilities of 100% ± 0% at distances up to 16 mm (35 mT) and 80% ± 18% at 20 mm (22 mT). A higher variance in collection

efficiencies was observed for the agitated microrafts with respect to the immediately collected microrafts. This could be a result of the larger variation in the initial displacements of microrafts during collection plate agitations compared to microraft translations during release. This collection method demonstrates the ability to obtain pure microstructures when an initial magnetic collection is not feasible.

3.3.7 Cell sorting and purification with magnetic microrafts. Direct collection of cells on microrafts whether or not a magnet is employed has been shown to be efficient, but purity may be limited due to non-target cells being shed from the array during the release procedure. To assess the viability and purity of single cells isolated from the array by magnetically enhanced collection, cell isolation experiments were performed using a heterogeneous population of cells plated on the array (Figure 3.10A). A minority population of HeLa cells stably expressing a nuclear eGFP was admixed with wild-type HeLa cells at a 1:3 ratio. To maximize the number of microrafts containing only a single cell, 15,000 cells were plated on an array of 44,000 two-layer microrafts (PS-AA top/1% magnetic PS-AA bottom) coated with collagen (Figure 3.10B-E). In three independent experiments, 60 microrafts containing a single cell possessing a fluorescent nucleus were released. Immediately after the collection procedure, all released microraft retained their attached cell (Figure 3.10F-G). After 7 days, 55 of the single cells (92 ± 5%) had expanded into a colony in which all cells possessed fluorescent nuclei with no non-fluorescent cells admixed (Figure 3.10H-I). Selective isolation of cells attached to magnetically collected microrafts was confirmed by releasing and magnetically collecting 20 microrafts without adherent cells from the microraft array plated with cells. Following 7 days culture, no cell colonies were observed on the collection plate. A cell collection

efficiency of 100% with 100% purity and a single-cell cloning efficiency of 92% was attained demonstrating the feasibility of creating highly purified clonal populations of cells from a heterogeneous population.

3.3.8 Magnetic purification of cells on microrafts. The ability to purify cells on previously sorted microrafts was demonstrated by releasing 20 magnetic microrafts containing single cells from an inverted array and magnetically purifying the microrafts, as described above. HeLa cells expressing a nuclear fluorescent protein (3,750 cells) were mixed with wild-type HeLa cells (11,250 cells) in suspension and were then plated on an array of 44,000 two-layer microrafts (PS-AA top/1% magnetic PS-AA bottom, 100 × 100 μm square, total raft thickness of 20 μm, 20 μm gap between rafts on the array) attached to a 6 mm high polycarbonate cassette. All microrafts were allowed to settle by gravity after release and then were magnetically collected on a glass collection dish. On examination, each microraft retained its single cell immediately following collection and 16 of these cells grew into individual colonies surrounding the microrafts after 7 days of incubation. No non-fluorescent cells were found amongst the collected fluorescent cells. These results demonstrate the utility of magnetic collection of microrafts for obtaining pure populations of cells from a heterogeneous population.

3.4 Conclusions

Magnetic microstructures were developed to enhance the manipulation and purity of cells isolated from a cell-based microarray. Nanoparticles composed of γFe_2O_3 were uniformly dispersed in a polystyrene-based polymer to provide biocompatible, transparent, magnetic microrafts. Through the use of multiple dip-coatings, microrafts composed of multiple layers could be easily fabricated. In this manner, microrafts were

created with layers composed of differing properties. For example, application of a polymer layer lacking nanoparticles over the magnetic layer overcame potential cell uptake of γFe_2O_3 from the culture surface. Viable cells cultured on the arrays of single- or two-layer magnetic microrafts could be viewed by brightfield, fluorescence and confocal imaging for identification and selection. Upon release, selected cells were magnetically collected efficiently and with high viability to achieve single-cell cloning rates of 92%. The magnetic properties of the microrafts enabled the attached cells to be readily separated from any contaminating cells shed from the array during the identification and release procedures. The magnetically enhanced retrieval process enabled 100% purity of collected cells to be achieved. These results demonstrated the utility of using magnet microrafts for obtaining highly pure and viable cells for cloning applications.[31]

3.5 Tables and Figures

Raft Material	Raft/Magnet Separation (mm)	B Field at Microraft Array	Collection Probability (%)	Collection Probability (%)
			Upright Array	Inverted Array Purification
0.01% γFe_2O_3 in PS-AA	1	449 ± 4	0 ± 0	0 ± 0
0.1% γFe_2O_3 in PS-AA	6	166 ± 6	100 ± 0	100 ± 0
	8	113 ± 7	76 ± 8	53 ± 26
	10	79 ± 3	0 ± 0	17 ± 8
1% γFe_2O_3 in PS-AA	12	57 ± 2	100 ± 0	100 ± 0
	16	35 ± 3	100 ± 0	100 ± 0
	20	22 ± 2	100 ± 0	100 ± 0
	24	18 ± 2	28 ± 17	20 ± 25
	28	15 ± 2	0 ± 0	4 ± 4
1% γFe_2O_3 in PS-AA bottom	12	57 ± 2	100 ± 0	100 ± 0
Native PS-AA Top	16	35 ± 3	100 ± 0	100 ± 0
	20	22 ± 2	73 ± 12	80 ± 18
	24	18 ± 2	0 ± 0	0 ± 0
Triplicate experiments (n = 20 rafts per experiment).				

Table 3.1 Collection of Magnetic Rafts.

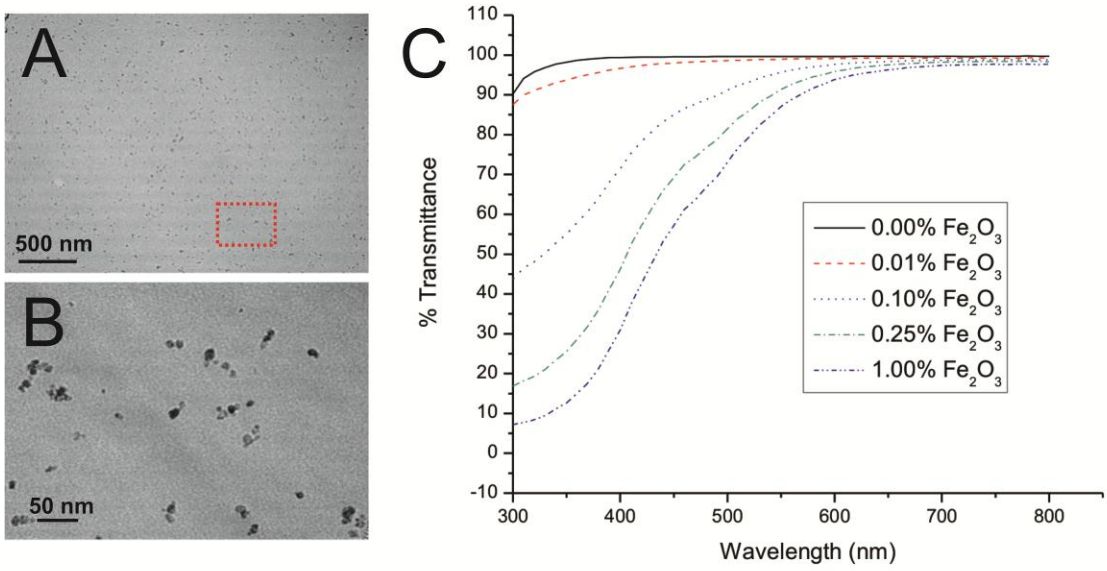

Figure 3.1 Magnetic PS-AA characterization. (A) TEM image of PS-AA containing 1% γFe_2O_3 nanoparticles. (B) The region in the box in (A) is shown at increased magnification. (C) Transmittance curves of films of PS-AA with various concentrations of embedded γFe_2O_3 nanoparticles.

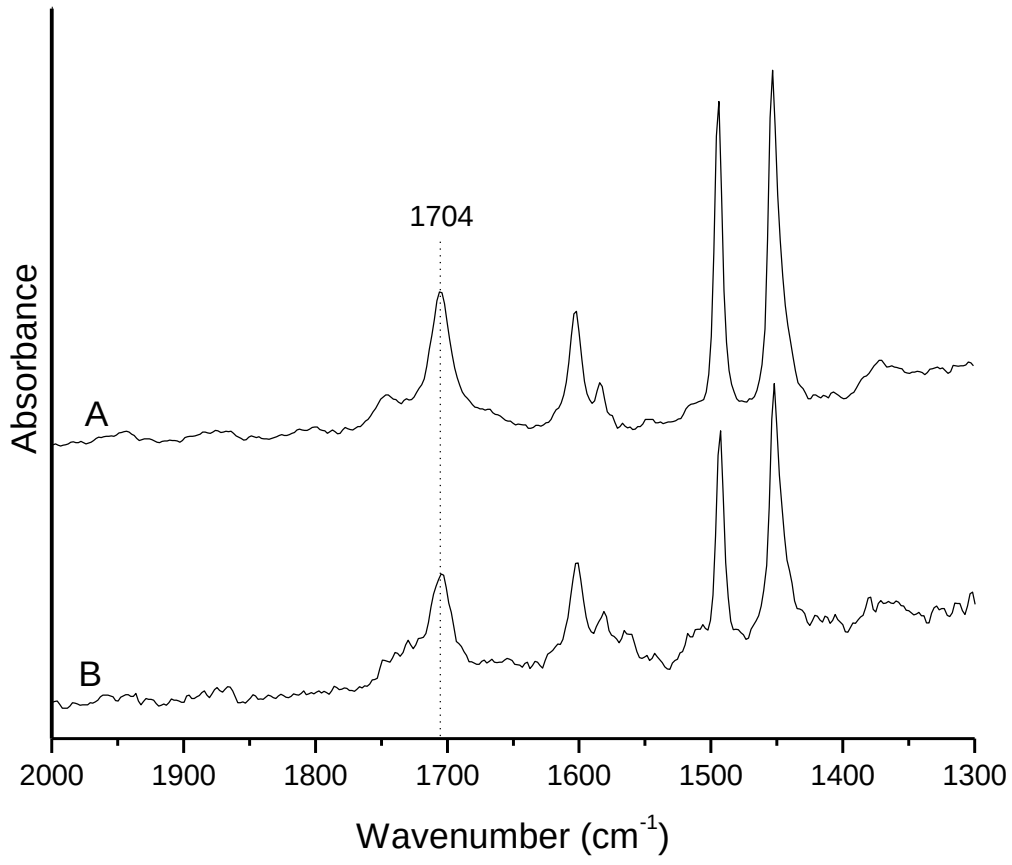

Figure 3.2 ATR-FTIR spectra of films consisting of (A) PS-AA or (B) PS-AA containing 1% γFe_2O_3. The peak at 1704 cm^{-1} is representative of a carbonyl group stretch and present only in the PS-AA and magnetic PS-AA. Peaks at 1602 cm^{-1} and 1493 cm^{-1}, characteristic of aromatic C=C bond stretching, along with the peak at 1452 cm^{-1}, resulting from bending of methylene groups, are all observed in polystyrene, PS-AA and magnetic PS-AA.

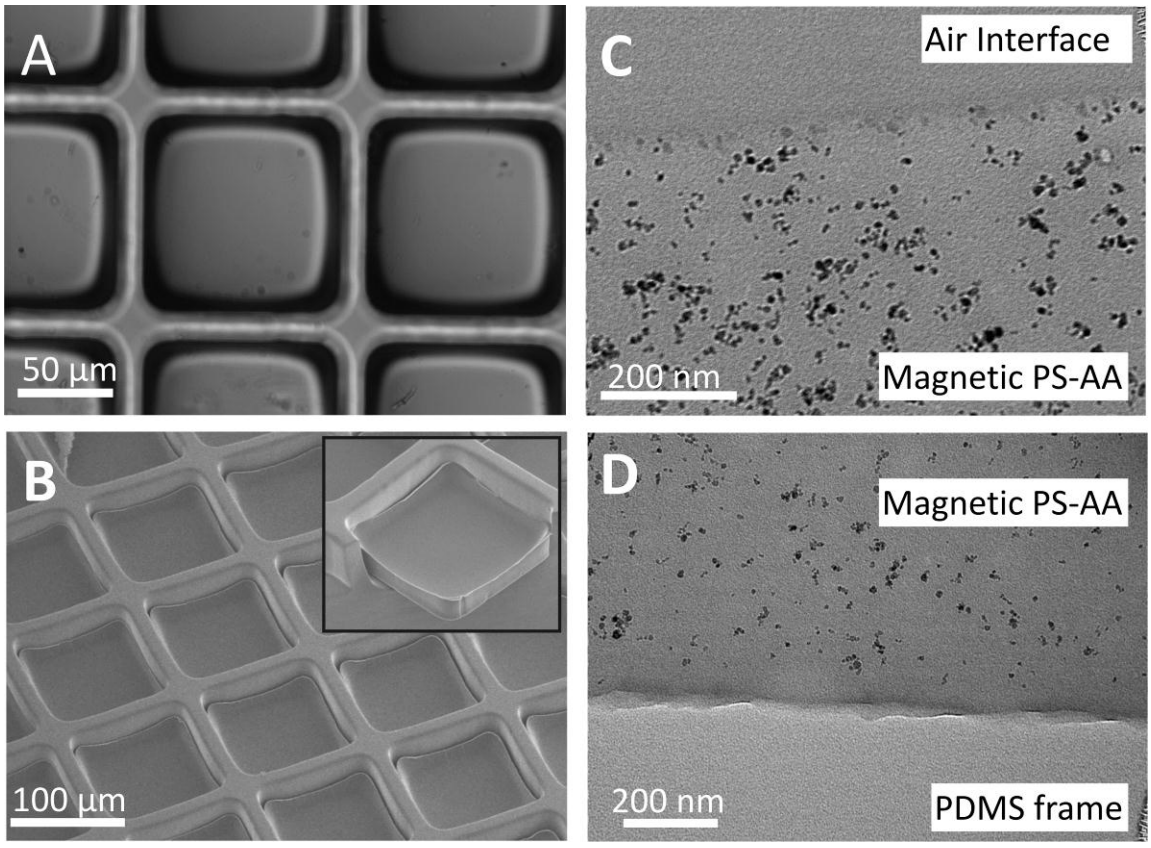

Figure 3.3 Fabrication of magnetic microrafts. (A) Brightfield and (B) SEM images of PS-AA microrafts containing 1% γFe_2O_3. Insert shows a side view of a raft with PDMS partially removed. (C) TEM images of microraft-air interface and (D) PDMS-microraft interface.

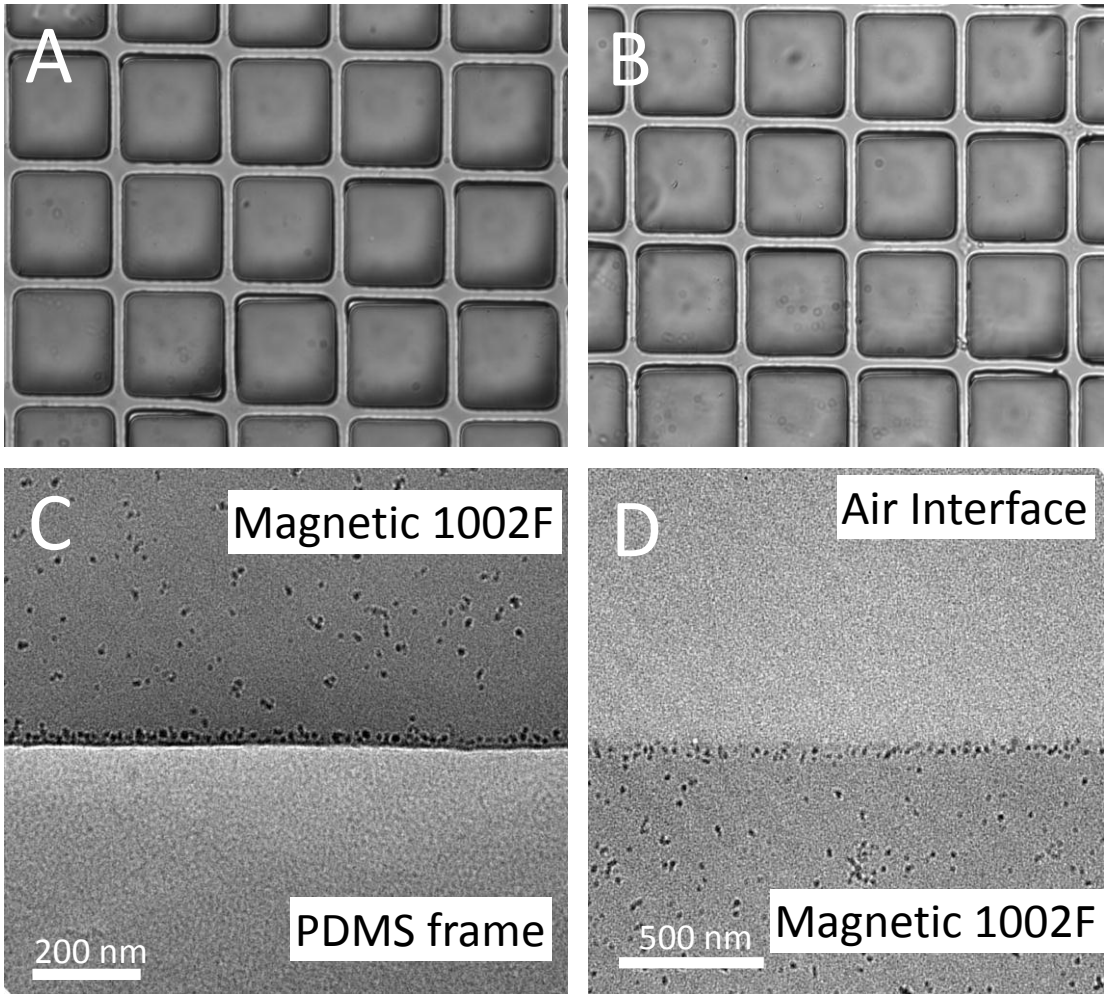

Figure 3.4 DIC images of microraft arrays developed from (A) 1002F containing 1% γFe_2O_3 or (B) SU8 containing 1% γFe_2O_3. TEM image of the base (C) and upper surface (D) of a microraft produced from 1002F containing 1% γFe_2O_3.

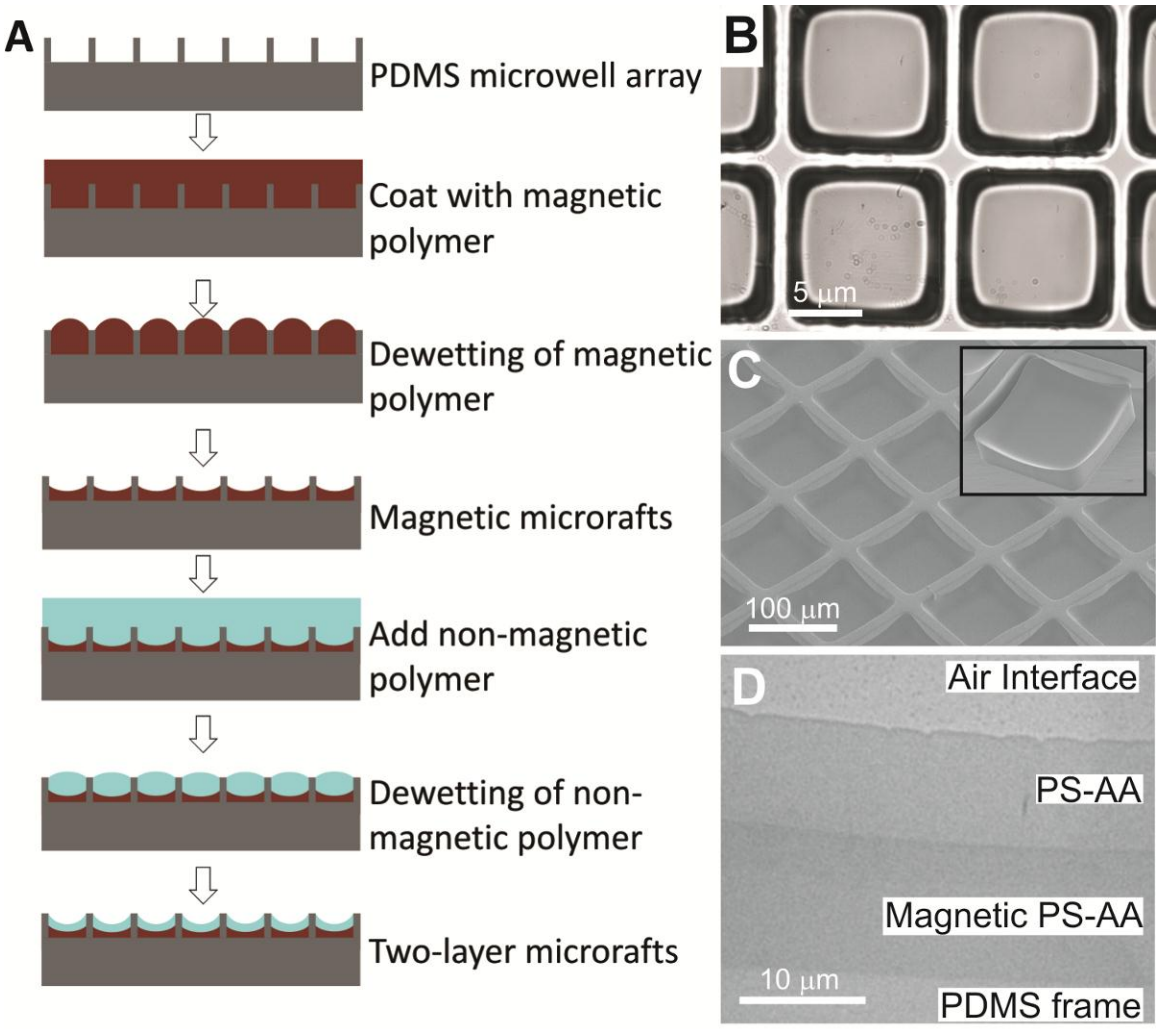

Figure 3.5 Two-layer magnetic raft fabrication. (A) Scheme of two-layer microraft fabrication. (B) Brightfield and (C) SEM images of a 2-layer microraft composed of a 1% γFe_2O_3 in PS-AA as the base with a PS-AA top layer. Insert shows a side view of a 2-layer microraft with PDMS partially removed. (D) TEM image of a cross section of a 2-layer microraft composed of a 10 μm magnetic PS-AA layer covered with an 8 μm thick layer of PS-AA.

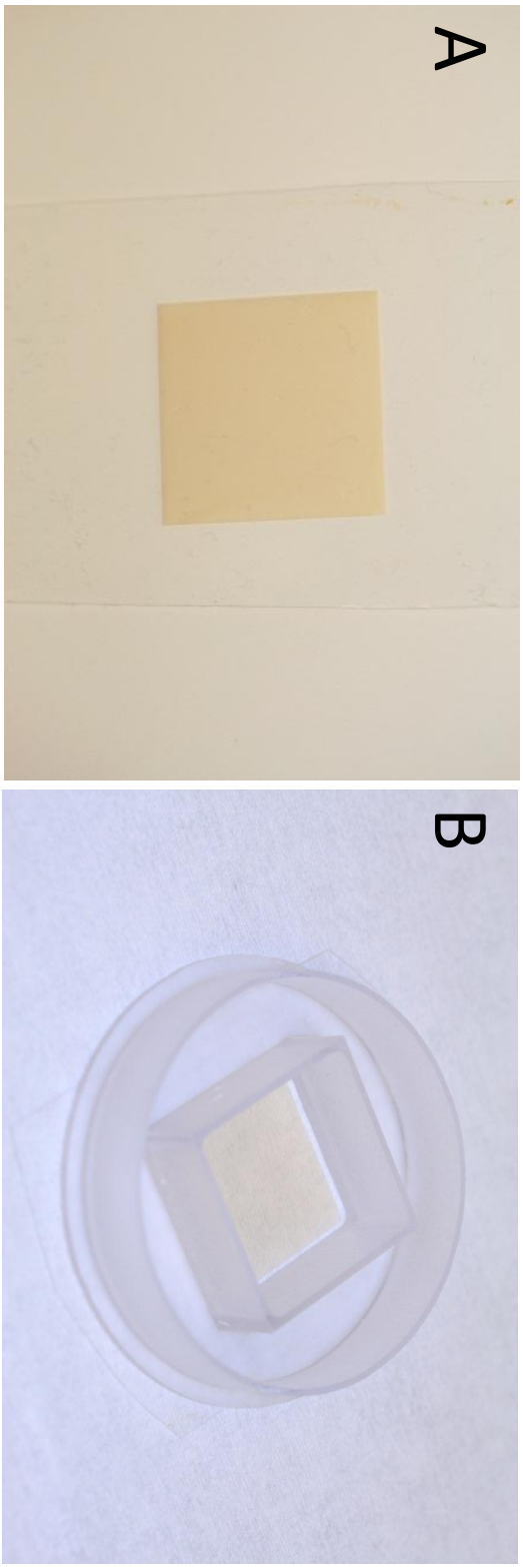

Figure 3.6 Image of a microraft array composed of PS-AA microrafts containing 1% γFe_2O_3 (A). Magnetic microraft array attached to a polycarbonate cassette (B).

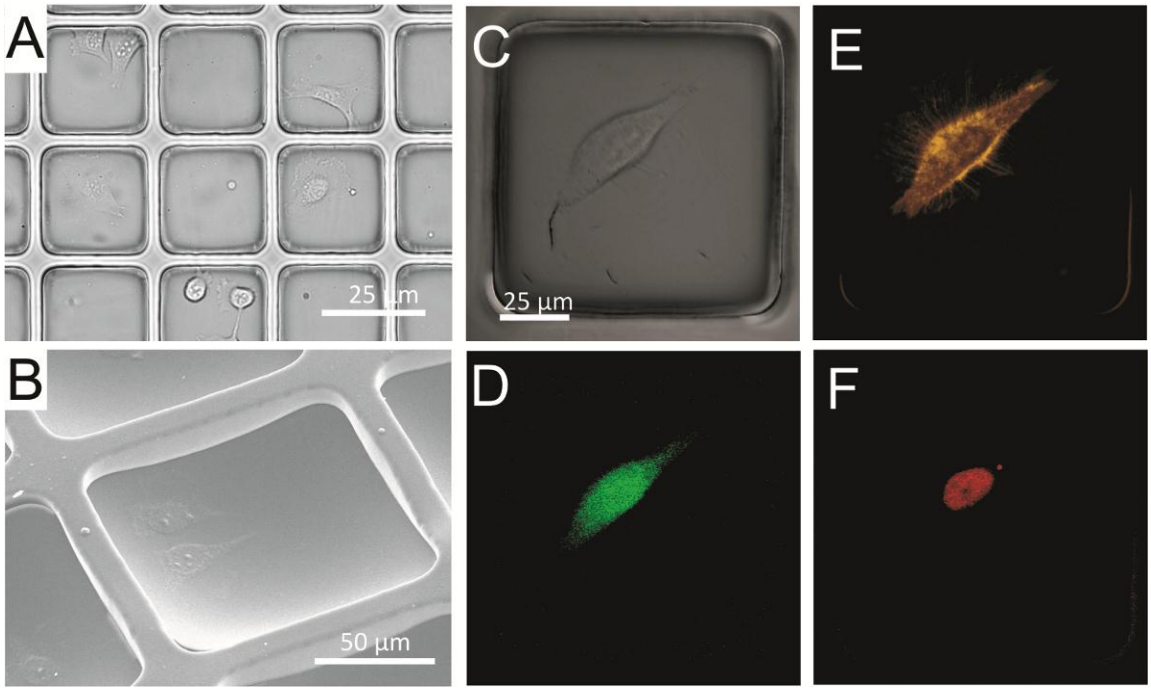

Figure 3.7 Imaging cells on magnetic microrafts. Brightfield (A) and SEM (B) images of HeLa cells adhered to 2-layer microrafts (100 µm) coated with collagen. DIC (C) and confocal fluorescence (D-F) images of a C2C12 cell loaded with fluorescent dyes. Individual fluorescent channels show the fluorophores introduced to the cell by transfection with an eGFP expressing plasmid (emission at 517 nm) (D), staining with CellMask^{TM} orange plasma membrane dye (emission 567 nm) (E) and DNA staining (Draq-5 emission at 697 nm) (F).

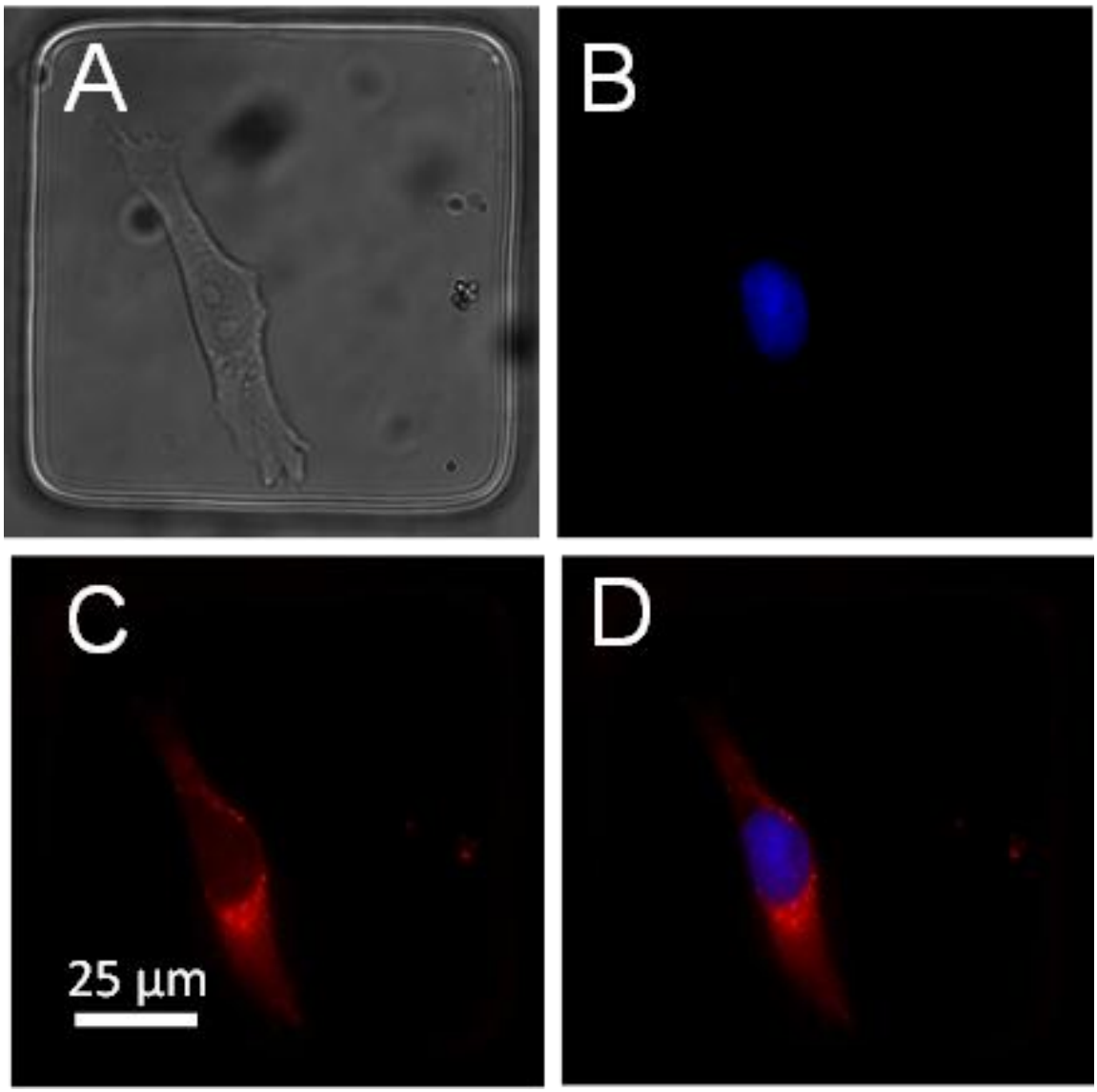

Figure 3.8 Brightfield (A) and fluorescence (B-D) images of a HeLa cell adhered to a 2-layer microraft (100-µm side). HeLa cells were stained with a nuclear dye, Hoechst 33342 (B) and a cytoplasmic dye CellTracker Red (C). A composite of the fluorescence images is shown (D).

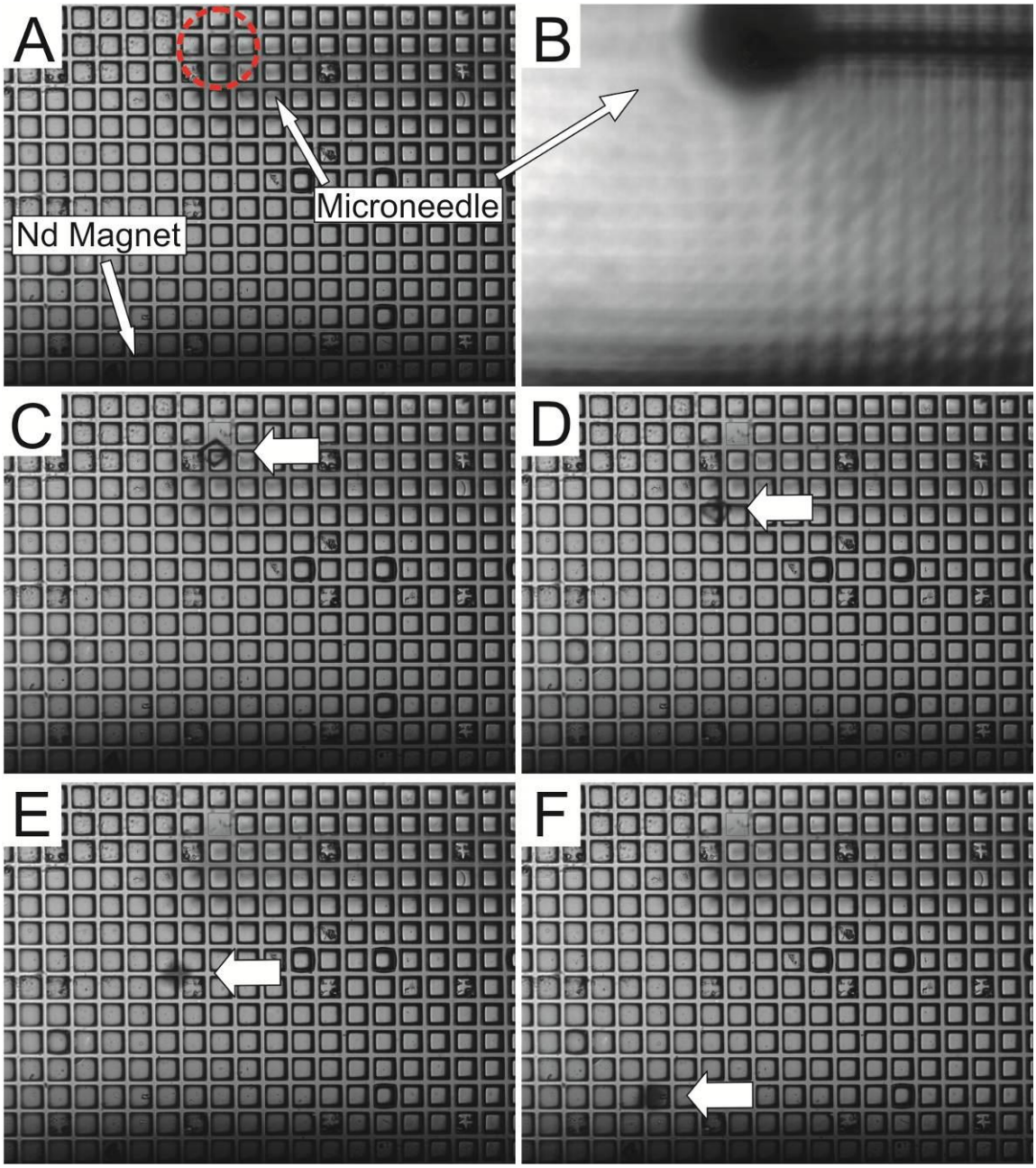

Figure 3.9 A series of time-resolved images demonstrating the release and magnetic collection of microrafts. In the displayed images, the neodymium magnet shown at the bottom of the image is 5 mm above the array and out of the focal plane. The microraft array composed of PS-AA containing 0.1% γFe_2O_3 (A) is deflected out of the focal plane by the microneedle during release of an individual microraft (B). The position of the microraft 1, 2, 3 and 4.3 s following release, panels (C-F) respectively, was monitored to assess the movement of a loose magnetic microstructure in a magnetic field. Microrafts are observed to move upward and thus out of focus as they are attracted to the magnet. Movie of micropallet collection provide in online version.

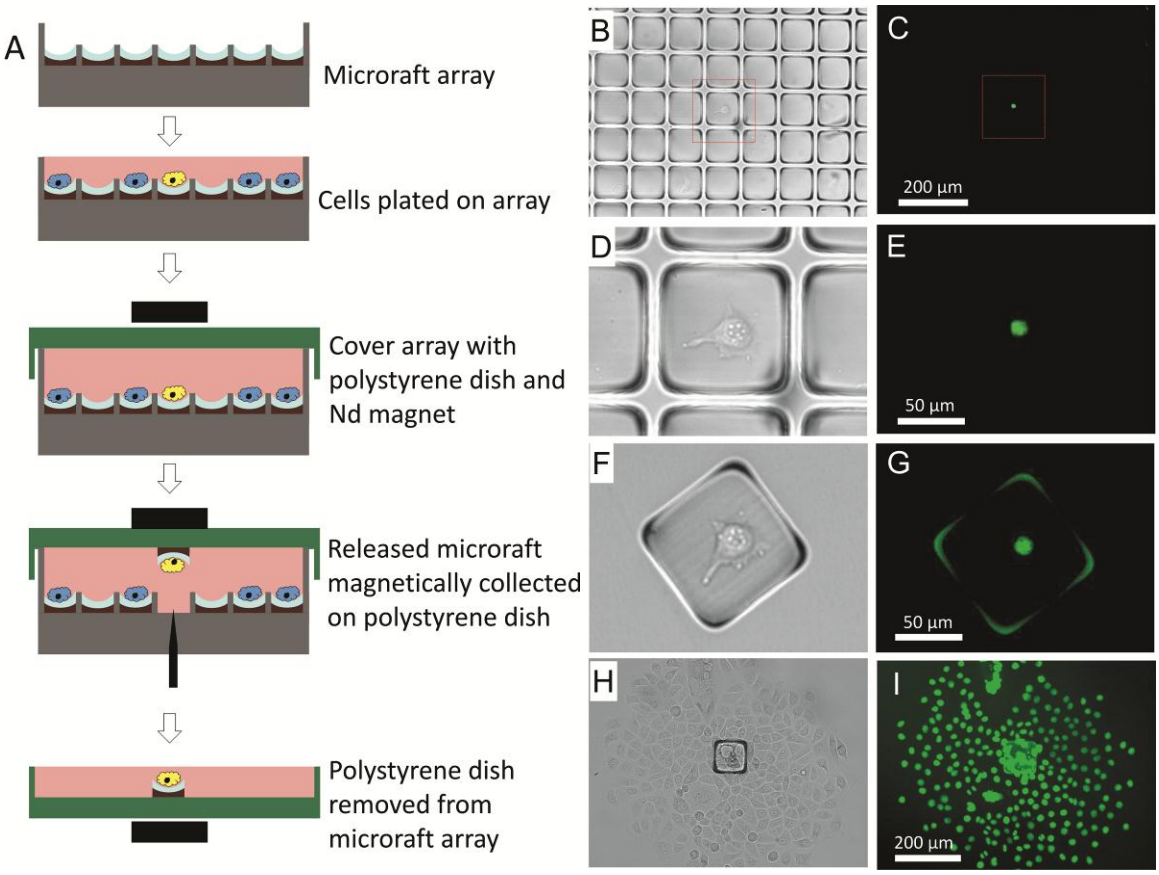

Figure 3.10 Single cell sorting with magnetic microrafts. (A) Scheme for the magnetic collection of microrafts. (B-H) Brightfield and fluorescence images of a HeLa cell expressing a fluorescent protein identified, isolated and expanded into a clonal colony. (B-E) A single HeLa cell possessing a fluorescent nucleus is identified on an array composed of two-layer microrafts (100 µm). (F-I) The cell seen in "B-E" immediately following magnetic-assisted collection (F,G) and after 7 days of incubation (H,I).

3.6 References

1. Patel D. Separating Cells. New York: Springer-Verlag; 2001.

2. Mori K, Kashiwagi A, Yomo T. Single-Cell Isolation and Cloning of Tetrahymena thermophila Cells with a Fluorescence-Activated Cell Sorter. *Journal of Eukaryotic Microbiology*. 2010;58(1):37-42.

3. Nagrath S, Sequist LV, Maheswaran S, et al. Isolation of rare circulating tumour cells in cancer patients by microchip technology. *Nature*. 2007;450(7173):1235-U1210.

4. Freshney RI. Culture of Animal Cells. New York: Wiley-Liss; 2000.

5. Shapiro HM. Practical Flow Cytometry (ed 4th). New York: Wiley-Liss; 2003.

6. Givan AL. Flow Cytometry First Principles (ed 2nd). New York: Wiley-Liss; 2001.

7. Kirkland DJ. Chemical transformation of Chinese hamster cells. I. A comparison of some properties of transformed cells. *British Journal of Cancer*. 1976;34:134-144.

8. Kemshead JT, Ugelstad J. Magnetic separation techniques: their application to medicine. *Molecular Cell Biochemistry*. 1985;67:11-18.

9. Schutze K, Posl H, Lahr G. Laser micromanipulation systems as universal tools in cellular and molecular biology and in medicine. *Cell Molecular Biology (Noisy-le-grand)*. 1998;44(5):735-746.

10. Kim JS, Hur D, Hwang JK, Chung C, Chang JK. Ongoing development of image cytometers. *Bioanalysis*. 2010;2(10):1755-1765.

11. Kovac JR, Voldman J. Intuitive, Image-Based Cell Sorting Using Opto-fluidic Cell Sorting. *Analytical Chemistry*. 2007;79:9321–9330.

12. Gascoyne PRC, Wang XB, Huang Y, Becker FF. Dielectrophoretic separation of cancer cells from blood. *Ieee Transactions on Industry Applications*. 1997;33(3):670-678.

13. Wang YL, Young G, Aoto PC, et al. Broadening cell selection criteria with micropallet arrays of adherent cells. *Cytometry Part A*. 2007;71A(10):866-874.

14. Wang YL, Phillips C, Xu W, et al. Micromolded arrays for separation of adherent cells. *Lab on a Chip*. 2010;10(21):2917-2924.

15. Miltenyi S, Muller W, Weichel W, Radbruch A. High-gradient magnetic cell-separation with MACS. *Cytometry*. 1990;11(2):231-238.

16. Liu W, Dechev N, Foulds IG, Burke R, Parameswaran A, Park EJ. A novel permalloy based magnetic single cell micro array. *Lab on a Chip*. 2009;9(16):2381-2390.

17. Adams JD, Thevoz P, Bruus H, Soh HT. Integrated acoustic and magnetic separation in microfluidic channels. *Applied Physics Letters*. 2009;95(25):3.

18. Pregibon DC, Toner M, Doyle PS. Magnetically and biologically active bead-patterned hydrogels. *Langmuir*. 2006;22(11):5122-5128.

19. Ino K, Okochi M, Konishi N, et al. Cell culture arrays using magnetic force-based cell patterning for dynamic single cell analysis. *Lab on a Chip*. 2008;8(1):134-142.

20. Lee H, Liu Y, Ham D, Westervelt RM. Integrated cell manipulation system - CMOS/microfluidic hybrid. *Lab on a Chip*. 2007;7(3):331-337.

21. Xia N, Hunt TP, Mayers BT, et al. Combined microfluidic-micromagnetic separation of living cells in continuous flow. *Biomedical Microdevices*. 2006;8(4):299-308.

22. Hagiwara M, Kawahara T, Yamanishi Y, Arai F. Driving method of microtool by horizontally arranged permanent magnets for single cell manipulation. *Applied Physics Letters*. 2010;97(1):3.

23. Sakar MS, Steager EB, Kim DH, Kim MJ, Pappas GJ, Kumar V. Single cell manipulation using ferromagnetic composite microtransporters. *Applied Physics Letters*. 2010;96(4):3.

24. Kim LN, Choi SE, Kim J, Kim H, Kwon S. Single exposure fabrication and manipulation of 3D hydrogel cell microcarriers. *Lab on a Chip*. 2011;11(1):48-51.

25. Ishihara H, Takeuchi S. Handling adherent cells with magnetically functionalized microplates. IEEE MEMS 2010 Conference; 2010:959-962.

26. Gach PC, Sims CE, Allbritton NL. Transparent magnetic photoresists for bioanalytical applications. *Biomaterials*. 2010;31(33):8810-8817.

27. Gunn NM, Chang R, Westerhof T, Li GP, Bachman M, Nelson EI. Ferromagnetic Micropallets for Magnetic Capture of Single Adherent Cells. *Langmuir*. 2010;26(22):17703-17711.

28. Massart R. Preparation of aqueous magnetic liquids in alkaline and acidic media. *Ieee Transactions on Magnetics*. 1981;17(2):1247-1248.

29. Bee A, Massart R, Neveu S. Synthesis of very fine maghemite particles. *Journal of Magnetism and Magnetic Materials*. 1995;149(1-2):6-9.

30. Jung H, Kwak B, Yang H, Tae G, Kim J, Shin K. Attachment of cells to poly(styrene-co-acrylic acid) thin films with various charge densities. *Colloids and Surfaces a-Physicochemical and Engineering Aspects*. 2008;313:562-566.

31. This chapter reproduced with permission from Gach P, Wang Y, Phillips C, Sims C, and Allbritton N. Isolation and manipulation of living adherent cells by micromolded magnetic rafts. *Biomicrofluidics*. 2011;5(3). Copyright 2011 American Institute of Physics.

Chapter 4: Precise manipulation and orientation of magnetic microstructures

4.1 Introduction

Technologies capable of precisely controlling the spatial positioning of objects have been demonstrated to be important in many areas of biology, physics and engineering.[1,2] Several approaches have been employed for controlling the location of microelements (microdevices, microbeads, single cells etc.) including; contact micromanipulation, optical trapping, magnetic tweezers and microfluidics.[3-7] Devices proficient at manipulating microstructures by non-invasive physical forces are especially useful for their ability to direct entities within closed systems.

Magnetism is a powerful tool for manipulating micron-scale objects with large and controllable forces. Magnetic actuation has been demonstrated to allow precise control of microelements such as microcantilevers, valves, turbines and microbeads attached to cells.[8-10] Manipulation of these magnetic microstructures is achieved by applying a magnetic field supplied by a permanent magnet or electromagnet. These systems are commonly employed to generate a wide range of magnetic forces ranging from femtonewtons to micronewtons. Manipulation of small microstructures 'microrobots' is typically accomplished in a single dimension with a solo magnetic or in multiple dimensions with multiple synchronously tuned magnetic poles (2 – 8).[11-13] While these technologies can provide control of microstructures in two dimensions across a substrate, a method for precisely transferring microdevices to a new substrate using magnetic field would be of great utility.

Along with the importance of item positioning, controlling the orientation of asymmetrical objects is critical for constructing microdevices and in tissue engineering.[14] Numerous strategies have been developed for controlling the 3-dimensional assembly of microstructures while attached to a substrate. However, greater control in device positioning is necessary for manipulating untethered microstructures. Optical tweezers are effective at trapping objects and controlling the item's position with high precision. Magnetic domains in microstructures may also be used to move and rotate an object using multiple synchronized electromagnets.[12,15] However, these technologies require very complex device fabrication and instrumentation and are low throughput. Assembly by parallel methods permits microstructure positioning with much higher throughput. Parallel self-assembly of microstructures has been performed by employing binding forces such as surface tension, capillary forces, electrostatic interactions and magnetic forces.[16-18] For example, when microstructures with hydrophobic surfaces were added to a substrate patterned with hydrophobic domains they bind selectively to the hydrophobic regions. Unfortunately, the majority of techniques for asymmetrically functionalizing the substrate and microdevices require complex fabrication procedures.

In this work, a simple method is developed for positioning untethered magnetic microstructures with high precision and controllable orientation. Typical procedures for achieving precise control of microelement positioning require complex microstructure geometries or instrumentation. Herein, the high susceptibility of magnetic microstructures to magnetic field gradients is exploited to achieve precision control of the elements by low cost methods. An external magnetic source combined with a metallic pole sharpened to a fine point was utilized to capture magnetic elements with high

precision. In addition to controlling the external magnetic fields, the integration of internal magnetic domains within microdevices were employed to magnetically rotate microstructures during collection.

These strategies for manipulating simple microstructures allow high efficiency collection of micropallets. The Allbritton group has previously demonstrated the utility of arrays of releasable elements microfabricated on glass substrates termed 'micropallets', for sorting single adherent cells.[19] Micropallet arrays have shown success for sorting single cells from a mixed cell population with low reagent requirements, high post-sorting yield and excellent viability. Individual micropallets with attached single cells have were collected onto a microwell array by gravity or magnetism and then cultured and expanded.[19,20] While effective at bulk isolation of micropallets these collection strategies offer little control of micropallet positioning. Magnetic poles were utilized to direct released micropallets to defined microwells with high efficiency and precision. Additionally, magnetic domains fabricated on the base of micropallets allowed orientation of micropallets during collection. These manipulation techniques serve to improve the collection efficiency and identification of collected micropallets and cells.

4.2 Materials and Methods

4.2.1 Reagents. The following materials were obtained from the Aldrich Chemical Company (St. Louis, MO): iron(III) chloride tetrahydrate, iron(III) chloride anhydrous, iron(III) nitrate nonahydrate, toluene (reagent grade), γ-butyralactone (GBL, 99+%), 1-methoxy-2-propanol (1002F developer, 98.5%). EPON resin 1002F (phenol, 4,4'-(1-methylethylidene)bis-, polymer with 2,2'-[(1-methylethylidene)bis(4,1-phenyleneoxymethylene]bis-[oxirane]) was obtained from Miller-Stephenson (Sylmar,

CA) and (heptadecafluoro-1,1,2,2-tetrahydrodecyl)-trichlorosilane was purchased from Gelest Inc (Morrisville, PA). Dulbecco's modified Eagle's medium (DMEM), fetal bovine serum (FBS), 1X phosphate buffered saline (PBS), pH 7.4, 0.05% trypsin with EDTA solution and penicillin/streptomycin were received from Invitrogen (Carlsbad, CA). Sylgard 184 silicone elastomer kit (PDMS) and UVI-6976 photoinitiator (triarylsulfonium hexafluorophosphate salts in 50% propylene carbonate) were received from Dow Corning (Midland, MI). All other chemicals were procured from Fisher Scientific (Pittsburgh, PA).

4.2.2 Fine-tipped magnetic pole fabrication. Ferromagnetic alloys were sharpened to radii of 25 μm by standard machining processes. Magnetic poles were fabricated from three different materials of varying magnetic saturations and permeabilities. Materials tested included: Vim Var low carbon magnetic iron (magnetic saturation = 2.15 mT, magnetic permeability = 10,000), EFI 50 (magnetic saturation = 1.45 mT, magnetic permeability = 100,000) and EFI 79 (magnetic saturation = 0.87 mT, magnetic permeability = 230,000), all obtained from Ed Fagen Inc. Franklin Lakes, NJ. 1.27-cm diameter ferromagnetic rods were sharpened to a point with a micromaching drill (UNC Physics Instrument Shop, University of North Carolina, Chapel Hill, NC) (Figure 4.1B). Machining a 1.27-cm diameter rod at a 63.4^{o} angle to a point produced a 1.27-cm tall cone (97^{o} tip angle). A 1.27-cm diameter rod machined at a 76.0^{o} angle to a point generated a 2.54-cm tall cone (37^{o} tip angle). A pole tip tapered in two stages was fabricated by initially shaping the 1.27-cm diameter rod at a 55.0^{o} angle to a height of 8-mm and 1.59-mm diameter. At this point the rod was sharpened at a 9.5^{o} angle to a point 4.76-mm tall (30^{o} tip angle).

4.2.3 Magnetic field characterization. Measurement of the field strength of the neodymium magnet used in all collection experiments was performed with a DC magnetometer (AlphaLab Inc). The magnetic field strength of the permanent magnet was profiled as a function of distance from the probe (Figure 4.1A). The magnetic field gradients at various distances from the magnetic poles were calculated by taking the average of the differences in the magnetic field strengths in 1 mm increments to a specified distance (Figure 4.1C).

4.2.4 Fabrication of micropallet arrays. Micropallets with dimensions 50×50×30 µm (L×W×H) and a 25 µm gap between micropallets were fabricated using standard photolithography techniques. Magnetic 1002F photoresist (61% EPON resin 1002F, 32.65% gamma-butyrolactone, 6.1% triarylsulfonium hexafluoroantimonate salts and 1.0% oleic acid functionalized γFe_2O_3 nanoparticles by weight percentage) was synthesized as described previously.[20] Prior to photoresist application, glass slides were cleaned with acetone, isopropyl alcohol, deionized water and treated in a plasma cleaner for 20 min (Harrick Plasma, Ithaca, NY). The magnetic photoresists were then spun to a 30 µm thick film on a microscope slide (75x38x1mm, Fisher Scientific, Pittsburgh, PA). Coated slides allowed to soft back in a 95^{o}C convection oven (Isotemp Oven, Fisher Scientific, Pittsburgh, PA) for 40 min. After the slides were allowed to cool the film was selectively exposed to UV light (Oriel Model #97435, Newport Inc., Stratford, CT) through a patterned chrome mask. Slides were post baked at 95^{o}C for a further 10 min and then allowed to cool to room temp. Film areas not exposed to UV light were then removed in a bath of SU-8 developer for 10 min. Arrays were then rinsed briefly with fresh SU-8 developer and isopropyl alcohol. Following solvent removal with a stream of

nitrogen gas the arrays were hard baked on a 120^{o}C hot plate for 1 h (825-HP, VWR, West Chester, PA). Following pallet fabrication, a PDMS ring was glued around the pallet array with PDMS. Virtual air walls were then developed through chemical vapor deposition of a hydrophobic perfluoroalkylsilane layer on the silicone oxide surface as described previously.[21]

4.2.5 Fabrication of hybrid micropallets. Two-layer microstructures were fabricated by spin coating a 55-µm layer of native 1002F over a 5-µm film of 1002F containing 1% γFe_2O_3 nanoparticles. Exposure of the photoresist through a patterned mask and subsequent development, as described for standard micropallets, generated 100 × 100 × 60 µm (L×W×H) microstructures.

Standard multilayer microfabrication procedures were adapted to fabricate microstructures possessing highly magnetic borders (Figure 4.3A). The first step involved fabricating an array of 5-µm tall magnetic borders by standard photolithography procedures, as described above. 1002F photoresist admixed with 10, 20 or 50% γFe_2O_3 nanoparticles was spin-coated onto a glass substrate at 3000 rpm.[20] Following a 45-min soft bake, a chrome mask etched with an array of 15-µm wide frames, i.e., the magnetic base borders, was aligned with the substrate and exposed to a UV source (76 mW/cm^2, Oriel Model #97435, Newport Inc., Stratford, CT). At concentrations above 1% in 1002F, the γFe_2O_3 nanoparticles were unstable and the nanoparticles formed micron size aggregates. Although the opaque nanoparticles prohibited direct exposure of photoresist directly below nanoparticles this material was still fully polymerized as a result of the scatter, diffraction of reflection of light around the nanoparticles.[22] Subsequent post-

baking, rinses with developer and hard-baking produced the magnetic borders comprising the hybrid micropallets.

Prior to application of the second layer of photoresist, the array of magnetic borders was treated for 20 min in a plasma cleaner. A 60-µm thick layer of 1002F photoresist was then spun over the array and baked for 1 h. A chrome mask patterned with an array of 100 x 100 µm elements was aligned to the array of magnetic borders and exposed to UV light (Karl Suss MA6/BA6, SUSS MicroTech, Garching, Germany). In some experiments the surface of each element was fabricated with an inverted"Z" on the top surface to allow identification of the orientation of the microstructures after collection (Figure 4.3B).[23] Slides were post baked at 95^{o}C for a further 10 min and then allowed to cool to room temp. Film areas not exposed to UV light were then removed in a bath of SU-8 developer for 10 min. Arrays were then rinsed briefly with fresh SU-8 developer and isopropyl alcohol. Following solvent removal with a stream of nitrogen gas, the arrays were hard baked on a 120^{o}C hot plate for 1 h. Following pallet fabrication, a PDMS ring was glued around the pallet array with PDMS. Virtual air walls were then developed through chemical vapor deposition of a hydrophobic perfluoroalkylsilane layer on the silicone oxide surface as described previously.[21]

4.2.6 Laser-based micropallet release. Micropallets were selectively released from the glass substrate using a laser-based approach as described previously.[24] Briefly, a laser pulse (5 ns, 532 nm Nd:YAG Polaris II laser, New Wave Research, Fremont, CA) was focused by a 20x microscope objective at the interface of the microstructure and glass substrate. The focused laser pulse generated a cavitation bubble at the base of the microstructure which upon expansion dislodged the selected element from the substrate.

Micropallets with dimensions 50×50×30 μm (L×W×H) were released with a single laser pulse (3.2 μJ). The hybrid micropallets with dimensions 100×100×60 μm (L×W×H) were released with multiple laser pulses (4.0 μJ, 5-8 pulses) directed at different regions of the element base.

4.2.7 Micropallet collection. An array of micropallets with dimensions 50×50×30 μm (L×W×H) containing 1% γFe_2O_3 nanoparticles enclosed by a PDMS chamber were filled with PBS and covered by a glass slide. Micropallets were released with a Nd:YAG laser and the precision of micropallet collection relative to the position of the magnetic pole was measured. To collect pallets, the pole tip was attached to an x-y-z translation stage so that the magnetized tip could be precisely positioned above the collection well of interest at various angles and displaced from the field of view of the microscope objective. Depending on the application, two mounting procedures were developed to control the position of the external magnet. The magnetic pole was placed in a fixed position relative the micropallet array by attaching the magnet to a platform placed directly on the transition stage. Alternatively, by mounting an x-y-z translation stage with attached magnetic pole to the microscope, the micropallet array could be manipulated independently to the magnetic pole (Figure 4.2A). Accuracy and efficiency of micropallet collection was evaluated by positioning various magnetic tips above the collection substrate and measuring the position of micropallet collection with respect to the pole tip.

4.2.8 Quantification of micropallet retention. Retention of collected micropallets on a glass slide, 100-μm PDMS film or PDMS multiwell plate was monitored under fluid flow. A PDMS channel (3-mm height, 7-mm width, 20-mm length) was sandwiched between a collection substrate and micropallet array and then filled with PBS. Magnetic

pallets were then released and collected with a Neodymium-iron-boron magnet (1.27-mm diam. 2.54-cm length) from Magcraft (Vienna, VA) onto a collection substrate. After pallet collection within the fluidic channel, the assembly was inverted so that the collection surface with attached pallets was now below the array. PBS was flowed at a known rate (1.8×10^{-7} m^3/s) through the PDMS channel for 30 s using a syringe pump (kdScientific, Holliston, MA) into the PDMS chamber through a 25 G needle (Becton Dickinson, Franklin Lakes, NJ). Pallet retention was monitored in real time with a 10x objective. Only pallets remaining in the initial field of view following fluid flow were marked as retained.

4.3 Results and Discussion

4.3.1 Fabrication/characterization of fine-tipped magnetic poles. Magnetic poles generate a wide range of forces for manipulating various biological and mechanical microelements with high precision. The magnitude of the magnetic field intensities generated by these devices is directly proportional with distance from the pole tip. This decline in the magnetic field strength at increasing distances from the pole makes maximization of the initial magnetic field strength critical for achieving high magnetic fields at large distances. Various magnetic materials and pole geometries were screened for their ability to maximize the magnetic field strength and magnetic field gradients near a fine-tipped pole (Figure 4.1). Three magnetic alloys of differing magnetic saturations and magnetic permeabilities were mated to a Nd magnet and transmission of the magnetic field measured (Figure 4.1A,C). The effectiveness of the various magnetic pole tips at conducting the magnetic fields was evaluated by comparing the product of the magnetic field strengths and magnetic field gradients at various distances from the pole (data not shown). The high saturation/low permeability material (Vim Var low carbon magnetic iron) produced larger magnetic field strengths (250 mT) near the pole tip than materials with lower

saturations and higher permeabilities, EFI 50 (235 mT) and EFI 79 (150 mT) and was therefore utilized in further experiments.

Geometry of the pole tip plays an important role in how the magnetic field lines directed by the pole.[25-27] A 1.27-mm diameter rod sharpened to point 1.27-mm tall yielded a broad 97^{o} tip (Figure 4.2D). This pole fabricated out of high carbon magnetic iron and attached to a Nd magnet generated a magnetic field strength of 250 mT (10472 mT/mm) at the pole tip. Conversely, the same material sharpened to a 37^{o} tip (2.54-cm tall cone) or 30^{o} tip (1.27-cm tall two-tapered tip) afforded magnetic fields of 129 mT (2884 mT/mm) and 127 mT (2532 mT/mm) at the respective pole tips. These results confirm previous finite element analysis simulations of magnetic pole tips which projected amplified magnetic forces at large distances as the tip radii and taper angles were increased.[25] These results imply that the choice of pole geometry necessitates a compromise between desired magnetic field strength and precision of the magnetic field gradient.

4.3.2 Collection of micropallets with magnetic poles. Precise positioning of unattached magnetic microstructures was demonstrated by collecting released magnetic micropallets with the magnetic fine-tipped poles. Magnetic capture of micropallets has previously been demonstrated to be effective for collecting micropallets at large distances ($\geq$ 15 mm) and at 100% efficiency; however, the precision of collection was not examined.[20] In this report, individual micropallets (dimensions 50 × 50 × 30 μm / L×W×H) containing 1% γFe_2O_3 nanoparticles were released by a Nd:YAG laser and their collection by a magnetic pole monitored (Figure 4.2A). Collection accuracy was assessed by measuring the axial displacement of 10 collected micropallets relative to the tip of the

magnetic pole, where the most accurate collection represents a micropallet displaced zero mm from pole tip (Figure 4.2B).

The accuracy and efficiency of micropallet collection was evaluated for different pole tip geometries and orientations (Table 4.1). Strategies giving collection efficiencies under 100% were deemed ineffective irrespective of the accuracy of collection. Micropallets were not efficiently collected when the magnetic field at the site of pallet release dropped below 40 mT as this field strength was insufficient to overcome gravity. Positioning the magnetic pole tip in relation to the micropallet array was initially tested by varying the angle of the broad 1.27-cm pole tip from 45^{o} – 90^{o} (Figure 4.2F-H). The highest accuracy of micropallet collection was achieved using a 90^{o} angle (241 ± 117 μm) and decreasing accuracy ensued as the pole tip was lowered to more acute angles. This effect was likely a result of the increased proximity of the magnetic pole sides to the collection substrate. Positioning the pole tip at a 90^{o} angle gave the most accurate micropallet collections; however, this orientation required positioning of the pole and magnet directly over the microscope objective leading to poor brightfield imaging. While setting the pole tip at a 60^{o} angle resulted in only slightly lower collection accuracies (433 ± 82 μm), this geometry allowed axial displacement of the pole tip with respect to the microscope objective (Figure 4.2A) thus accommodating real-time brightfield imaging of micropallets.

The effect of the magnetic field localization on microstructure capture was evaluated by tracking changes in micropallet collection as the geometry of the magnetic pole was altered. The tapered pole tip provided the highest collection accuracy (75 ± 31 μm) of micropallets with a 1 mm PDMS spacer (Figure 4.2C). The tapered pole

outperformed the broader 1.27-cm and 2.54-cm cones because of the higher localized magnetic field generated by the sharper tip. Unfortunately, this tip only reliably captured micropallets with $\leq$3 mm gap between the array and collection substrate. For many applications the tapered pole transmits sufficient magnetic fields to effectively collect magnetic microstructures. However, some systems require greater magnetic field intensities over large working distances, such as when taller PDMS spacers are preferred or if the microstructures have a low saturation magnetization. For these circumstances the broader 1.27-cm magnetic pole can generate an adequate magnetic field at the micropallet array to collect the released microstructures. The broad 1.27-cm magnetic pole was successful at capturing microstructures released 9 mm from the pole with an accuracy of 440 ± 241 μm. These results demonstrate a complementary pair of pole tips for magnetically collecting microstructures over a wide range of accuracies and working distances.

4.3.3 Microstructure retention on collection substrates. Adhesion between microstructures and the surrounding substrate can play a pivotal role in the effectiveness of a device. Technologies employing microcantilevers,[28] microactuators[9] or microelement flow through channels[29] would benefit from substrates with low adhesion to the device. Conversely, adhesive surfaces are favorable for substrates upon which microstructures are to be immobilized. Microstructure adhesion to various substrates was examined by applying a variety of forces and monitoring microstructure release from the surface (Table 4.2). Micropallet attraction was quantified by recording the retention of micropallets containing 1% γFe_2O_3 nanoparticles (dimensions 50x50x30 μm^3) collected with a 1-mm PDMS spacer onto a collection substrate consisting of glass, hydrophobic

PDMS films, hydrophilic PDMS films or PDMS microwells. Successfully detained pallets were those which remained within the same field of view at the conclusion of each experiment (n = 20 micropallets, 3 experiments).

Efficient collection of multiple magnetic micropallets requires retention of collected micropallets during repositioning of the magnetic pole. Micropallet adhesion against gravity was examined by removing the Nd magnetic after micropallet collection. All substrates except the hydrophilic PDMS film effectively secured the micropallets under static conditions. Plasma treatment of PDMS generated deprotonated silanol groups which did not provide good binding to the hydrophobic 1002F microstructures.[30] Vibrations to the system occur during adjustment of the pole tip and repositioning of the micropallet array. Consistent application of these stresses was applied by dropping a 44 g weight onto the microscope stage holding the pallet array. Again the glass substrate and untreated PDMS showed excellent retention of micropallets (>90%) whereas all micropallets were released from the hydrophilic PDMS film. Micropallet adhesion to glass and untreated PDMS in the absence of a magnetic field make these good substrates for collecting microstructures using the magnetic poles.

Removal of contaminating cells, media exchanges and even transportation of collection substrates may generate fluid motion within the microsystem. Micropallet arrest onto various substrates with and without magnetic attraction under the application of fluid flow was assessed in a fluidic channel. For these studies the square PDMS chamber was replaced with a PDMS channel (3-mm height, 7-mm width, 20-mm length) connected to a syringe pump which injected PBS into the channel at a constant volumetric flow rate of 1.8×10^{-7} m^3/s. Following collection, the apparatus was inverted

and fluid flowed over the collected micropallets for thirty seconds. Micropallets showed poor adhesion to glass slides (29 ± 4%) even in the presence of a magnetic field (36 ± 7%). Untreated PDMS films provided improved detainment as a result of hydrophobic interactions between the micropallets and PDMS allowing a ≥ 70% retention. The PDMS microwell plate afforded the best pallet capture (≥85%) due to both hydrophobic interactions and fluidic barriers created by the microwells. These outcomes show that micropallet retention to a collection substrate may be tailored through adjustment of the local magnetic field, substrate hydrophobicity and fluid flow profile.

4.3.4 Fabrication of hybrid micropallets. Localization of magnetic materials within a microstructure generates asymmetry in the forces applied to the device when introduced to a magnetic field gradient. These uneven forces have been exploited to provide directional and rotational control of several microdevices.[2,31-34] Unfortunately, typical strategies for machining microstructures with highly magnetic segments generally requires complex fabrication. In this report, microstructures possessing magnetic regions were fabricated by simple photolithography. A single-exposure step was used to fabricate a 100 × 100 × 60 μm (L×W×H) microstructure comprised of a 5-μm base of 1% magnetic 1002F and a 55-μm 1002F top (Figure 3B). Alternatively, a two-step procedure was employed to construct 100 × 100 × 60 μm (L×W×H) micropallets framed by 15-μm wide/ 5-μm tall border of 1002F containing 10, 20 or 50 % γFe_2O_3 (Figure 4.3A). Magnetic 1002F formulations with greater than 1% γFe_2O_3 have large nanoparticle aggregates that make imaging through the microstructures difficult.[35] Fabrication of the magnetic regions along the boundary of the microstructure bases produced highly

magnetic micropallets while retaining transparency at the center of the device (Figure 4.3C-D).

*4.3.5 Controlling microstructure orientation***.** Micropallet tracking and cell visualization following collection is plagued by the random orientations of micropallets on a surface following collection.[19] Micropallets landing in an upright orientation are preferential because imbedded numbers/letters can be easily read. It is impossible to identify micropallets from their tracking numbers if they are collected on their side. Additionally, if a micropallet is collected in a sideways orientation cell morphology and intracellular components cannot be adequately imaged. Tracking micropallets captured in an inverted orientation is undesirable due to difficulties with processing inverted numbers and letters. If properly localized, highly magnetic regions within a micropallet will move towards an external magnetic and provide control over the orientation of the collected micropallets. In triplicate experiments, 20 hybrid micropallets were released and magnetically assembled onto a glass substrate, after which their orientation was assessed (Table 4.3). These elements were labeled with an inverted "Z" to allow easy assessment of the orientation following collection (Figure 4.3B-D). Micropallets were collected in three different orientations: upright (inverted "Z"), upside down ("Z") or sideways. Micropallets with 5-μm magnetic bases (1% magnetic 1002F) and 55-μm 1002F tops were randomly positioned following collection (Figure 4.3E,F). Hybrid pallets with magnetic borders (15-μm wide, 5-μm tall) possessing 10, 20 and 50 % γFe_2O_3 below a 60-μm 1002F top yielded optically clear pallets with the majority of magnetic particles at the base and edges of the pallet. Hybrid micropallets with 20% and 50% magnetic frames were collected in an upright orientation with an efficiency of 72 ± 8% and 25 ±

5%, respectively. The high concentrations of γFe_2O_3 in the borders resulted in the microstructures becoming brittle and disintegrating during release. The ensuing uneven magnetism rendered incorrect collection of these pallets. Micropallets containing 10% magnetic borders were correctly oriented with 90 ± 10% efficiency using a 5-mm PDMS spacer. A 1 mm separation between released pallets and a 1 mm axial separation of the Nd magnetic and pallet improved the correct orientation of hybrid pallet collection to 100 ± 0% (Figure 4.3G).

4.4 Conclusions

A method for controlling microstructure positioning was developed by modifying the magnetic field gradient and localization of the magnetic material within a microstructure. Magnetic rods sharpened to fine tips were employed to generate highly focused magnetic fields and were demonstrated to capture magnetic micropallets with a accuracy as low as 75 μm. A previous report described a method for magnetically collecting molded microstructures referred to as 'microrafts'.[36] The fine-tipped magnetic pole could also be employed to precisely capture the microrafts with high precision following their microneedle-based release. It was observed that the choice of collection substrate played an essential role in the effectiveness of micropallet collection. Additionally, integration of a localized highly magnetic domain within a microstructure was exploited to control the orientation of the element on a surface following release and collection. In addition to localization of the micropallets' magnetism, these highly magnetic borders provided opaque borders. This non-transparent border surrounding a central transparent pallet can greatly enhance the effectiveness of cellular imaging. Light scattering occurs at the edges of conventional pallets due to the difference in the

refractive index between the pallet and surrounding media and the surface roughness of the sides of the pallets.[37] The dark border should absorb a large fraction of the scattered light and permit improved imaging which is required for sensitive fluorescence measurements. Strategies described for controlling the manipulation of microstructures through rational placement of magnetic materials and fields will be applicable to many areas of biomedical engineering.

4.5 Tables and Figures

Collection Pole	Pallet/Magnet Separation (mm)	Collection Probability (%)	Axial Pallet Drift (μm)
1.27 cm Tall Tip	1	100	539 ± 233
	5[a]	100	838 ± 263
	5	100	433 ± 82
	5[b]	100	241 ± 117
	9	80	440 ± 241
2.54 cm Tall Tip	1	100	109 ± 46
	3	50	112 ± 45
1.27 cm Tall	1	100	75 ± 31
Tapered Tip	3	100	80 ± 42
	5	30	67 ± 47

n = 10 micropallets per experiment [a] 45° Pole Angle [b] 90° Pole Angle

Table 4.1 Accuracy of micropallet collection by magnetic poles.

Stress test	Substrate	Percentage remaining
Magnet Removal	Glass slide	98 ± 3
	Untreated PDMS film	100 ± 0
	Hydrophilic PDMS film	40 ± 10
44 g Weight Drop	Glass slide	98 ± 3
	Untreated PDMS film	98 ± 3
	Hydrophilic PDMS film	0 ± 0
Fluid Flow	Glass slide	29 ± 4
Magnet Removed	Untreated PDMS film	70 ± 7
	Untreated PDMS microwell	85 ± 4
Fluid Flow	Glass slide	36 ± 7
	Untreated PDMS film	100 ± 0
	Untreated PDMS microwell	98 ± 2
Triplicate experiments (n = 20 micropallets per experiment)		

Table 4.2 Micropallet retention to various substrates.

Hybrid Micropallet	Pallet/Magnet	Micropallets	Initial Orientation | Orientation After Glass Removal					
Material	Separation (mm)	Collected (%)	Correct		Incorrect		Side	
1% γFe_2O_3 base layer	1	100 ± 0	27 ± 3	30 ± 5	33 ± 10	32 ± 8	40 ± 13	38 ± 6
	5	100 ± 0	7 ± 3	35 ± 5	8 ± 8	57 ± 8	85 ± 5	8 ± 3
	9	0 ± 0	N/A		N/A		N/A	
10% γFe_2O_3 border	1	100 ± 0	67 ± 16	58 ± 8	0 ± 0	17 ± 6	33 ± 8	25 ± 5
	5	100 ± 0	80 ± 13	90 ± 10	0 ± 0	8 ± 6	20 ± 5	2 ± 3
	9	48 ± 9	50 ± 9	63 ± 15	0 ± 0	13 ± 8	30 ± 5	8 ± 3
	1*	100 ± 0	75 ± 9	83 ± 8	0 ± 0	8 ± 3	25 ± 5	8 ± 8
	5*	100 ± 0	100 ± 0	100 ± 0	0 ± 0	0 ± 0	0 ± 0	0 ± 0
	9*	100 ± 0	83 ± 6	83 ± 6	0 ± 0	8 ± 10	16 ± 10	8 ± 6
20% γFe_2O_3 border	5	100 ± 0	77 ± 10	72 ± 8	5 ± 5	5 ± 5	18 ± 8	23 ± 8
50% γFe_2O_3 border	5	90 ± 5	32 ± 8	25 ± 5	8 ± 3	7 ± 8	50 ± 5	58 ± 8
Triplicate experiments (n = 20 pallets per experiment), *denotes magnet axially shifted 1 mm								

Table 4.3 Hybrid micropallet collection.

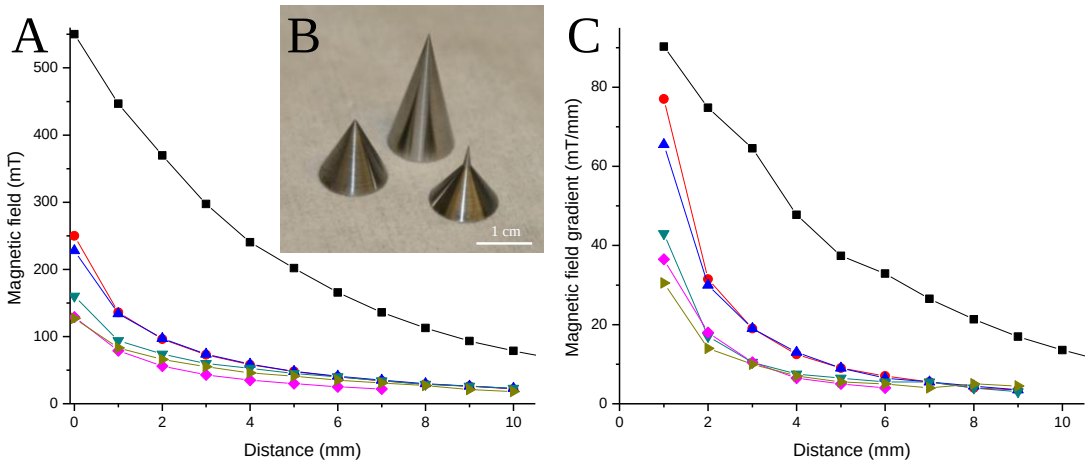

Figure 4.1 Characterization of magnetic poles. A) Magnetic field strength (in mT) and C) magnetic field gradients (in mT/mm) of the Nd magnet (black square), 1.27-cm long cone made from vim var iron (red circle), 1.27-cm cone fabricated from EFI50 (blue triangles), 1.27-cm cone made from EFI79 (green triangle), 1.27-cm long tapered pole comprised of vim var iron (tan triangle) and 2.54-cm cone made from carbon iron (pink triangle). B) Images of magnetic poles: structures from from left to right represent a 1.27-cm diameter/1.27-cm tall pole, 1.27-cm diameter/2.54-cm tall pole and a 1.27-cm diameter/1.27-cm long tapered pole.

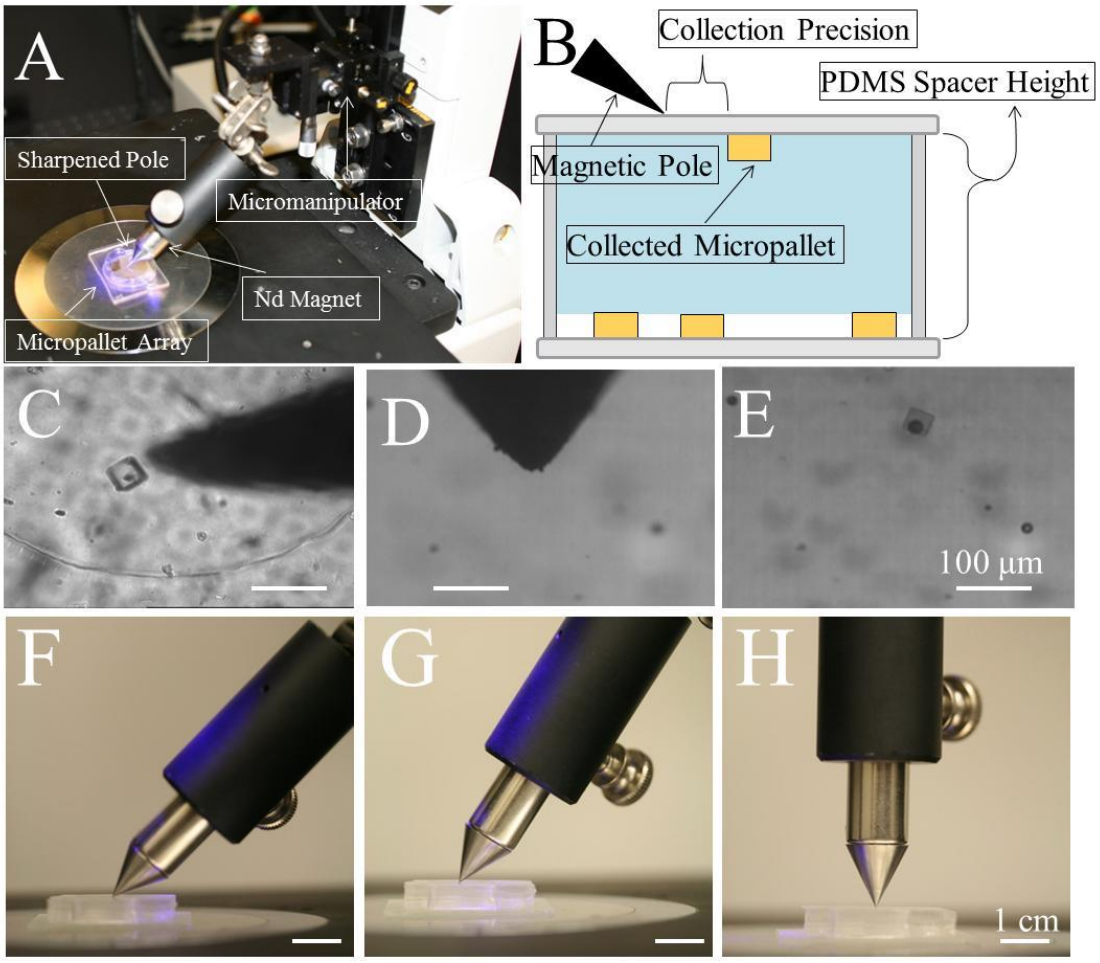

Figure 4.2 Micropallet collection by magnetic pole tips. A) Image of magnetic pole system with magnetic tip positioned over collection substrate of a micropallet array device. B) Schematic of micropallet collection with a magnetic pole tip. C) Brightfield image of magnetic micropallet collected by a 1.27-cm tapered pole tip. D) Brightfield image of magnetic micropallet following collecting by a 1.27-cm magnetic pole and E) corresponding image after removal of the pole. F-H) Images of a 1.27-cm magnetic pole aligned over a micropallet array at an angle of 45^{o}, 60^{o} and 90^{o}, repectively.

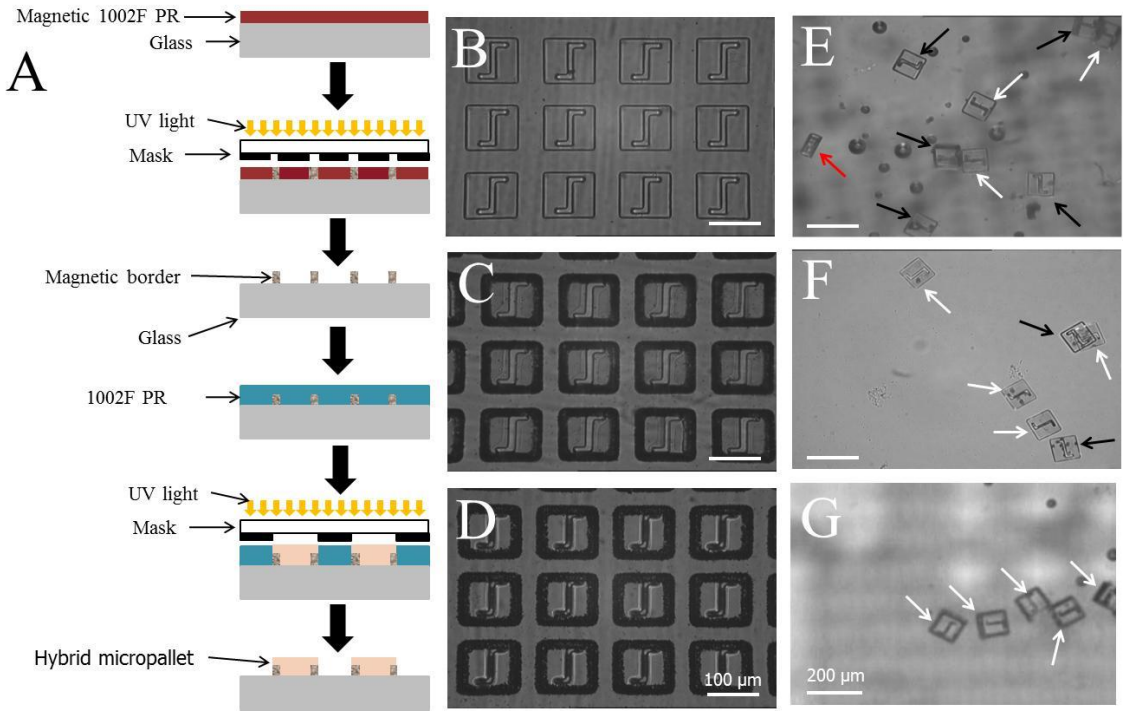

Figure 4.3 Fabrication and collection of hybrid micropallets. A) Schematic of the process flow for fabrication of the hybid micropallets. Images of hybid micropallets composed of a 60-µm 1002F micropallet with B) 1% γFe_2O_3 base, C) 10% γFe_2O_3 border or D) 50% γFe_2O_3 border. Collection of hybrid micropallets composed of a 1% γFe_2O_3 base E) immediately following collection and F) after separation of the micropallet array. G) Capture of hybrid micropallets comprising a 10% γFe_2O_3 border immediately following collection. White arrows represent micropallets collected in upright orientation, black arrows represent micropallets collected in an inverted orientation and red arrows represent micropallets captured on their side.

4.6 References

1. Whitesides G, Grzybowski B. Self-assembly at all scales. *Science*. 2002;295(5564):2418-2421.

2. Abbott J, Nagy Z, Beyeler F, Nelson B. Robotics in the small - Part I: microrobotics. *Ieee Robotics & Automation Magazine*. 2007;14(2):92-103.

3. MacLachlan R, Becker B, Tabares J, Podnar G, Lobes L, Riviere C. Micron: An Actively Stabilized Handheld Tool for Microsurgery. *Ieee Transactions on Robotics*. 2012;28(1):195-212.

4. Neuman K, Block S. Optical trapping. *Review of Scientific Instruments*. 2004;75(9):2787-2809.

5. Roman G, Chen Y, Viberg P, Culbertson A, Culbertson C. Single-cell manipulation and analysis using microfluidic devices. *Analytical and Bioanalytical Chemistry*. 2007;387(1):9-12.

6. Pamme N. Magnetism and microfluidics. *Lab on a Chip*. 2006;6(1):24-38.

7. Chronis N, Lee L. Electrothermally activated SU-8 microgripper for single cell manipulation in solution. *Journal of Microelectromechanical Systems*. 2005;14(4):857-863.

8. Gibbs M. Applications of magmems. *Journal of Magnetism and Magnetic Materials*. 2005;290:1298-1303.

9. Yamanishi Y, Sakuma S, Onda K, Arai F. Powerful actuation of magnetized microtools by focused magnetic field for particle sorting in a chip. *Biomedical Microdevices*. 2010;12(4):745-752.

10. Yamanishi Y, Sakuma S, Kihara Y, Arai F. Fabrication and Application of 3-D Magnetically Driven Microtools. *Journal of Microelectromechanical Systems*. 2010;19(2):350-356.

11. Hagiwara M, Kawahara T, Yamanishi Y, Arai F. Driving method of microtool by horizontally arranged permanent magnets for single cell manipulation. *Applied Physics Letters*. 2010;97(1).

12. Floyd S, Pawashe C, Sitti M. Two-Dimensional Contact and Noncontact Micromanipulation in Liquid Using an Untethered Mobile Magnetic Microrobot. *Ieee Transactions on Robotics*. 2009;25(6):1332-1342.

13. Sakar M, Steager E, Kim D, Kim M, Pappas G, Kumar V. Single cell manipulation using ferromagnetic composite microtransporters. *Applied Physics Letters*. 2010;96(4).

14. Chung B, Lee K, Khademhosseini A, Lee S. Microfluidic fabrication of microengineered hydrogels and their application in tissue engineering. *Lab on a Chip*. 2012;12(1):45-59.

15. Ishihara H, Takeuchi S. Handling adherent cells with magnetically functionalized microplates: IEEE Proc. in MEMS; 2010:959 - 962.

16. Srinivasan U, Liepmann D, Howe R. Microstructure to substrate self-assembly using capillary forces. *Journal of Microelectromechanical Systems*. 2001;10(1):17-24.

17. Tien J, Terfort A, Whitesides G. Microfabrication through electrostatic self-assembly. *Langmuir*. 1997;13(20):5349-5355.

18. Ramadan Q, Uk Y, Vaidyanathan K. Large scale microcomponents assembly using an external magnetic array. *Applied Physics Letters*. 2007;90(17).

19. Wang Y, Young G, Bachman M, Sims C, Li G, Allbritton N. Collection and expansion of single cells and colonies released from a micropallet array. *Analytical Chemistry*. 2007;79(6):2359-2366.

20. Gach P, Sims C, Allbritton N. Transparent magnetic photoresists for bioanalytical applications. *Biomaterials*. 2010;31(33):8810-8817.

21. Wang Y, Sims C, Marc P, Bachman M, Li G, Allbritton N. Micropatterning of living cells on a heterogeneously wetted surface. *Langmuir*. 2006;22(19):8257-8262.

22. Damean N, Parviz B, Lee J, Odom T, Whitesides G. Composite ferromagnetic photoresist for the fabrication of microelectromechanical systems. *Journal of Micromechanics and Microengineering*. 2005;15(1):29-34.

23. Wang Y, Young G, Bachman M, Sims CE, Li GP, Allbritton NL. Collection and expansion of single cells and colonies released from a micropallet array. *Analytical Chemistry*. 2007;79:2359-2366.

24. Quinto-Su P, Salazar G, Sims C, Allbritton N, Venugopalan V. Mechanisms of pulsed laser microbeam release of SU-8 polymer "Micropallets" for the collection and separation of adherent cells. *Analytical Chemistry*. 2008;80(12):4675-4679.

25. Xiang Y, Miller J, Sica V, Lavan D. Optimization of force produced by electromagnet needles acting on superparamagnetic microparticles. *Applied Physics Letters*. 2008;92(12).

26. Matthews B, LaVan D, Overby D, Karavitis J, Ingber D. Electromagnetic needles with submicron pole tip radii for nanomanipulation of biomolecules and living cells. *Applied Physics Letters*. 2004;85(14):2968-2970.

27. Barbic M, Mock J, Gray A, Schultz S. Scanning probe electromagnetic tweezers. *Applied Physics Letters*. 2001;79(12):1897-1899.

28. Suter M, Ergeneman O, Zurcher J, et al. Superparamagnetic photocurable nanocomposite for the fabrication of microcantilevers. *Journal of Micromechanics and Microengineering*. 2011;21(2).

29. Jensen-McMullin C, Bachman M, Li G. Microfabricated micropallets for enhancement of biomolecular techniques. *Microfluidics and Nanofluidics*. 2008;5(2):225-234.

30. Duffy DC, McDonald JC, Schueller OJA, Whitesides GM. Rapid Prototyping of Microfluidic Systems in Poly(dimethylsiloxane). *Analytical Chemistry*. 1998;70:4974-4984.

31. Kummer M, Abbott J, Kratochvil B, Borer R, Sengul A, Nelson B. OctoMag: An Electromagnetic System for 5-DOF Wireless Micromanipulation. *Ieee Transactions on Robotics*. 2010;26(6):1006-1017.

32. Kim L, Choi S, Kim J, Kim H, Kwon S. Single exposure fabrication and manipulation of 3D hydrogel cell microcarriers. *Lab on a Chip*. 2011;11(1):48-51.

33. Sakar M, Steager E, Kim D, et al. Modeling, control and experimental characterization of microbiorobots. *International Journal of Robotics Research*. 2011;30(6):647-658.

34. Pawashe C, Floyd S, Sitti M. Multiple magnetic microrobot control using electrostatic anchoring. *Applied Physics Letters*. 2009;94(16).

35. Gach PC, Sims CE, Allbritton NL. Transparent magnetic photoresists for bioanalytical applications. *Biomaterials*. 2010;31(33):8810-8817.

36. Gach P, Wang Y, Phillips C, Sims C, Allbritton N. Isolation and manipulation of living adherent cells by micromolded magnetic rafts. *Biomicrofluidics*. 2011;5(3).

37. Shadpour H, Zawistowski J, Herman A, Hahn K, Allbritton N. Patterning pallet arrays for cell selection based on high-resolution measurements of fluorescent biosensors. *Analytica Chimica Acta*. 2011;696(1-2):101-107.

Chapter 5: Isolation of viable rare cells by large micropallet arrays

5.1 Introduction

Cancer accounts for approximately 25% of deaths in the United States with most mortality due to metastases.[1,2] Growth of tumors at sites distant from the primary location arises from intravasation of tumor cells followed by extravasation and growth in new locations. Only a small percentage of tumor cells circulating in the blood stream are competent to engraft and form new tumors.[3,4,5] These successful cells are thought to possess stem cell-like attributes enabling the cells to divide, reproducing additional cancer stem cells as well to produce cells differentiating into the proliferating cells comprising the tumor. Cancer stem cells have been identified in many tumor systems including; breast cancer,[6] prostate cancer,[7] the hematopoietic system[8] and the central nervous system.[9] Breast cancer is an important system clinically because it is the most common malignant disease of women in the United States and the death rates from individuals diagnosed with metastatic breast cancer remain high. The subset of cells expressing stem-like properties identified in breast cancers are characterized by their expression of CD44 (a marker of stem cells) and lack of CD24 surface markers (characteristic of epithelial cell differentiation).[6] $CD44^{+}/CD24^{-/low}$ cells have recently been reported to exhibit greater invasive and proliferative properties[10] than other cell populations and are competent to form tumors in mouse xenograft models.[6]

Difficulties in monitoring and characterizing these cancer stem cells are due to their low abundance in the heterogeneous tumor cell population. The majority of research

directed at analyzing and sorting these low abundance cells types employs fluorescence-activated cell sorting (FACS).[6,11,12] For successful FACS sorting of cancer stem cells; the adherent tumor cells are stripped from their growth surfaces, labeled with surface-marker specific antibodies and the cancer stem cells isolated by FACS. FACS has been demonstrated to be successful for isolating viable mammalian cells by utilizing a range of selection parameters and relatively high throughputs (>10,000 cells/s). However, FACS systems are not effective at isolating rare target cells (frequencies below 0.01%).[13] Isolation of rare cells by FACS is often preceded by an enrichment step, such as magnetic-activated cell sorting (MACS), prior to sorting for the best outcome.[14,15,16] However, MACS sorting becomes complicated when positive and negative selection is necessary, as in the case for the $CD44^{+}/CD24^{-/low}$ breast cancer stem cells. Several microfluidic technologies have recently been developed to achieve isolation and analysis of rare cells. These systems operate on a wide variety of sorting parameters including: immunoaffinity interactions,[17] magnetism,[18] size,[19] and DEP responses.[20,21] These strategies all offer suboptimal sorting efficiencies because they necessitate removal of adherent cells from their growth surfaces which is accompanied by a changing of the cell morphology, reduced cellular surface markers and altered cell physiology. Intense manipulation, sample handling and the prolonged removal of adherent cells from their growth surfaces all lead to low recovery and viability of cells sorted by these flow-based sorting strategies.[22]

Microscopy-based cell imaging devices eliminate challenges associated with examining adherent cells in suspension by allowing analysis of cells while still attached to their growth surfaces. Additionally, these methods permit evaluation of subcellular

components, temporal responses and cell-cell interactions. Several imaging cytometry systems have shown success at enumerating rare cells.[23,24] Unfortunately, few devices have successfully incorporated cell sorting capabilities with high-throughput microscopy-based detection. The Allbritton group has previously demonstrated the utility of arrays of releasable elements microfabricated on glass substrates termed 'micropallets' for sorting single adherent cells and small colonies while the cells remain adhered to the micropallet suface.[25] This technology has shown success in sorting single cells present at rarity down to 1% in a mixed cell population with low reagent requirements and at a high post sorting yield and viability.[26] However, the minute quantity of many tumorigenic cancer cells makes standard micropallet arrays (comprising 10,000 – 50,000 elements) ineffective platforms for isolating these cells. In the present work, the potential for using micropallet arrays to sort rare cell types, comprising 1 cell of interest per $10^4 - 10^6$ non-target cells is examined. For these purposes a large array of approximately 1.3 million micropallets was developed along with a high-throughput array screening procedure. A high-resolution wide-field microscope and automated image processing were utilized to identify low abundance target cells on the array. Isolation of viable rare cells by the micropallet arrays was then achieved and results directly compared to FACS sorting.

5.2 Materials and Methods

5.2.1 Reagents. The following materials were obtained from the Aldrich Chemical Company (St. Louis, MO): iron(III) chloride tetrahydrate, iron(III) chloride anhydrous, iron(III) nitrate nonahydrate, toluene (reagent grade), triarylsulfonium hexafluorophosphate salts, mixed, 50% in propylene carbonate, γ-butyralactone (GBL, 99+%), 1-methoxy-2-propanol (SU8 developer, 98.5%). EPON resin 1002F (phenol,

4,4'-(1-methylethylidene)bis-, polymer with 2,2'-[(1-methylethylidene) bis(4,1-phenyleneoxymethylene]bis-[oxirane]) was obtained from Miller-Stephenson (Sylmar, CA) and (heptadecafluoro-1,1,2,2-tetrahydrodecyl)trichlorosilane was purchased from Gelest Inc (Morrisville, PA). Dulbecco's modified Eagle's medium (DMEM), fetal bovine serum (FBS), 1X phosphate buffered saline (PBS), pH 7.4, 0.05% trypsin with EDTA solution and penicillin/streptomycin were received from Invitrogen (Carlsbad, CA). Sylgard 184 silicone elastomer kit (PDMS) was received from Dow Corning (Midland, MI). Fibronectin extracted and purified from human plasma was obtained from Chemicon International Inc. (Temecula, CA). Wild-type HeLa cells were purchased from the American Type Culture Collection (ATCC, Manassas, VA). All other chemicals were procured from Fisher Scientific (Pittsburgh, PA).

5.2.2 Fabrication of micropallet arrays and PDMS chambers. Magnetic 1002F photoresist (61% EPON resin 1002F, 32.65% gamma-butyrolactone, 6.1% triarylsulfonium hexafluoroantimonate salts and 0.25% oleic acid functionalized γFe_2O_3 nanoparticles by weight percentage) was synthesized as described previously.[27] The magnetic photoresists was then spin-coated to a 75 µm thick film on a glass slide (B270 150mm diam. x 0.9mm thick, Valley Design Corp., Santa Cruz, CA). Prior to photoresist application, glass slides were cleaned with acetone, isopropyl alcohol, deionized water and treated in a plasma cleaner for 20 min (Harrick Plasma, Ithaca, NY). Coated slides were covered with foil and allowed to soft bake in a 95^{o}C convection oven (Isotemp Oven, Fisher Scientific, Pittsburgh, PA) for 1 h. After the slides cooled, the film was exposed to UV light (Karl Suss MA6/BA6, SUSS MicroTech, Garching, Germany) through a chrome mask. Slides were post baked at 95^{o}C for a 10 min and then cooled to

room temperature. Film areas not exposed to UV light were then removed by incubation in SU-8 developer for 10 min. Arrays were rinsed briefly with fresh SU-8 developer and isopropyl alcohol. Following solvent removal with a stream of nitrogen gas, the arrays were hard baked on a 120^{o}C hot plate for 1 h (825-HP, VWR, West Chester, PA). Large arrays were composed of a 1350x950 array of micropallets with dimensions of 50 × 50 × 75 μm (L × W × H) and a 25 μm gap between micropallets. Every 50th and 51st micropallet was replaced with a 125 × 125 μm square element with 50 μm embedded numbers to assist in identifying micropallet coordinates. This generated an array with a total size of 101.225 × 71.250 mm consisting of 1,280,448 micropallets and 513 numbered micropallets. Following pallet fabrication, a plastic cassette was glued around the pallet array with PDMS. The 105 × 75 × 6 mm culture chamber was machined from 3mm ABS filament (MakerBot Industries, Brooklyn, NY) with a BFB 3000 plus 3D printer (3D systems, Rock Hill, SC). A small side chamber was included on the culture chamber to allow removal of air bubbles from the micropallet array chamber when cells were cultured. The array was coated with hydrophobic perfluoroalkylsilane layer ((heptadecafluoro-1,1,2,2-tetrahydrodecyl)trichlorosilane) by chemical vapor deposition as described previously.[28] The arrays were sterilized by rinsing with 95% ethanol and dried in a tissue culture hood. Excess ethanol was removed with five 1X PBS rinses. Top surfaces of the micropallets on the array were then coated with 5 mL of 25 μg/mL fibronectin in PBS for one hour at room temperature. Following surface coating the array was rinsed ×5 with 1X PBS.

5.2.3 Cell culture. All cells were cultured in DMEM supplemented with FBS (10%), L-glutamine (584 mg L^{-1}), penicillin (100 units mL^{-1}) and streptomycin (100 μg

ml^{-1}) in a 37^{o}C incubator with a 5% CO_2 atmosphere. To culture cells on the micropallet arrays, the 1X PBS was replaced with cell culture media and suspensions of HeLa cells intermixed with various quantities of GFP-HeLa cells were added to the array at a cell:pallet ratio yielding <1 cell per pallet (10 mL of 50,000 cells/mL). Cells were allowed to settle and adhere to the array for 8 h unless otherwise stated in the text.

Conditioned media was developed by growing subconfluent cultures of HeLa cells in DMEM supplemented with FBS (10%), L-glutamine (584 mg L^{-1}), penicillin (100 units mL^{-1}) and streptomycin (100 µg ml^{-1}) for 48 h. The supernatant was centrifuged (3,000 g, 20 min), stored at -20^{o}C and thawed immediately prior to use.

5.2.4 Microscopy. A computer-controlled (ProScan^{TM} III motorized stage system, Prior Scientific Inc., Rockland, MA) XY translational stage (H138A/C ProScan^{TM} upright microscope stage, Prior Scientific Inc., Rockland, MA) was mounted on an Olympus MVX10 MacroView microscope (Olympus, Center Valley, PA) with a Hamamatsu ORCA-Flash4.0 CMOS camera (Hamamatsu, Bridgewater, NJ) for imaging. Focus adjustments were controlled by a motorized focus drive (H122SZX Focus Kit, Prior Scientific Inc., Rockland, MA). Automated array screening was achieved through a custom MatLab program. The boundaries and focal plane of the array were identified, then the array was screened with a 1X objective and 2X zoom which generated 166 individual 6.85 × 6.85 mm images consisting of 8,100 micropallets each. Micropallet arrays were imaged in a raster scan pattern with brightfield microscopy and fluorescence microscopy using FITC, Texas Red, and DAPI fluorescent filter sets; fluorescence illumination was achieved via a Lumen 200 arc lamp (Prior Scientific Inc., Rockland, MA).

5.2.5 Image processing and analysis. Raw images were saved to the computer hard drive and the data segmented by a custom Matlab program. Morphological filtering was employed to subtract background illumination from uneven lighting and autofluorescence from the images. First, a morphological closing was implemented to eliminate dark areas between the pallets, then a modified top hat filter (morphological opening of the closed image subtracted from the original image) was used to eliminate the image background fluorescence in each image. The images were segmented using a user-defined absolute thresholding approach. The threshold value was determined for each filter set to maximize the sensitivity of the cytometry. Size exclusion filters were employed to eliminate light scattering particles larger or smaller than a user-defined maximum and minimum diameter respectively. Negative control fluorescence images were then subtracted from the fluorescence image of the target cell. The resulting cell coordinates were then manually imaged to confirm cellular identification.

5.2.6 Micropallet release and collection. Following identification of target cells, the glass cover was replaced with a multiwell collection substrate. The collection substrate consisted of a 100 × 70 array of 1 × 1 mm PDMS wells 100 μm in depth fabricated as described previously.[25] A plastic cassette was attached to the multiwell plate using PDMS as a glue. The 103 × 73 × 2 mm cassette was manufactured from 3mm ABS filament (MakerBot Industries, Brooklyn, NY) with a BFB 3000 plus 3D printer (3D systems, Rock Hill, SC). The cassette was autoclaved, rinsed with ethanol and allowed to air dry in a tissue culture hood. The chamber was then incubated with 25 μg/mL fibronectin in 1X PBS for 2 hrs. Prior to use, the wells were rinsed ×5 with 1X PBS. The collection cassette was then mated to the micropallet cassetteso that 1X PBS filled the

space between the arrays. The array was then transferred to a Nikon Eclipse TE300 inverted microscope (Nikon Instruments Inc., Melville, NY) and micropallets holding target cells were released. Detached micropallets were collected by applying a magnetic field using a 1.27 cm diam. × 2.54 cm thick axially magnetized neodymium magnet (K&J Magnetics, Inc., Jamison, PA).[27] Following collection of all target micropallets, the small magnet was replaced by a 10.16 × 10.16 × 1.27 cm (L × W × H) neodymium magnet (K&J Magnetics, Inc., Jamison, PA) and transferred to a sterile hood. The magnet was held in contact with the collection plate during removal of the cassette and replacement of the 1X PBS with conditioned media. The magnet was then removed and the collection plate moved to an incubator for culture of isolated cells

5.2.7 Fluorescence-activated cell sorting (FACS). GFP-HeLa cells were mixed with HeLa cells at ratios of $1:10^4$, $1:10^5$ and $1:10^6$ in complete media. For the $1:10^4$ and $1:10^5$ ratios, a total of 1,000,000 cells were used while 4 X 10^6 cells were employed for the $1:10^6$ mixture. The cell mixtures were then split into two aliquots, one to be separated by FACS and the other cultured on the pallet arrays with the goal of isolating the GFP-HeLa cells. Cells were separated based on forward and side scatter, and GFP fluorescence using a singlet-cell gate and 100 μm tip (MoFlo, Beckman-Coulter, Brea, CA). Single cells were deposited into wells of a 96 well glass bottom plate preloaded with 100 μL of conditioned media (Auto Clone, Beckman-Coulter, Brea). Wells with cells were identified by microscopy and cultured in conditioned media for 7 days. After that time, the cells were again examined and colony formation was determined. In addition to the aliquot of cells to be sorted, the FACS system also utilized an additional 10,000 cells (50:50 HeLa/GFP-HeLa) to set the sort parameters.

5.3 Results and Discussion

5.3.1 Design of large-scale micropallet arrays. To identify cells occurring at frequencies as low as 1 in 10^6, arrays accommodating large numbers of cells were fabricated. Arrays (10.1 × 7.1 cm) with 1.3 million micropallets (50 × 50 × 75 μm (L × W × H) 25 μm interpallet gap) were fabricated on a glass substrate (Fig. 1A).[25] Every 50^{th} and 51^{st} element was replaced with a single 125 × 125 μm square pallet imprinted numbers to assist in identifying pallet location on the array. The micropallets were composed of 1002F photoresist with 0.25% γFe_2O_3 nanoparticles wt./wt. to enable efficient collection of released elements within a magnetic field.[27] These large-scale arrays contained 130 times the number of micropallets as a standard size micropallet arrays (10,000 micropallets). This substantially reduced the fabrication costs, time and reagents necessary for assaying large numbers of cells.

5.2.2 Image acquisition. Screening of large-scale arrays for rare events requires an efficient means of imaging the array and identifying cells of interest. Numerous factors should be addressed when developing a system for high-throughput imaging including: screening duration, cellular fluorescence intensity and pixel number per cell. Minimizing array screening time was desired to reduce experimental times and diminish cell exposure to room temperature/atmospheric CO_2 levels.[29] Array imaging times were dominated by the time for image acquisition and stage movement. Analysis of fluorescence images demands cellular fluorescence to be significantly brighter than the background signal. Fluorescence illumination of cells should be minimal to reduce imaging time along with photobleaching[30] and phototoxicity.[31] Another preference of image acquisition is for a

pixel size that maximizes the number of pixels/cell to generate high resolution images and to reduce the impact of camera noise.

An automated wide-field epifluoresence imaging system was designed to meet the above requirements for efficient screening of large micropallet arrays. A MVX10 macroview microscope was employed to generate high quality images at low magnification. This microscope offers large field of view with microscope objectives (0.63 X – 2.0 X) of high numerical apertures (N.A.) ranging from 0.15 to 0.50. Additionally, the microscope body possessed a variable zoom drive that expanded the total magnification of the microscope from 0.4 to 12.6. A high N.A. objective was crucial to efficiently collecting the fluorescence signal since the light gathering power of an objective for epi-illumination (F_{epi}) is governed by the equation:

$$F_{epi} = 10^4 \text{ x } NA_{obj}^4 \text{ / } M^2$$

where M is the magnification. This equation exemplifies the utility of the 1 X MVX10 objective (N.A. 0.25) for wide-field imaging which provides 1526 × greater F_{epi} than that generated by a standard 1 X objective (N.A. 0.04), such as the 1X Nikon Plan UW. When this system was combined with an ORCA-Flash4.0 sCMOS camera, a large field of view ranging from 1,225 mm^2 to 1.17 mm^2 was achievable (Table 1). The ORCA-Flash 4.0 was utilized because it offered excellent sensitivity (>50% from 450 – 750 nm), low noise (1.3 e- at 100 frames/s), high-speed (100 frames/s) and high field of view/resolution (4.0M pixels at 6.5 µm x 6.5 µm). This imaging system generated pixel sizes of 17.10 µm – 0.53 µm as the field of view changed from 1,225 mm^2 to 1.17 mm^2, respectively.

The camera imaging, microscope stage and focus adjustments were controlled by a custom Matlab program to automate image acquisition. The efficiency of system

automation was assessed by screening a 10.1 cm × 7.1 cm micropallet array. Prior to imaging the corners of the arrays were identified to define the array perimeter along with the focal plane of micropallet surfaces. During optimization of the image acquisition process the light exposure time was fixed at 200 ms and the microscopy magnification set using both the objective and a variable magnification zoom within the microscope. Complete imaging of the array required between 0.27 and 121 min. as the total magnification changed from 0.4 to 12.6, respectively (Table 1). A 1 X objective with 2 X magnification (166 images/array, 8,100 pallets/image) yielded the most acceptable compromise between pixel size (3.34 μm/pixel) and image acquisition time (3 min 51 s) (Figure 1A insert). This configuration allowed sequential imaging of the 10.1 cm × 7.1 cm micropallet array with brightfield and 3 filter sets, as described below, in approx. 15 min. Additionally, the small pixel size provides multiple pixels per cell (ave. mammalian cell size 10 – 20 μm) which aids in cellular analysis.

5.3.3 Imaging workflow. A defined series of steps are integral to automating micropallet array screening, image processing and cell identification as outlined in Figure 1B. Initially, the system parameters were user defined in a Matlab graphical user interface (GUI) that included: setting imaging channels and exposure times, size exclusion limits and a threshold intensity value. Micropallet array boundaries and the pallet array focal plane were acquired by manually imaging the corners of the array by brightfield microscopy. Although the glass slide and microscope stage have excellent flatness, micron size particles on either substrate can skew the focal plane by several microns over the length of the array. The micropallet array was then sequentially screened using both brightfield and fluorescence microscopy. Brightfield images were

acquired to aid in cell identification and to report micropallet addresses using the numbered micropallets. Fluorescence images were acquired at the appropriate fluorescence wavelengths for the fluorophore in the target cells and at other wavelengths for identification of non-cellular artifacts. The system parameters for imaging a 10.1 × 7.1 cm array were optimized by screening an array containing GFP-HeLa cells intermixed with an abundance of HeLa cells. GFP-HeLa cells were utilized as target cells due to their high, stable fluorescence intensity. The system was optimized for identifying target cells by imaging the array with a FITC (Ex. 470±20, Dichroic 495, Em. 525±25) (GFP-HeLa cells), DAPI (Ex. 350±25nm, Dichroic 400, Em. 460±25nm) and TxRED (Ex. 545±15, Dichroic 570 Em. 620±30) filter set. Imaging parameters were screened for their effectiveness in correctly identifying GFP-HeLa cells while minimizing false positive reports.

5.3.4 Image processing. Before cell identification, image acquisition and pre-processing of raw images were necessary to reduce background noise. Reduction in the background signals resulting from small air bubbles and autofluorescence of the micropallets will allow improved discrimination between target cells and artifacts during image analysis. The system parameters were optimized by analyzing four images acquired from a pallet array loaded with a 1:10 mixture of GFP-HeLa cells to HeLa cells. Strategies for improving the quality of images prior to analysis were evaluated by measuring the signal-to-noise (S/N) ratio. For this initial image processing, a "signal" was defined as any item that when illuminated with light generated a fluorescence signal irrespective of whether it was due to cellular fluorescence or non-cellular light scatter. The "noise" was a product of the autofluorescence generated by the micropallets and air

bubbles. The signal-to-noise (S/N) ratio was maximized by optimizing the exposure dose for each filter set, as shown in Figure 3A. Optimal exposure times were selected as that in which increasing the time no longer sufficiently increased the S/N ratio. For GFP-HeLa cells, optimal exposure times were determined to be 182 ± 7 ms, 196 ± 4 ms and 304 ± 12 ms for the FITC, Texas Red, and DAPI filter sets, respectively. The FITC channel had a definite peak whereas the Texas Red and DAPI channels reached a plateau in the S/N ratio. The S/N peak in the FITC channel was due to saturation of the camera pixels by the highly fluorescent GFP-HeLa cells at 182 ± 7 ms exposures. Conversely, the signal intensity afforded by the noncellular debris did not saturate the camera over the exposure times examined but rather reached an inflection point where the light scatter intensity increased proportionately with the background.

Increases in the S/N ratio was further attained by performing noise filtering and background subtraction on the images.[32] Various methods were screened for their ability to distinguish the micropallet autofluorescence and large bright areas (such as scatter from large bubbles) from objects of interest (Figure 3C-F). Five different were tested to increase the S/N ratio for the FITC images: adaptive wiener filtering (Figure 3B.2), two top hat filtering strategies (Figure 3B.3 and 3B.5) and a combination of noise filtering and background subtraction (Figure 3B.4 and 3B.6). The background subtraction strategy that provided the greatest increase in the S/N ratio was the modified morphological top hat filter without any adaptive noise filtering (97 ± 7% S/N increase). The modified morphological top hat filter also generated high S/N ratios when applied to the DAPI and TxRED images (data not shown). Along with improving the S/N ratio, the modified top hat filter corrected for uneven illumination in the epi-fluorescent system. For these

reasons this image processing strategy was employed prior to data analysis in all subsequent experiments.

5.3.5 Image analysis. To quickly identify cells on the array, background subtracted images were segmented, excluding signals with low intensity and those created by the light scatter of non-cellular artifacts. These imaging parameters were screened for their effectiveness at achieving high sensitivity while minimizing false positive reports. Sensitivity in the FITC channel was defined as the percentage of user-identified GFP-HeLa cells that were counted following image processing and segmentation. For the DAPI and Texas Red channels, sensitivity was reported as the percentage of user-identified highly fluorescent artifacts (dust, air bubbles, etc.) that were correctly categorized. Initially the fluorescence intensity thresholds (minimum pixel intensity cutoffs) were established to remove low intensity fluorescence signals generated by micropallet autofluorescence and small air bubbles. In order to minimize false positives, the largest threshold value was selected that maintained 100% sensitivity. Optimal threshold values of 2010 ± 180, 345 ± 40 and 90 ± 20 were identified for FITC, DAPI and Texas Red filter sets respectively (Figure 4). These fluorescence threshold cutoffs were implemented prior to further image analysis.

The remaining false positive signals created by light scattering artifacts were reduced in the FITC images through sized-based filtering and by subtracting signals recorded in the negative-control filter sets (DAPI, Texas Red). A size filter which eliminates objects with an area larger or smaller than a user-defined maximum and minimum was able to eliminate 30 ± 14% false positive results while maintaining 100% sensitivity (minimum: 5 μm diameter, maximum: 40 μm diameter). The minimum pixel

count per cell must be > 1 to allow removal of the small artifacts while not affecting the sensitivity. Some non-cellular entities generate a greater fluorescence signal than the threshold cutoff and cannot be removed by size filtering, thereby increasing the false positive count.

Many of the artifacts that scatter light in the FITC channel also generate signals when imaged by other fluorescence filter sets; demonstrated by the dust particle that scatters light with the FITC, DAPI and Texas Red filter sets (Figure 2C-G). This phenomenon was exploited to remove these signals from the FITC images. Subtraction of the DAPI and Texas Red images from the FITC data yielded a reduction in false positives of 46 ± 11%. Both negative control filter sets were employed because many artifacts demonstrated varied intensities of light scatter at different wavelengths. When both negative control filters and size filters were used together, the false positive results were reduced by 68 ± 14% while still maintaining 100% sensitivity. Target cell positions were then identified by their absolute position on the XY stage and manually by utilizing brightfield images and the numbered pallets of the large array. This allowed the user to quickly screen through the objects of interest at a higher magnification and confirm true positives.

5.3.4 Isolation of rare cells. The efficiency of the micropallet system for enumerating and isolating low abundance cells was evaluated by sorting GFP-expressing HeLa cells intermixed with wild type HeLa cells at ratios of $1{:}10^4$, $1{:}10^5$ and $1{:}10^6$. Arrays were imaged for the GFP-HeLa cells using the optimal conditions and automated imaging analysis software described above. GFP-HeLa cells were identified in the samples with target to background cell ratios of $1{:}10^4$, $1{:}10^5$ and $1{:}10^6$ with efficiencies

of 96%, 100% and 100%; respectively (Figure 5). The optimized image processing and analysis gave on average 48 ± 20 false positive signals over the total of 6 arrays analyzed. Enumeration sensitivities were confirmed by inspecting the micropallet arrays for GFP-HeLa cells following removal of the identified target cells as described below. Following 7 days incubation of the post-sorted arrays, the arrays were manually screened for the presence of small GFP-HeLa cell colonies. No GFP-HeLa cells could be found indicating that there were no false-negative cells but rather the 96% enumeration sensitivity for the $1:10^4$ cell sample was a result of statistical variations common when working with small cell quantities.

Full utility of the micropallet technology lies not merely in the enumeration of cells but in the ability to isolate individual cells from the heterogeneous population. Along with the fluorescence-based target identification, the array was imaged with brightfield microscopy to ascertain the coordinates of the target cells. Numbered micropallets were distributed throughout the array so that the micropallets with GFP-HeLa cell could be located when transferred to an inverted microscope paired with an external Nd:YAG laser. The GFP-HeLa cells cultured at abundances of $1:10^4$, $1:10^5$ and $1:10^6$ identified in the previous section were each detached from the array and then magnetically collected onto numbered PDMS multiwell plates with 100% collection efficiency. Following 7 days of incubation; 45, 5 and 2 of the single GFP-HeLa cells formed small colonies from the micropallets collected from the arrays plated with GFP-HeLa cells at ratios of $1:10^4$ (48 cells collected), $1:10^5$ (5 cells collected) and $1:10^6$ (2 cells collected), respectively (Figure 5). Additionally, no contaminating nonfluorescent HeLa cells were present on the collection plate which demonstrates the high purity

attained in isolating rare cells on micropallets. These results suggested that large arrays of micropallets combined with sensitive image acquisition and analysis can efficiently enumerate and isolate low abundance cells.

5.3.5 Comparison of rare cell sorting with FACS. A direct comparison of micropallet sorting with FACS for sorting 10^3 or 10^6 cells where the ratio of target fluorescent cells to background cells was 1:99 has been previously reported.[26] The FACS system was unable to isolate cells when loaded with 10^3 cells but could efficiently isolate target cells from samples composed of 10^6 cells. Here a comparison was made between micropallet technology and FACS for isolating low numbers of rare target cells. Standard mixtures of GFP-HeLa cells and HeLa cells in complete media at ratios of $1:10^4$, $1:10^5$ and $1:10^6$ were first generated and split into two aliquots for analysis by each technology. Half the sample, 500,000 cells for the ratios of $1:10^4$ and $1:10^5$ and 2,000,000 cells for the ratio of $1:10^6$, were sorted using the micropallet arrays as described in the previous section. In parallel experiments the other half of the sample was sorted by FACS. The FACS system was very accurate at identifying the GFP-HeLa cells, though calibration with a concentrated cell suspension was required prior to cell sorting to attune the system gating. Target cells were sorted into individual chambers of a 96 well plate and allowed to culture for 7 days. When imaged for the presence of colony formation; 5 colonies were observed for the $1:10^4$ mixture (50 cells sorted), no cell colonies present for the $1:10^5$ mixture (5 cells sorted) and no colonies formed from the $1:10^6$ mixture (2 cells sorted) (Figure 5). High loss of cells and low collection viability are common drawbacks of FACS which result in low sorting yields for rare cells. These weaknesses for the basis for the recommendation that FACS systems not be used for isolating single cells from

mixtures at frequencies less 0.01%.[14] For these reasons numerous rounds of sorting or sample enrichment are commonly employed prior to isolating rare cells by FACS. Conversely, cells sorted by micropallet arrays formed colonies with excellent efficiency. The ability to adjust the imaging analysis parameters during or following image acquisition and prior to sorting decisions provides high sorting efficiencies of unknown rare specimens which are not feasible with single time frame sorting techniques such as FACS and microfluidics.

5.4 Conclusions and Future Work

An array in excess of 1 million micropallets has been developed for capturing and isolating rare cells from a heterogeneous mixture. To quickly identify cells on the array, image processing and analysis was automated. Important factors in the successful identification of rare cells include the camera exposure time, image background subtraction, threshold selection and reduction of false positives by size-based filtering and negative control filter sets. Efficient sorting of adherent cells expressed at abundances down to one in a million was demonstrated. The ability to isolate rare cells without the need for multiple rounds of sorting will allow new biological applications where the inability to proficiently acquire the required cells is prohibited. Automated thresholding techniques are currently being evaluated for their effectiveness at identifying target cells which would eliminate the necessity of calibrating the imaging parameters with control cells.[33] Importantly, this technique will allow multi-parameter and adjustable image cytometry permitting efficient identification of unknown rare cell types without the requirement of any control measurements. Though automated screening of the array can be performed in <15 min, the precise micropallet positions are manually recorded and

the arrays are transferred to an inverted microscope for user controlled release of select micropallets. Incorporation of a Nd:YAG laser integrated inverted microscope with the MVX10 Macroview system would allow high resolution image analysis of initially screened micropallets followed by automated microstructure release.

Cell lines possessing low abundance cancer stem cell subpopulations will be screened on the large micropallet arrays to demonstrate the utility of this technology for isolating rare cell. The MCF-7 cell line has been identified as having cancer stem cells at low frequencies $<10^5$.[10] These breast cancer stem cells will be identified by their expression of CD44 and absence of CD24 surface markers. Micropallets carrying target cells will then be isolated from the array and the rare cell cultured to form small $CD44^+/CD24^{-/low}$ colonies. The large micropallets arrays will also allow isolation of slow growing or non-proliferating cells not easily obtainable by other techniques in which the target cells are easily overgrown by other cell types, such as cells transfected with a low efficiency tumor suppressor gene. This technology can also be adapted for isolating viable circulating tumor cells directly from whole blood without the requirement removal of the erythrocytes and lymphocytes, as described in Chapter 6. Micromolded microraft arrays could benefit from these advances as they have shown promise for easily fabricating large arrays[34] and isolating cells with high efficiency and low contamination.[35] The strategies developed in this report to quickly scan and analyze a large area will be useful for identifying cells on other platforms such as various other large microarrays, high throughput parallel microfluidic devices and centrifugal cell sorting devices. Along with sorting rare cells the advances developed in this report will find utility in isolating stem cell colony portions. These studies require a very low density

of cells plated on an array to reduce cross contamination as colonies expand and a large enough population of cells plated to isolate a significant quantity of cells for further applications.

5.5 Tables and Figures

Objective/Mag	Pixel Size (um)	Field of View (mm^2)	Images per Array[a]	Imaging Time (min)[ab]
0.63X/0.63	17.10	1225.88	7	0.27
0.63X/2.00	5.27	116.46	67	1.73
0.63X/6.30	1.68	11.79	657	13.65
1X/0.63	10.64	475.25	17	0.55
1X/2.00	3.34	46.74	166	3.85
1X/6.30	1.05	4.60	1685	32.94
2X/0.63	5.40	122.32	64	1.67
2X/2.00	1.68	11.84	654	13.58
2X/6.30	0.53	1.17	6616	120.66

[a] Image number and time from screening of a 10.1 x 7.1 cm array [b] All images taken at 200 ms exposure

Table 5.1 Effects of MVX-10 microscope objective on imaging parameters.

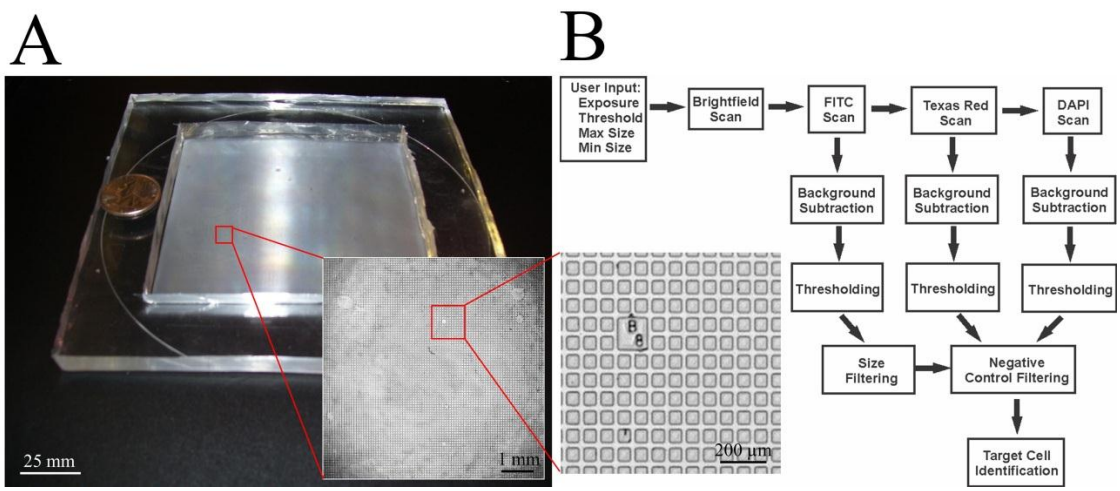

Figure 5.1 (A) Photograph of large micropallet array. Inserts show a region of the array magnified ×4.3 and ×30. (B) Schematic of the process flow for image acquisition and data analysis.

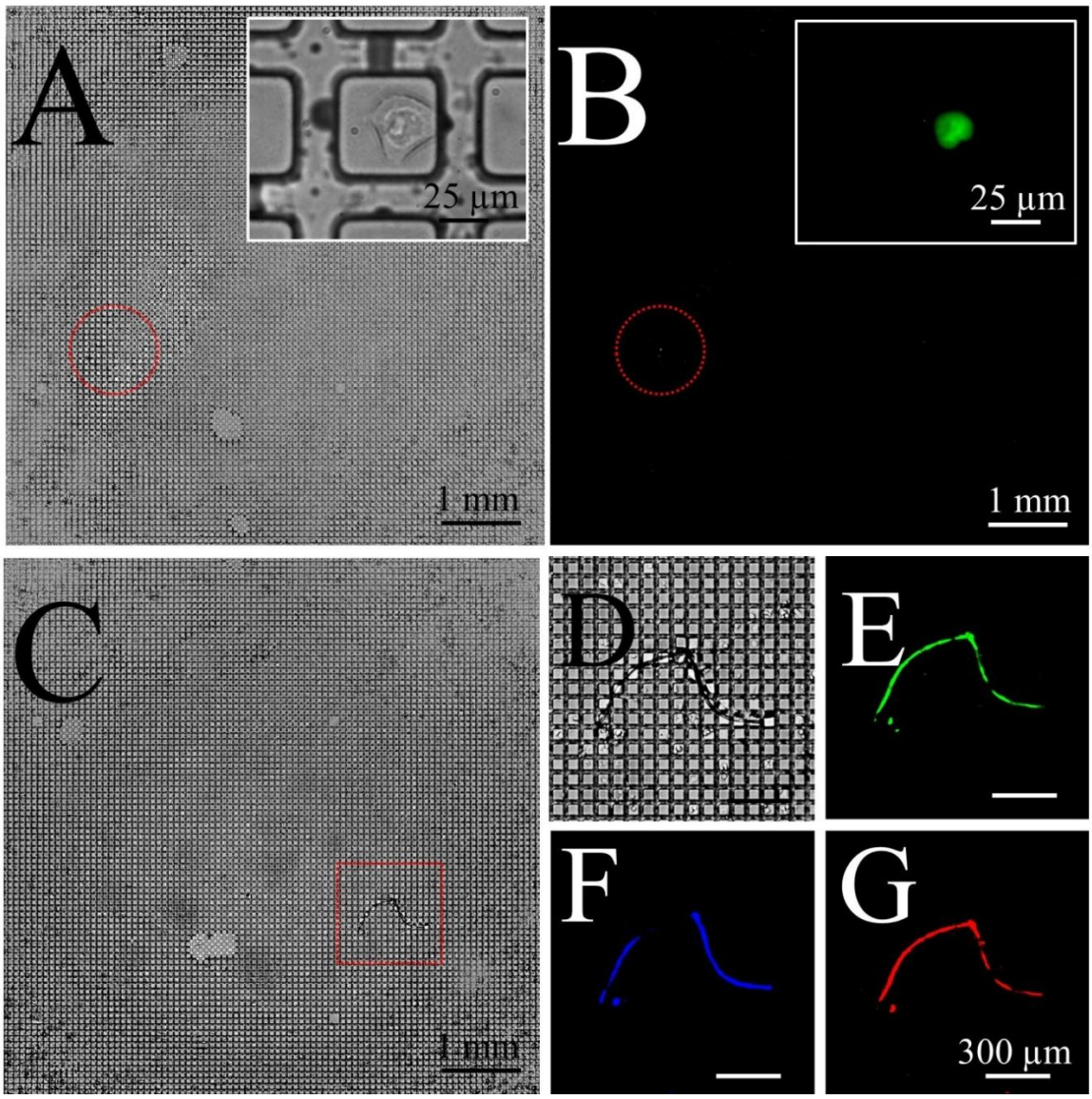

Figure 5.2 Micrographs of HeLa cells admixed with a low abundance of GFP-HeLa cells on micropallets. Raw brightfield and fluorescence images taken with the MVX-10 microscope (1X objective/ 2X zoom) showing identification of a single GFP-HeLa cell (A-B). Insets are of the same GFP-HeLa cell aquired by an inverted microscope with a 60X objective. Brightfield image of a different region of the same array showing the presence of a piece of dust (C) magnified in (D). Magnified fluorescence images highlighting the light scatter generated by the same debris particle when imaged by FITC (E), DAPI (F) and TxRed (G) filter sets.

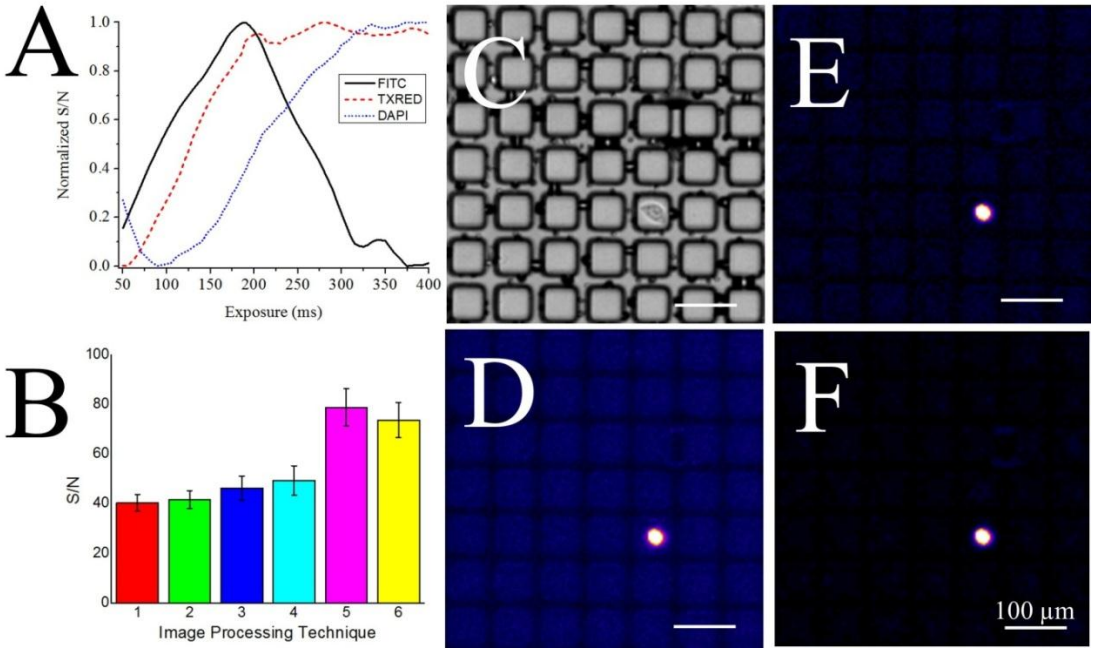

Figure 5.3 Image processing. Normalized S/N from images of micropallet arrays (n = 4) vs exposure time for three different filter sets; DAPI (Ex. 350±25nm, Dichroic 400, Em. 460±25nm), FITC (Ex. 470±20, Dichroic 495, Em. 525±25) and TxRed (Ex. 545±15, Dichroic 570 Em. 620±30) (A). The S/N ratio was normalized from 0 to 1 for each filter. Optimal exposure times were selected where increasing the exposure no longer sufficiently increased the S/N ratio for varying background subtraction techniques. S/N ratio for varying background subtraction techniques applied to fluorescence images of GFP-HeLa cells on micropallets (B). The S/N ratio was calculated for the raw image (1) and image following background subtraction by adaptive wiener filtering (2), top hat filtering (3), adaptive wiener filtering (4), adaptive top hat filtering (5) and modified top hat filtering (6). The top hat filter used a disk shaped structuring element 50 µm in diameter. The modified top hat used a morphologically closed (square structing element of 75 × 75 µm) which was then morphologically opened (disk structuring element 50 um in diameter) and subtracted from the orifinal image. Optical (C) and fluorescence (D-F) images of a GFP-HeLa cell on an array of micropallets imaged with a FITC filter set. Pseudocolor fluorescence images are of the raw image (D) and following background subtraction by adaptive wiener filtering (E) and modified top hat filtering (F).

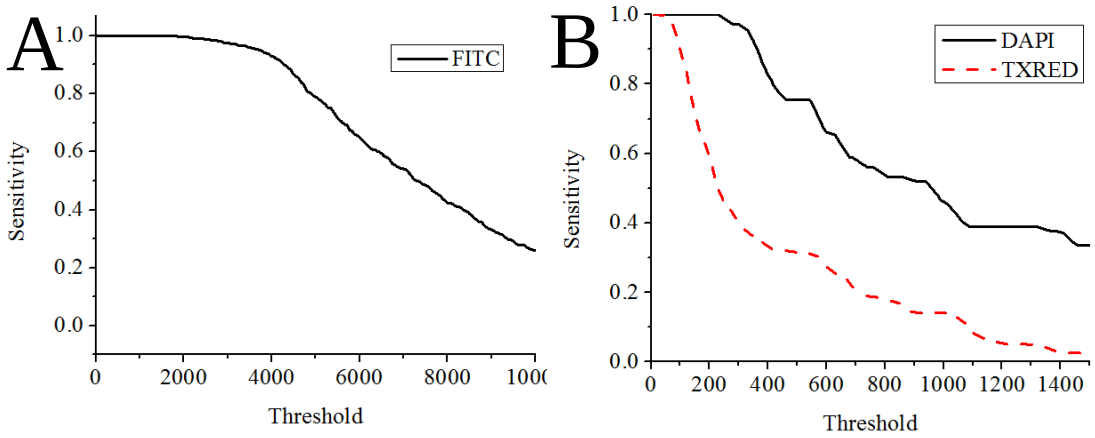

Figure 5.4 Sensitivity vs Threshold value curves to optimize selected threshold values for each filter set in order to achieve 100% sensitivity and minimize false positives.

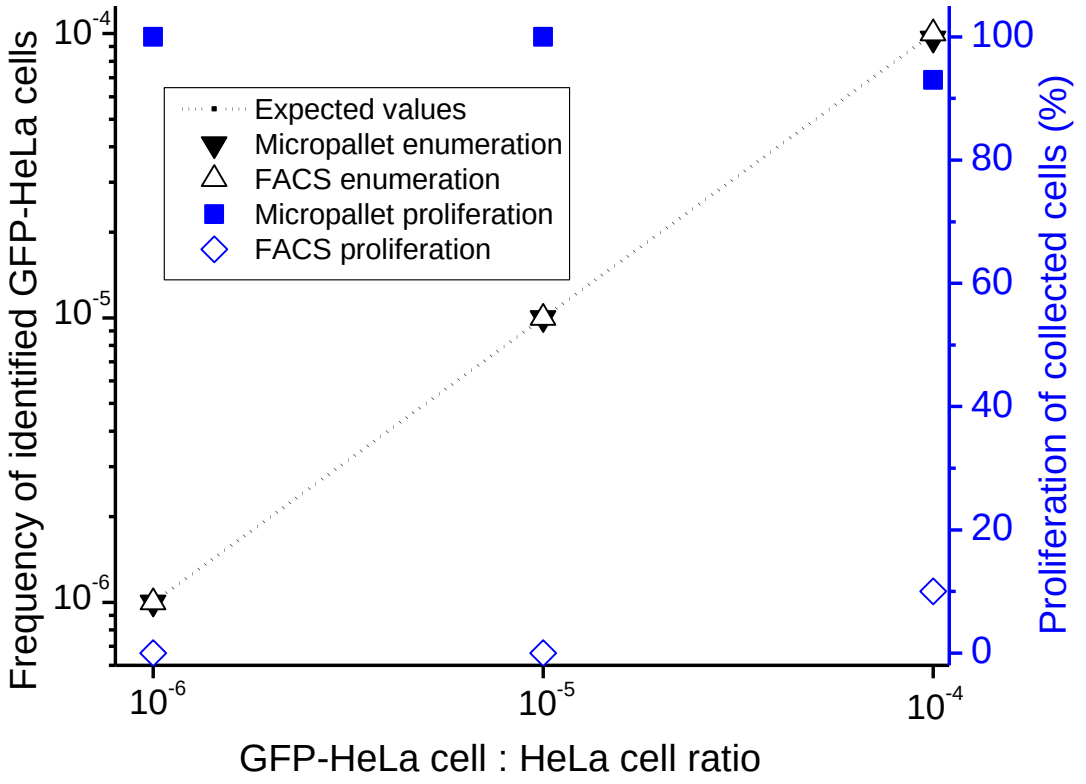

Figure 5.5 Efficiencies of low abundance GFP-HeLa cell sorting by micropallet arrays and FACS. GFP-HeLa cells admixed into a population of HeLa cells at frequencies of 10^{-6} – 10^{-4} were detected by their fluorescence in FITC channels (black triangles). Following sorting into a multiwell plate the proliferation was recorded as the percentage of cells that formed small colonies after 7 days incubation (blue squares).

5.6 References

1. Siegel R, Naishadham D, Jemal A. Cancer Statistics, 2012. *CA: A Cancer Journal For Clinicians*. 2012;62(1):10-29.

2. Chambers A, Groom A, MacDonald I. Dissemination and growth of cancer cells in metastatic sites. *Nature Reviews Cancer*. 2002;2(8):563-572.

3. Luzzi KJ, MacDonald IC, Schmidt EE, et al. Multistep nature of metastatic inefficiency - Dormancy of solitary cells after successful extravasation and limited survival of early micrometastases. *American Journal of Pathology*. 1998;153(3):865-873.

4. Weiss L. Metastatic Inefficiency. *Advances in Cancer Research*. 1990;54:159-211.

5. Reya T, Morrison SJ, Clarke MF, Weissman IL. Stem cells, cancer, and cancer stem cells. *Nature*. 2001;414(6859):105-111.

6. Al-Hajj M, Wicha M, Benito-Hernandez A, Morrison S, Clarke M. Prospective identification of tumorigenic breast cancer cells. *Proceedings of the National Academy of Sciences of the United States of America*. 2003;100(7):3983-3988.

7. Collins AT, Berry PA, Hyde C, Stower MJ, Maitland NJ. Prospective identification of tumorigenic prostate cancer stem cells. *Cancer Research*. 2005;65(23):10946-10951.

8. Bonnet D, Dick JE. Human acute myeloid leukemia is organized as a hierarchy that originates from a primitive hematopoietic cell. *Nature Medicine*. 1997;3(7):730-737.

9. Singh SK, Hawkins C, Clarke ID, et al. Identification of human brain tumour initiating cells. *Nature*. 2004;432(7015):396-401.

10. Sheridan C, Kishimoto H, Fuchs RK, et al. CD44(+)/CD24(-) breast cancer cells exhibit enhanced invasive properties: an early step necessary for metastasis. *Breast Cancer Research*. 2006;8(5).

11. Gudjonsson T, Villadsen R, Nielson HL, Ronnov-Jensen L, Bissell MJ, Petersen OW. Isolation, immortalization, and characterization of a human breast epithelial cell line with stem cell properties. *Genes & Development*. 2002;16:693-706.

12. Ponti D, Costa A, Zaffaroni N, et al. Isolation and in vitro propagation of tumorigenic breast cancer cells with stem/progenitor cell properties. *Cancer Research*. 2005;65(13):5506-5511.

13. Scriba TJ, Purbhoo M, Day CL, et al. Ultrasensitive detection and phenotyping of CD4+ T cells with optimized HLA class II tetramer staining. *Journal of Immunology*. 2005;175(10):6334-6343.

14. Ibrahim S, van den Engh G, Kumar A, Galaev I, Mattiasson B. Flow cytometry and cell sorting. *Cell Separation: Fundamentals, Analytical and Preparative Methods*. 2007;106:19-39.

15. Ibrahim S, van den Engh G. High-speed cell sorting: fundamentals and recent advances. *Current Opinion in Biotechnology*. 2003;14(1):5-12.

16. Cristofanilli M, Budd G, Ellis M, et al. Circulating tumor cells, disease progression, and survival in metastatic breast cancer. *New England Journal of Medicine*. 2004;351(8):781-791.

17. Nagrath S, Sequist LV, Maheswaran S, et al. Isolation of rare circulating tumour cells in cancer patients by microchip technology. *Nature*. 2007;450(7173):1235-1239.

18. Kang JH, Krause S, Tobin H, Mammoto A, Kanapathipillai M, Ingber DE. A combined micromagnetic-microfluidic device for rapid capture and culture of rare circulating tumor cells. *Lab on a Chip*. 2012;12(12):2175-2181.

19. Vona G, Sabile A, Louha M, et al. Isolation by size of epithelial tumor cells - A new method for the immunomorphological and molecular characterization of circulating tumor cells. *American Journal of Pathology*. 2000;156(1):57-63.

20. Gascoyne P, Noshari J, Anderson T, Becker F. Isolation of rare cells from cell mixtures by dielectrophoresis. *Electrophoresis*. 2009;30(8):1388-1398.

21. Hu X, Bessette P, Qian J, Meinhart C, Daugherty P, Soh H. Marker-specific sorting of rare cells using dielectrophoresis. *Proceedings of the National Academy of Sciences of the United States of America*. 2005;102(44):15757-15761.

22. Seidl J, Knuechel R, Kunz-Schughart LA. Evaluation of membrane physiology following fluorescence activated or magnetic cell separation. *Cytometry*. 1999;36(2):102-111.

23. Krivacic R, Ladanyi A, Curry D, et al. A rare-cell detector for cancer. *Proceedings of the National Academy of Sciences of the United States of America*. 2004;101(29):10501-10504.

24. Hsieh H, Marrinucci D, Bethel K, et al. High speed detection of circulating tumor cells. *Biosensors & Bioelectronics*. 2006;21(10):1893-1899.

25. Wang Y, Young G, Bachman M, Sims C, Li G, Allbritton N. Collection and expansion of single cells and colonies released from a micropallet array. *Analytical Chemistry*. 2007;79(6):2359-2366.

26. Wei X, Sims C, Allbritton N. Microcup Arrays for the Efficient Isolation and Cloning of Cells. *Analytical Chemistry*. 2010;82(8):3161-3167.

27. Gach P, Sims C, Allbritton N. Transparent magnetic photoresists for bioanalytical applications. *Biomaterials*. 2010;31(33):8810-8817.

28. Wang Y, Sims C, Marc P, Bachman M, Li G, Allbritton N. Micropatterning of living cells on a heterogeneously wetted surface. *Langmuir*. 2006;22(19):8257-8262.

29. Freshney RI. Culture of Animal Cells, 6th Ed.: John Wiley & Sons, Inc.; 2010.

30. Song L, van Gijlswijk RP, Young IT, Tanke HJ. Influence of fluorochrome labeling density on the photobleaching kinetics of fluorescein in microscopy. *Cytometry*. 1997;27(3):213-223.

31. Stephens DJ, Allan VJ. Light microscopy techniques for live cell imaging. *Science*. 2003;300(5616):82-86.

32. Soille P. Morphological Image Analysis: Principles and Applications. New York: Springer; 1999.

33. Sezgin M, Sankur B. Survey over image thresholding techniques and quantitative performance evaluation. *Journal of Electronic Imaging*. 2004;13(1):146-168.

34. Wang Y, Phillips C, Xu W, et al. Micromolded arrays for separation of adherent cells. *Lab on a Chip*. 2010;10(21):2917-2924.

35. Gach P, Wang Y, Phillips C, Sims C, Allbritton N. Isolation and manipulation of living adherent cells by micromolded magnetic rafts. *Biomicrofluidics*. 2011;5(3).

Chapter 6: Capture and Isolation of CTCs Directly from Whole Blood with Micropallet Arrays

6.1 Introduction

Advances in clinical technologies have revealed the significance of low abundance biomolecules or cells for monitoring patient health. Many studies have demonstrated the utility of a non-invasive liquid biopsy towards monitoring disease progression or patient health by analyzing rare biomolecules in blood.[1,2] Recent reports have hypothesized the importance of information that circulating tumor cells (CTCs) may provide regarding the phenotype and metastatic behavior of an individual's primary tumor.[3-5] Efficient strategies to isolate these low abundance cells from peripheral blood may enable novel clinical diagnostics as well as better understanding of cancer cell biology. Many recent studies have sought to capture CTCs from the peripheral blood of patients or animal models with cancer. Magnetic-activated cell sorting (MACS) and fluorescence-activated cell sorting (FACS) are the oldest methods in use for isolating CTCs. MACS technology utilizes antibody-labeled magnetic beads specific against the CTCs surface markers, typically epithelial cell adhesion molecule (EpCAM). Numerous studies interested in the enumeration and analysis of CTCs utilize MACS; including the MagSweeper[6] and CellSearch, the only FDA-approved CTC detection strategy. However, MACS sorting is only capable of collecting CTCs based on their surface markers, rarely provides 100% collection efficiency and is plagued by contaminating cells such as lymphocytes and other nonspecifically captured cells. FACS is a commonly used

technology for retrieving pure cells from a heterogeneous population. However, the low abundance of CTCs present in blood makes this serial analysis technique inefficient in isolating the CTCs. Sample preparation is therefore required to remove the erythrocytes prior to cell sorting; common strategies include erythrocyte lysis, gradient centrifugation and MACS.[7] However, these protocols often result in by loss of CTCs as well as reduced cell viability.

The inefficiency of these technologies at isolating CTCs has spurred the development of a multitude of new capture technologies to sort and analyze CTCs. Microfluidic based devices to isolate CTCs enhance substrate-cell interactions by increasing the effective surface area[8,9] or by generating chaotic cell mixing.[10,11] While these technologies have been demonstrated to be highly efficient at capturing and analyzing CTCs, their utility for collecting viable CTCs is limited due to the strong antibody binding. Helzer et al. isolated cells cultured on a plastic CTC-chip by releasing the micropillers by laser pressure catapulting (LPC), however, this protocol required removal of the fluid and consequently did not allow isolation of viable CTCs.[12] Microfluidic devices have also achieved isolation of CTCs from blood by employing enrichment within microwell arrays,[13] fluidic switching[14] and inertial focusing.[15,16] Other strategies for collecting cells following enrichment via antibody binding have sought to release cells from the substrate by trypsin digestion of the antibody-antigen bonds[17-19] or introduction of a releasable linker to the antibody-substrate complex.[20,21] While efficient at capturing CTCs with known surface proteins, these devices are not well suited for capturing unknown CTCs or releasing and collecting individual CTCs. Devices capable of CTC capture based on their native cellular properties have been developed to account

for these limitations. Dielectrophoresis has been utilized to enrich CTCs, however, this technique requires removal of the erythrocytes to obtain a reproducible dielectrophoretic response of the CTCs.[22] Numerous devices have taken advantage of the size different between CTCs and the smaller erythrocytes and lymphocytes, which constitute the majority of whole blood. Size-selective microfilters have been developed in a variety of geometries to effectively capture CTCs from whole blood[23-25] These size-based collection strategies are able to capture and collect CTCs with excellent viability, however, they are unsuccessful at capturing small CTCs and also suffer from clogging by lymphocytes when high blood volumes are filtered. Generally the demonstration of device utility for these size-based methods is limited to blood with added tissue-cultured tumor cell lines such as MCF-7 cells. Though the tissue-cultured cells captured by these devices retain a high level of proliferation; few reports have successfully demonstrated the ability to culture CTCs acquired from animal models and culture of CTCs from patients has not yet been achieved.[26-28] Isolation and culture of these CTCs could be useful in understanding the requirements for CTC extravasation and metastasis formation.

Our lab has previously demonstrated the utility of arrays of releasable elements microfabricated on glass substrates teamed 'micropallets' for sorting single adherent cells.[29] Micropallet arrays have shown success in sorting single cells in a mixed cell population with low reagent requirements and at a high post sorting yield and viability. Additionally, this technology has been demonstrated to be highly versatile for isolating a small numbers of target cells from mixed populations especially when the target cells are present at low abundance.[29] Functionalization of the micropallet surfaces with extracellular matrixes (ECM) or capture antibodies has previously been demonstrated to

provide pre-enrichment of target cells prior to sorting.[30,31] In this report, the potential for using micropallet arrays to isolate tumor cells directly from whole blood is examined. As a proof-of-principle, MCF-7 cells were mixed into whole blood and loaded directly onto micropallet arrays functionalized with either fibronectin or anti-EpCAM. The capture efficiency of MCF-7 cells intermixed diluted varying amounts into blood was compared for both surface modifications.

6.2 Materials and Methods

6.2.1 Reagents. The following materials were obtained from the Aldrich Chemical Company (St. Louis, MO): iron(III) chloride tetrahydrate, iron(III) chloride anhydrous, iron(III) nitrate nonahydrate, toluene (reagent grade), triarylsulfonium hexafluorophosphate salts, mixed, 50% in propylene carbonate, γ-butyralactone (GBL, 99+%), 1-methoxy-2-propanol (1002F developer, 98.5%), N-(3-dimethylaminopropyl)-N´-ethylcarbodiimide hydrochloride (EDC), cerium(IV) ammonium nitrate and acrylic acid. EPON resin 1002F (phenol, 4,4'-(1-methylethylidene)bis-, polymer with 2,2'-[(1-methylethylidene) bis(4,1-phenyleneoxymethylene]bis-[oxirane]) was obtained from Miller-Stephenson (Sylmar, CA) and (heptadecafluoro-1,1,2,2-tetrahydrodecyl)trichlorosilane was purchased from Gelest Inc (Morrisville, PA). Dulbecco's modified Eagle's medium (DMEM), fetal bovine serum (FBS), 1X phosphate buffered saline (PBS), pH 7.4, 0.05% trypsin with EDTA solution and penicillin/streptomycin were received from Invitrogen (Carlsbad, CA). Sylgard 184 silicone elastomer kit (PDMS) was received from Dow Corning (Midland, MI). Fibronectin extracted and purified from human plasma was obtained from Chemicon

International Inc. (Temecula, CA). All other chemicals were procured from Fisher Scientific (Pittsburgh, PA).

6.2.2 Fabrication of micropallet arrays and PDMS chambers. Micropallets were fabricated out of 1002F photoresist containing 0.25% oleic acid functionalized γFe_2O_3 nanoparticles by weight percentage, as described previously.[32] Large micropallet arrays with a total size of 101.2×71.3 mm possessing 1,280,448 micropallets on a 1350×950 array (50×50×75 μm (L×W×H) 25 μm gap) were fabricated on large glass slides (B270 150mm diam. x 0.9mm thick, Valley Design Corp., Santa Cruz, CA), as described in chapter 5. A numbered was placed on the surface of every 50th micropallet on the array. Small scale experiments were performed on arrays consisting of 113×113 micropallets (8.45×8.45mm array) of dimensions 50×50×75 μm (L×W×H) with a 25 μm gap between micropallets fabricated on a microscope slide (75x38x1mm, Fisher Scientific, Pittsburgh, PA), approximately 1:100th the area of the larger micropallet arrays. A plastic cell culture chamber was glued around the array with PDMS and arrays were treated with a hydrophobic perfluoroalkylsilane layer to form virtual air walls.[33]

6.2.3 Micropallet functionalization. Micropallet surfaces were treated with various proteins to aid in cell capture and improve array biocompatibility. Prior to loading with cells, pallet arrays and films were sterilized by rinsing with 95% ethanol and dried in a sterile hood. Excess ethanol was removed with five PBS rinses. For capture of adherent cells, the top surfaces of the pallets on the array were coated with 1 mL of 25 μg/mL fibronectin in PBS for one hour at room temperature. Following surface coating, the array was rinsed 5x with PBS.

Alternatively, pallet tops were functionalized with anti-EpCAM antibody to allow capture of all cells expressing epithelial surface marker antigens. Following creation of the virtual air walls, epoxide rings on the 1002F surface were opened yielding hydroxyl groups by soaking arrays in 1 M nitric acid containing 0.1 M CAN for 2 h as described previously.[34] CAN was then removed by rinsing with deionized water and the arrays were treated for 2 h with a mixture of 10% acrylic acid, 7.5 mM CAN and 75 mM sulfuric acid. The array was then rinsed 5x with deionized water and incubated in PBS for 2 h. Arrays were then rinsed with sodium phosphate buffer (20 mM, pH 4.5) and then placed in 2 wt% N-(3-dimethylaminopropyl)-N´-ethylcarbodiimide hydrochloride (EDC) in sodium phosphate buffer (20 mM, pH 4.5) for 2 h. Following 5 rinses with PBS, protein A/G or FITC-protein A was covalently coupled to the PAA by incubation with 500 µg/mL of the protein in PBS for 2 h. After rinsing the array functionalized with protein A/G with PBS 5x, 100 ug/mL antihuman-epithelial cell adhesion molecule (anti-EpCAM) or FITC-EpCAM in 1X PBS was added for 2 h. All samples were then rinsed 5x with PBS prior to further applications.

6.2.4 Cell culture and array plating. All cells were cultured in DMEM supplemented with FBS (10%), L-glutamine (584 mg L^{-1}), penicillin (100 units mL^{-1}) and streptomycin (100 µg ml^{-1}) in a 37^{o}C incubator with a 5% CO_2 atmosphere. To ascertain the capture efficiency of adherent cell lines from whole blood, GFP-HeLa cells or MCF-7 cells were mixed into sheep's blood (BioChemed Services, Winchester, VA). The sample was then mixed with 20mL media and added to a fibronectin or anti-EpCAM functionalized pallet array and transferred to an incubator for at least a 2 h, to allow the adherent cells time to settle and attach to the substrate. The array was rinsed 5-10x with

PBS to selectively remove the blood components. The cassette was then filled with PBS and covered by a glass slide.

6.2.5 Microscopy. Screening for rare cells over the large micropallet array was achieved through automated array imaging with an MVX-10 macroview microscope (Olympus, Center Valley, PA) paired with image analysis software as described in Chapter 5. Imaging small micropallet arrays and high resolution imaging was performed on an inverted microscope (Eclipse TE300, Nikon, Melville, NY).[29,32]

6.3 Results and Discussion

6.3.1 Micropallet functionalization with anti-EpCAM. Epithelial cell adhesion molecule (EpCAM) antibodies are frequently utilized to capture CTCs owing to the overexpression of EpCAM in numerous human carcinomas.[35] To provide capture of EpCAM-expressing CTCs the micropallet surfaces were functionalized with EpCAM antibody. The epoxide rings of the 1002F were opened to generate hydroxyl groups capable of reacting with the acrylic acid monomer and PAA was grafted onto the pallet top surfaces.[34] Proteins possessing free amino groups could then be covalently linked to the grafted PAA through carbodiimide-mediated amide formation. Effective binding of biomolecules to the micropallet tops was demonstrated by the binding of FITC-labeled protein A. The average fluorescence of the FITC-protein A-coated micropallets was 8520 ± 290, much greater than that for native micropallets (210 ± 30) or native micropallets incubated with FITC-labeled protein A (1080 ± 140). The time required for the grafting process (12 h) was greatly reduced for micropallet functionalization compared to that reported previously (84 h)[34] since the longer incubation times with CAN destroyed the virtual air walls between the micropallets. The extent and amount of EpCAM antibody

loaded on to the pallets was measured by incubation of FITC-EpCAM with arrays possessing native micropallets or protein A/G-functionalized micropallets. A much greater fluorescence intensity was observed for the micropallets coated with protein A/G with respect to native micropallets incubated with FITC-EpCAM or untreated micropallets; 2050 ± 380, 490 ± 100 and 190 ± 40, respectively (Figure 1). Replacement of the virtual air walls by a more rugged micropallet boundary such as; poly(ethylene glycol) (PEG) walls[36], oil walls or through use of microraft arrays which utilize PDMS walls[37] could allow prolonged incubation periods with the CAN solution and likely improve the quantity of anti-EpCAM immobilization to the array surfaces.

6.3.2 Cell capture on micropallets by anti-EpCAM. MCF-7 cells were utilized to model capture of CTCs by anti-EpCAM binding. MCF-7 cells are a breast cancer cell line that exhibits a high expression of EpCAM (509,500 molecules/cell) an order of magnitude higher than the EpCAM expression observed in most CTCs.[38] The effectiveness of cell capture on micropallet surfaces was demonstrated by loading MCF-7 cells onto arrays coated with PAA-protein A/G-anti-EpCAM. MCF-7 cells (10,000 cells) were plated onto the functionalized pallet arrays (with 12,769 micropallets) and incubated for 10 min. Ten images were acquired covering a fraction of the array's total area and the cells in each image were counted. 1127 cells were identified on the 2430 micropallets that were visualized (Figure 2A). The arrays were then inverted and gently agitated to remove unbound and loosely attached MCF-7 cells. Images of the same array were then acquired and the cells counted. 90 ± 8% (n = 3) of the cells remained attached to the arrays (Figure 2B). To determine the specificity of cell capture, 10,000 HeLa cells were added to the anti-EpCAM functionalized arrays and following a 10 min-incubation

imaged as described above (n = 3 arrays, 2430 micropallets imaged, 988 total cells identified). HeLa cells were used as a control for anti-EpCAM binding as they are known to express little to no EpCAM.[39] Only 12 ± 5% of the HeLa cells (118 total cells identified) were retained following inversion and agitation of the array (Figure 2C,D). The reduced collection of HeLa cells relative to MCF-7 cells demonstrated that the mechanism of cell capture was primarily a function of antibody-antigen binding as opposed to non-specific cell adhesion to the substrate.

6.3.3 Tumor cell capture from whole blood. Enrichment of viable CTCs, the tumor cells capable of metastasis formation, has previously been demonstrated by the selective capture of these proliferative cells onto an extracellular matrix.[40] Micropallet arrays are a promising platform for capturing viable CTCs directly from whole blood. As a proof-of-principle, 100 MCF-7 cells were mixed into 1, 10 or 100 µL of whole blood for sorting on the micropallet arrays functionalized with fibronectin. For ease of analysis arrays consisting of 12,769 elements were utilized in place of the larger micropallet arrays. The quantity of blood added to the smaller arrays was equivalent to adding 0.1, 1 and 10 mL of whole blood, respectively to large micropallet arrays, used below. DMEM (2 mL) was added to the blood/MCF-7 mixture to dilute the sample and prevent cell overcrowding in culture. The arrays were placed in an incubator for 8 h to allow the MCF-7 cells time to settle onto and attach to the micropallet tops (Figure 3). Prior to imaging, arrays were rinsed with PBS to remove the majority of the blood cells and enable identification of the MCF-7 cells. The efficiency of erythrocyte and lymphocyte depletion was dependent on the number of PBS washes. Following 10 rinses with PBS, less than 100 erythrocytes and less than 5 lymphocytes remained on an 0.8 mm^2 area of

the array. Of the MCF-7 cells mixed into 1, 10 or 100 µL whole blood, 95 ± 2%, 92 ± 5% and 55 ± 16% of the cells attached to the micropallets (n = 3 arrays). The maximal 95% capture efficiency corresponds to the percentage of living cells within a typical MCF-7 culture since the rapidly growing cells exhibit a high percentage of senescent cells. The low capture efficiency of MCF-7 cells when mixed into 100 µL whole blood was likely to the dense layer of erythrocytes on the array. As the blood cells are sufficiently dilute, MCF-7 cells are able to encounter the array surface and adhere to the micropallets.

6.3.4 anti-EpCAM enrichment of MCF-7 cells from whole blood. The majority of CTCs in circulation are either apoptotic or non-proliferating.[41] These cells need to be captured in order to determine the total CTC cell count. These cells may also possess valuable information as to why not all CTCs are successful at forming engrafting. The effectiveness of tumor cell enrichment from whole blood by anti-EpCAM coated micropallets was evaluated by measuring the capture of MCF-7 cells mixed into whole blood. In triplicate experiments, 100 MCF-7 cells were added to 1, 10 or 100 µL of whole blood which was then diluted with cell culture media (2 mL) prior to loading onto an array of 12,769 anti-EpCAM functionalized micropallets. Arrays were transferred to an incubator for 2 h to provide the MCF-7 cells time to attach to the micropallets. The arrays were then washed with PBS to remove the majority of erythrocytes and lymphocytes. Of the MCF-7 cells mixed into 1, 10 or 100 µL whole blood, 85 ± 10%, 87 ± 12% and 38 ± 25% of the cells adhered to the micropallets. These values are similar to the capture efficiencies obtained with micropallets coated with fibronectin. It is possible that the MCF-7 cell capture on the anti-EpCAM functionalized micropallets was due to cell capture by the antibody and nonspecific cell attachment to the PAA coating on the

micropallets. Enrichment of tumor cells by antibody-based binding ensures collection of the majority of antigen expressing CTCs from a sample.

6.4 Conclusions

The current work demonstrated the capability of tumor cell isolation directly from whole blood with the micropallet technology. Micropallets functionalized with either fibronectin or anti-EpCAM were able to efficiently isolate MCF-7 cells from 1 mL of whole blood with very minimal sample processing i.e. dilution. Future work will achieve laser-based release and culture of MCF-7 cells isolated from whole blood. The clinical utility of the micropallet arrays for sorting CTCs will be demonstrated by isolating tumor cells directly from the whole blood of mice bearing pancreatic ductal adenocarcinoma (PDAC) patient-derived xenografts (PDX). Following capture of viable CTCs on the micropallet arrays the cells may be cultured into small colonies that encompass multiple micropallets. Individual micropallets carrying portions of the cell colony can then be removed and analyzed over the lifespan of the developing tumor and compared to tumor growth *in-vivo*. While static conditions lead to low capture efficiencies with larger volumes of blood, micropallet bases with high aspect ratio poles grafted with anti-EpCAM could feasibly be incorporated into a microfluidic channel increasing the volumes of blood processed by these arrays. A combined micropallet-microfluidic device could take advantages of the high throughput cell capture rates offered by microfluidics with gentle release of micropallets holding captured CTCs. Beyond its applications with micropallet technology, a novel method for immobilizing anti-EpCAM antibodies to polymers via immobilization to the antibody to protein A/G bound to PAA grafted substrates is reported. This strategy holds great promise for functionalizing various other

microdevies with anti-EpCAM or other antibodies for the capture of CTCs. Micromolded microraft arrays would also benefit from these advances as they have shown promise for easily fabricating large arrays and isolating cells with high efficiency and low contamination.[37,42]

6.5 Figures

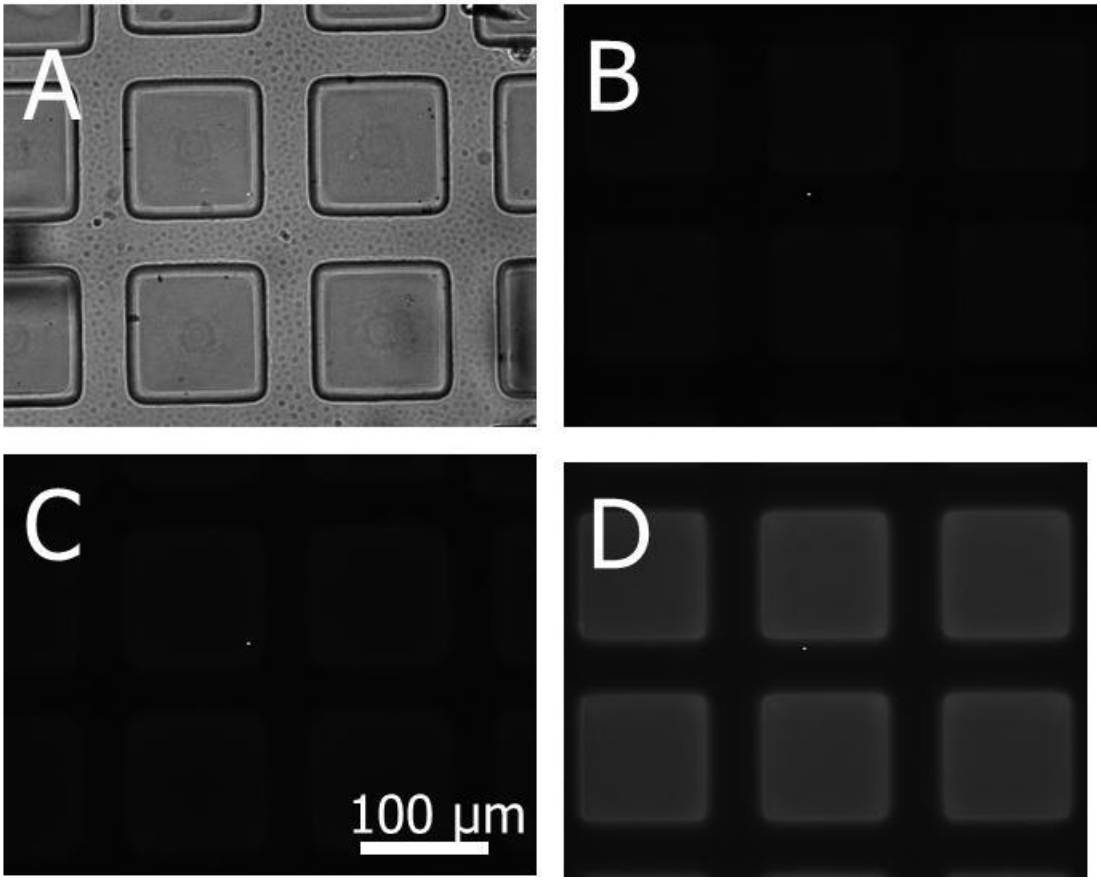

Figure 6.1 anti-EpCAM functionalization of micropallets. Brightfield image of micropallets (A) and fluorescence images of untreated micropallets (B), FITC-EpCAM physically absorbed to micropallets (C) and FITC-EpCAM attached to micropallets grafted with PAA and covalently attached protein A/G (D).

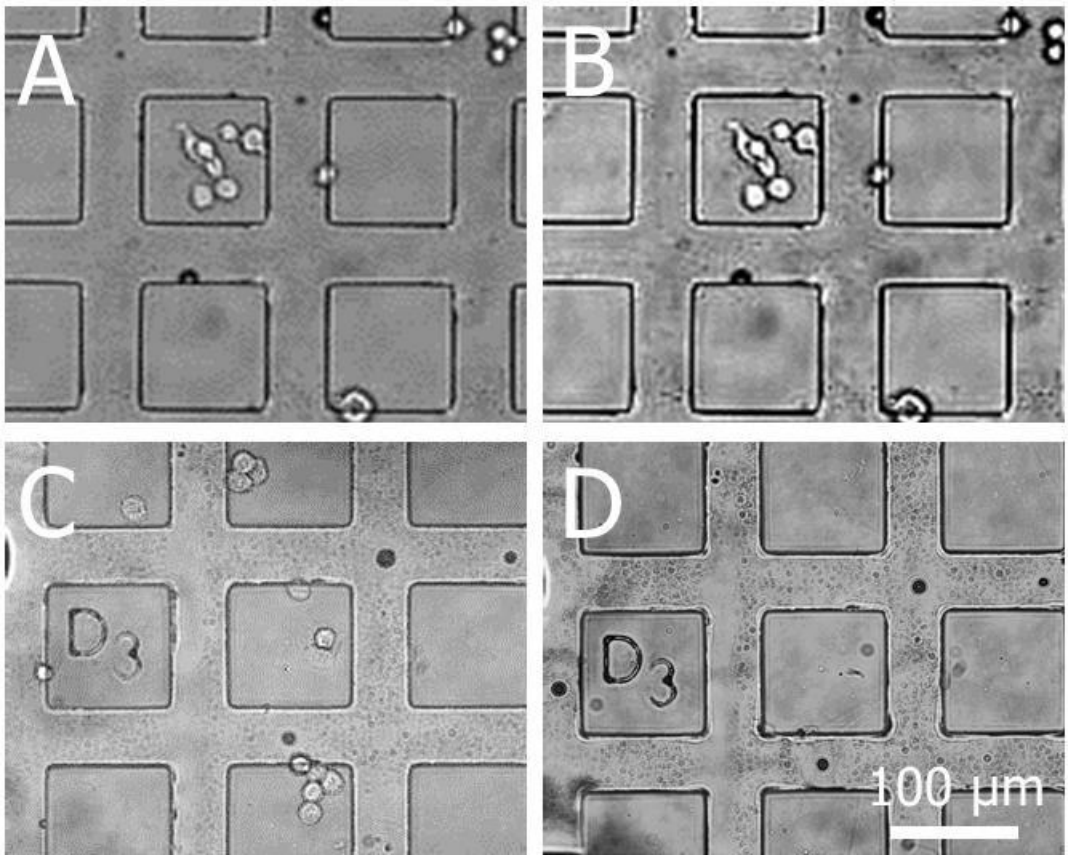

Figure 6.2 Selective cell capture on EpCAM functionalized micropallets. MCF-7 cells on micropallet array before (A) and after rinsing (B). HeLa cells on micropallet array before (C) and after rinsing (D).

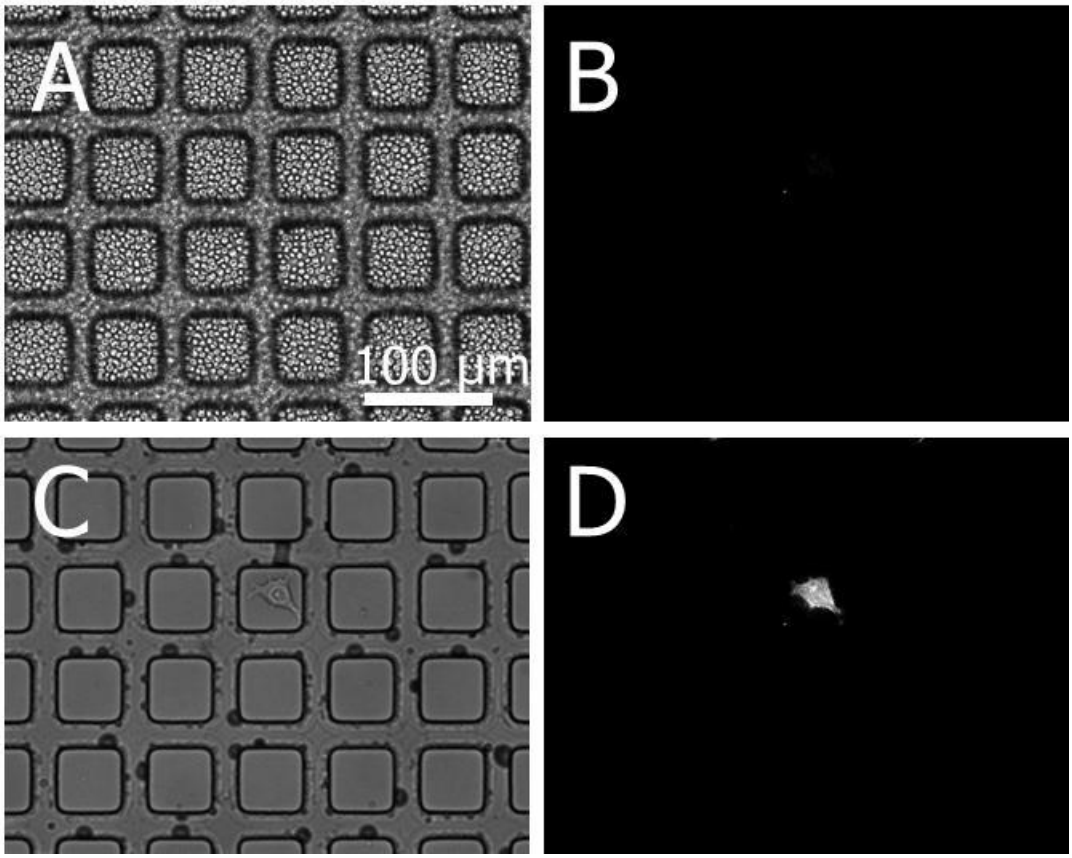

Figure 6.3 Capture of MCF-7 cells from peripherial blood. Brightfield (A) and fluorescence images (B) of fibronectin-coated arrays overlaid with whole blood containing MCF-7 cells prior to removal of the blood by washing. Brightfield (C) and fluorescence images (D) of the same array in A and B after washing.

6.6 References

1. Rissin D, Kan C, Campbell T, et al. Single-molecule enzyme-linked immunosorbent assay detects serum proteins at subfemtomolar concentrations. *Nature Biotechnology*. 2010;28(6):595-U525.

2. Toner M, Irimia D. Blood-on-a-chip. *Annual Review of Biomedical Engineering*. 2005;7:77-103.

3. Cohen S, Punt C, Iannotti N, et al. Relationship of circulating tumor cells to tumor response, progression-free survival, and overall survival in patients with metastatic colorectal cancer. *Journal of Clinical Oncology*. 2008;26(19):3213-3221.

4. Cristofanilli M, Budd G, Ellis M, et al. Circulating tumor cells, disease progression, and survival in metastatic breast cancer. *New England Journal of Medicine*. 2004;351(8):781-791.

5. Paterlini-Brechot P, Benali N. Circulating tumor cells (CTC) detection: Clinical impact and future directions. *Cancer Letters*. 2007;253(2):180-204.

6. Talasaz A, Powell A, Huber D, et al. Isolating highly enriched populations of circulating epithelial cells and other rare cells from blood using a magnetic sweeper device. *Proceedings of the National Academy of Sciences of the United States of America*. 2009;106(10):3970-3975.

7. Takao M, Takeda K. Enumeration, Characterization, and Collection of Intact Circulating Tumor Cells by Cross Contamination-Free Flow Cytometry. *Cytometry Part A*. 2011;79A(2):107-117.

8. Nagrath S, Sequist LV, Maheswaran S, et al. Isolation of rare circulating tumour cells in cancer patients by microchip technology. *Nature*. 2007;450(7173):1235-1239.

9. Gleghorn J, Pratt E, Denning D, et al. Capture of circulating tumor cells from whole blood of prostate cancer patients using geometrically enhanced differential immunocapture (GEDI) and a prostate-specific antibody. *Lab on a Chip*. 2010;10(1):27-29.

10. Stott S, Hsu C, Tsukrov D, et al. Isolation of circulating tumor cells using a microvortex-generating herringbone-chip. *Proceedings of the National Academy of Sciences of the United States of America*. 2010;107(43):18392-18397.

11. Wang S, Liu K, Liu J, et al. Highly Efficient Capture of Circulating Tumor Cells by Using Nanostructured Silicon Substrates with Integrated Chaotic Micromixers. *Angewandte Chemie-International Edition*. 2011;50(13):3084-3088.

12. Helzer KT, Barnes HE, Day L, Harvey J, Beilings PR, Forsyth A. Circulating Tumor Cells Are Transcriptionally Similar to the Primary Tumor in a Murine Prostate Model. *Cancer Research*. 2009;69(19):7860-7866.

13. Kang JH, Krause S, Tobin H, Mammoto A, Kanapathipillai M, Ingber DE. A combined micromagnetic-microfluidic device for rapid capture and culture of rare circulating tumor cells. *Lab on a Chip*. 2012;12(12):2175-2181.

14. Schiro PG, Zhao M, Kuo JS, Koehler KM, Sabath PDE, Chiu PDT. Sensitive and high-throughput isolation of rare cells from peripheral blood with ensemble-decision aliquot ranking. *Angewandte Chemie*. 2012;51(19):4618-4622.

15. Hur S, Mach A, Di Carlo D. High-throughput size-based rare cell enrichment using microscale vortices. *Biomicrofluidics*. 2011;5(2):-.

16. Bhagat A, Hou H, Li L, Lim C, Han J. Pinched flow coupled shear-modulated inertial microfluidics for high-throughput rare blood cell separation. *Lab on a Chip*. 2011;11(11):1870-1878.

17. Adams A, Okagbare P, Feng J, et al. Highly efficient circulating tumor cell isolation from whole blood and label-free enumeration using polymer-based microfluidics with an integrated conductivity sensor. *Journal of the American Chemical Society*. 2008;130(27):8633-8641.

18. Dharmasiri U, Balamurugan S, Adams A, Okagbare P, Obubuafo A, Soper S. Highly efficient capture and enumeration of low abundance prostate cancer cells using prostate-specific membrane antigen aptamers immobilized to a polymeric microfluidic device. *Electrophoresis*. 2009;30(18):3289-3300.

19. Dharmasiri U, Njoroge S, Witek M, et al. High-Throughput Selection, Enumeration, Electrokinetic Manipulation, and Molecular Profiling of Low-Abundance Circulating Tumor Cells Using a Microfluidic System. *Analytical Chemistry*. 2011;83(6):2301-2309.

20. Vickers D, Hincapie M, Hancock W, Murthy S. Lectin-mediated microfluidic capture and release of leukemic lymphocytes from whole blood. *Biomedical Microdevices*. 2011;13(3):565-571.

21. Gurkan UA, Anand T, Tas H, et al. Controlled viable release of selectively captured label-free cells in microchannels. *Lab on a Chip*. 2011;11(23):3979-3989.

22. Gascoyne P, Noshari J, Anderson T, Becker F. Isolation of rare cells from cell mixtures by dielectrophoresis. *Electrophoresis*. 2009;30(8):1388-1398.

23. Vona G, Sabile A, Louha M, et al. Isolation by size of epithelial tumor cells - A new method for the immunomorphological and molecular characterization of circulating tumor cells. *American Journal of Pathology*. 2000;156(1):57-63.

24. Tan S, Yobas L, Lee G, Ong C, Lim C. Microdevice for the isolation and enumeration of cancer cells from blood. *Biomedical Microdevices*. 2009;11(4):883-892.

25. Zheng S, Lin H, Lu B, et al. 3D microfilter device for viable circulating tumor cell (CTC) enrichment from blood. *Biomedical Microdevices*. 2011;13(1):203-213.

26. Glinskii A, Smith B, Jiang P, et al. Viable circulating metastatic cells produced in orthotopic but not ectopic prostate cancer models. *Cancer Research*. 2003;63(14):4239-4243.

27. Glinsky GV, Glinskii AB, Berezovskaya O, et al. Dual-color-coded imaging of viable circulating prostate carcinoma cells reveals genetic exchange between tumor cells in vivo, contributing to highly metastatic phenotypes. *Cell Cycle*. 2006;5(2):191-197.

28. Ameri K, Luong R, Zhang H, et al. Circulating tumour cells demonstrate an altered response to hypoxia and an aggressive phenotype. *British Journal of Cancer*. 2010;102(3):561-569.

29. Wang Y, Young G, Bachman M, Sims C, Li G, Allbritton N. Collection and expansion of single cells and colonies released from a micropallet array. *Analytical Chemistry*. 2007;79(6):2359-2366.

30. Gunn N, Bachman M, Li G, Nelson E. Fabrication and biological evaluation of uniform extracellular matrix coatings on discontinuous photolithography generated micropallet arrays. *Journal of Biomedical Materials Research Part A*. 2010;95A(2):401-412.

31. Shadpour H, Sims C, Allbritton N. Enrichment and Expansion of Cells Using Antibody-Coated Micropallet Arrays. *Cytometry Part A*. 2009;75A(7):609-618.

32. Gach P, Sims C, Allbritton N. Transparent magnetic photoresists for bioanalytical applications. *Biomaterials*. 2010;31(33):8810-8817.

33. Wang Y, Sims C, Marc P, Bachman M, Li G, Allbritton N. Micropatterning of living cells on a heterogeneously wetted surface. *Langmuir*. 2006;22(19):8257-8262.

34. Wang Y, Pai J, Lai H, et al. Surface graft polymerization of SU-8 for bio-MEMS applications. *Journal of Micromechanics and Microengineering*. 2007;17(7):1371-1380.

35. Went P, Lugli A, Meier S, et al. Frequent EpCam protein expression in human carcinomas. *Human Pathology*. 2004;35(1):122-128.

36. Wang Y, Salazar G, Pai J, Shadpour H, Sims C, Allbritton N. Micropallet arrays with poly(ethylene glycol) walls. *Lab on a Chip*. 2008;8(5):734-740.

37. Wang Y, Phillips C, Xu W, et al. Micromolded arrays for separation of adherent cells. *Lab on a Chip*. 2010;10(21):2917-2924.

38. Rao C, Chianese D, Doyle G, et al. Expression of epithelial cell adhesion molecule in carcinoma cells present in blood and primary and metastatic tumors. *International Journal of Oncology*. 2005;27(1):49-57.

39. Sekine J, Luo S, Wang S, Zhu B, Tseng H, Yu H. Functionalized Conducting Polymer Nanodots for Enhanced Cell Capturing: The Synergistic Effect of Capture Agents and Nanostructures. *Advanced Materials*. 2011;23(41):4788-+.

40. Paris P, Kobayashi Y, Zhao Q, et al. Functional phenotyping and genotyping of circulating tumor cells from patients with castration resistant prostate cancer. *Cancer Letters*. 2009;277(2):164-173.

41. Chambers A, Groom A, MacDonald I. Dissemination and growth of cancer cells in metastatic sites. *Nature Reviews Cancer*. 2002;2(8):563-572.

42. Gach P, Wang Y, Phillips C, Sims C, Allbritton N. Isolation and manipulation of living adherent cells by micromolded magnetic rafts. *Biomicrofluidics*. 2011;5(3).

Chapter 7: Microfabricated Arrays for Splitting and Assay of Clonal Colonies

7.1 Introduction

Microfabricated devices aimed at efficient culture and manipulation of mammalian cells offer the promise of providing protocols that dramatically reduce the time and effort needed to create molecularly engineered cell lines. Conventional methods for viable cell selection for cell line generation are often based on cell-surface proteins and can usually be accomplished by magnetic or fluorescence activated cell sorting (FACS) using labeled antibodies against a surface protein. However, most proteins are intracellular and can only be detected by FACS in fixed (dead) cells unless co-expressed with a fluorescent marker, such as green fluorescent protein (GFP).[1-3] Unfortunately, these fluorescent reporter genes do not always accurately reflect the expression of the gene or protein of interest.[4] When a cell-destructive assay such as immunocytochemistry of an intracellular protein is used for cell line identification, significant effort is required to classify large numbers of clones while maintaining viable cells for subsequent use. FACS, cloning ring, or limiting dilution protocols must first be used to isolate single cells and create clonal colonies. These are then expanded in culture over many weeks to produce clonal populations large enough to manually split and assay in a cell-destructive manner.[5,6] High-throughput, automated instruments for colony picking are available, but suffer from very high cost, and are limited to only a few cell types. Once picked, colonies must still be split and assayed serially, thus limiting any savings in time and manpower.[7-

In recent years, microfabricated devices based on microfluidic, dielectrophoretic, optical or magnetic principles have been developed for culture and screening of cells; although, almost all have been directed at bulk sorting of single cells, not parallel assay and manipulation of individual colonies.[11-16] A few reports have involved whole colony retrieval and a very limited number have described colony printing or isolation of partial colonies.[11,17-19] Thermo-responsive polymers have been used to effect release of cells[20] or arrayed colonies[21] *en masse*, but an effective means for clonal colony retrieval has not yet been presented. Laser microdissection has been used to selectively divide hepatocyte colonies patterned on a microarray, but the cells were fixed and nonviable prior to collection.[22] In one of the only descriptions of molecular characterization while maintaining viable cells in a sampled colony, Villa-Diaz *et al* sampled cells from a stem-cell colony cultured within a microchannel.[23] By subjecting various portions of the colony to a laminar flow stream, cells from one region could be selectively exposed to trypsin to enzymatically free cells from the colony for downstream collection and subsequent analysis by PCR. This procedure is an elegant solution to the need for sub-sampling a colony, but required large-sized colonies (>1 mm) and was only demonstrated for a single colony at a time due to the discrete fluidic architecture required to sample each colony. The Allbritton Group reported a microarray of pedestal-like elements termed pallets on which small clonal colonies could be produced, followed by colony division and collection.[24] While the technique demonstrated feasibility, sampling all of the colonies on an array required serial release and collection of a large number of pallets. Manipulation of the numerous microscale samples proved tedious, suffered from high losses, and presented complications in maintaining registration with the original colonies.

The current work describes a new technique to achieve parallel splitting of very large numbers of colonies of mammalian cells in a single step followed by highly parallel performance of a destructive assay to identify target colonies. A platform composed of two matching arrays of three-dimensional microstructures was designed. Due to the need for accurate alignment of the microstructures on each array, a system was devised and tested for mating the arrays with a tolerance of ≤30 μm. The dimensions of the array structures were optimized to enhance cell migration between the aligned array microstructures. Tests of viability and phenotype were performed to confirm that viable colonies bridging the arrays were generated and separation of the arrays produced mirror-image colonies on the two arrays. The cells on one array then served as samples for a destructive assay in a parallel format while the second array preserved the matching colonies in a viable state. A proof-of-principle experiment compared this printing array method with a FACS-based technique to generate clones with decreased Coronin 1B expression using a lentiviral vector carrying a short hairpin interfering RNA (shRNA).

7.2 Experimental Section

7.2.1 Materials. EPON resin 1002F [phenol, 4,4'-(1-methylethylidene)bis-, polymer with 2,2'-[(l-methylethylidene)bis(4,1-phenyleneoxymethylene)]bis(oxirane)] was obtained from Miller-Stephenson (Sylmar, CA). UVI-6976 photoinitiator (triarylsulfonium hexafluoroantimonate salts in propylene carbonate) was purchased from Dow Chemical (Torrance, CA). SU-8 developer (1-methoxy-2-propyl acetate) was received from MicroChem Corp. (Newton, MA, USA). All other photoinitiators and resins were from Sigma-Aldrich (St. Louis, MO) as was γ-butyrolactone (GBL). (Heptadecafluoro-1,1,2,2-tetrahydrodecyl) trichlorosilane was from Gelest Inc.

(Morrisville, PA). Poly(dimethylsiloxane) (PDMS, Sylgard 184 silicone elastomer kit) was purchased from Dow Corning (Midland, MI). Dulbecco's Modified Eagle Medium (DMEM), fetal bovine serum (FBS), 0.05% Trypsin-EDTA, bovine serum albumin (BSA), Calcein Red-Orange AM, AlexaFluor568 dye conjugated phalloidin, and penicillin/streptomycin were obtained from Life Technologies (Carlsbad, CA). Cy5 secondary antibody conjugate was obtained from Jackson Immunoresearch (West Grove, PA). Transwell® inserts, glass microscope slides, fibronectin and all other reagents were procured from Fisher Scientific (Pittsburgh, PA). The microfabrication masks were drawn using TurboCAD (IMSI/Design, LLC, Novato, CA) and then printed and fabricated by Fineline Imaging (Colorado Springs, CO).

7.2.2 Fabrication of the arrays. Fabrication of the pallet and printing arrays used standard process photolithography as previously described.[25] Briefly, a layer of 1002F (120 µm thick for the pallet array and 50 µm for the printing array) was spin-coated on a 75 mm × 50 mm glass microscope slide, and then soft baked (65 °C for 20 min followed by 95 °C for 90 min [pallets] or 60 min [printing array bases]). After soft baking, a chrome mask was placed on the top of the 1002F films and exposed using a Newport 97485 UV exposure system. The slide was then hard baked (1 min at 65 °C and 8 min at 95 °C). After cooling, a second layer of 1002F-50 was spin-coated onto the 1002F-coated slide to the desired thickness (50 µm for the pallet array and 20 - 120 µm for the printing array) and the slide was soft baked as described above. A second chrome mask was placed on top of the slide, aligned and exposed using an aligner (MA6, SUSS Microtec,Germany). The slide was then hard baked as described above. Finally, the slide was immersed in SU-8 developer for 10 min, sprayed with isopropyl alcohol and dried

with compressed nitrogen. The array was baked at 95 °C for 5 min and then baked at 120 °C for 1 h to remove remaining solvent from the photoresist.

Arrays composed of either 1296 or 3000 pallets with dimensions of 150 μm (L) × 150 μm (W) × 120 μm (H) and a 150 μm gap were fabricated for the experiments described in the current work. At the edges of the pallet array, two cross structures each with dimensions of 8 mm (L) × 5 mm (W) × 170 μm were also fabricated on the substrate for alignment purposes. For the printing array, the base dimensions were 250 μm (L) × 250 μm (W) × 50 μm (H) with a 50 μm inter-base gap. Dimensions of the printing posts were varied during the course of optimization as described in the results and ranged from 30 -250 μm (L) × 30 -250 μm (W) × 20 -120 μm (H) with a 270 μm inter-post gap. The printing array possessed an identical number of microstructures as the pallet array and two alignment crosses (overall dimensions of 1.2 cm [L] × 8 mm [W], see Figures 7.2 and 7.3). To mate with the alignment markers on the pallet array, the printing alignment structures contained an inner groove with dimensions of 8.06 mm (L) × 5.06 mm (W) × 70-170 μm (depth depending on post height) into which the crosses of the pallet array nested.

After microfabrication, both the pallet and printing arrays were treated with perfluoroalkyl silane to generate hydrophobic regions between the pallets or printing bases.[26] This enabled the creation of a "virtual wall" formed by a continuous air bubble entrapped between the microelements of an array when immersed in media. The air wall acted to localize cells and their descendants to their original pallet or base surface as previously described.[27,28] Before use, a PDMS ring surrounding the pallet array was constructed to provide a temporary chamber for housing the cells and media during

plating and culture prior to the printing step. To create the ring, Sylgard 184 resin with curing reagent (ratio 10:1) was poured into a plastic mold and the assembly was heated in an 80 °C oven for 20 min. The PDMS ring was attached to the pallet array's upper surface by simply pressing the PDMS against the glass substrate. A circular chamber was created on the backside of the printing array by removing the polycarbonate membrane of a Transwell® (Corning Inc., Corning, NY) and then attaching the polystyrene housing to the back side of the array substrate with PDMS. This structure aided in handling the printing array during alignment and created a chamber that when filled with fluid acted as a weight to press the printing array onto the pallet array (see Figures 7.1 and 7.4). Before use, both arrays were sterilized by soaking in 70% ethanol for 20 min and then dried with compressed nitrogen.

*7.2.3 Cell printing***.** HeLa, a human cervical carcinoma cell line; NIH 3T3, a murine fibroblast cell line; IA32, a mouse embryonic fibroblast cell line; A549, a human alveolar adenocarcinoma cell line, and HT1080, a human fibrosarcoma cell line, were used in the current studies. Both wild-type HeLa cells and a molecularly engineered HeLa cell line stably expressing a nuclear GFP fusion with the histone H1 protein were utilized. After cells were plated on the pallet array, they were cultured for 72 h to allow small clonal colonies to form. The PDMS ring was removed under sterile conditions and media was added to the Petri dish containing the array such that the level of the media was ~2 mm above the array. The fibronectin pre-coated printing array was then placed in contact with the pallet array with the patterned side facing the pallet array. Using manual placement with the aid of the alignment structures, the posts of the printing array were positioned near the center and in contact with the pallets on the pallet array. Sterile fluid

(4 mL of media) was then added to the chamber formed by an open chamber on the backside of the printing array to weight the array, thus keeping it in position. The mated arrays were returned to a standard tissue culture incubator. After 24 h, the two arrays were separated under sterile conditions. Immediately upon separation, the printing array was immersed in media (10 mL media in a 100 mm Petri dish). Both the pallet and the printing arrays were maintained in media and then imaged to identify the percentage of replicated colonies or to carry out viability assays. Unless otherwise specified, in each experiment 3 identical arrays and 50 elements per array were analyzed to generate the data.

7.2.4 Alignment system. An important aspect of the design was an easy and accurate manual alignment system for the two arrays, since each printing post needed to be positioned in register with each pallet. Alignment was facilitated by incorporating large cross-shaped structures on the substrate near the edge of the arrays. These alignment structures fit together in a "tongue and groove" manner when the two arrays were mated (Figure 7.2). The tongue sides of the alignment structures were fabricated on the pallet array. The grooved structures were placed on the printing array. The height of the grooved structures varied from 70 to 170 μm depending on the post height. Maintenance of the alignment and maximal contact between the pallets and posts required weighting of the upper array. This was accomplished by adding a clear, fluid-filled chamber on top of the mated arrays (Figures 7.2 and 7.3).

7.2.5 Measuring pallet height. Pallet heights were measured using a P-15 surface profiler (KLA Tencor, San Jose, CA). The profilometer stylus was scanned across a row of pallets over multiple regions of the original and printing arrays. The stylus tip (2 μm

tip radius and 60^{o} cone angle) was unable to fall between the high aspect ratio microstructures so pallet bases were determined by extending the scan of the stylus to the glass substrate at the edge of the array.

7.2.6 Fabrication of the collection plate. The mold for a microwell collection plate was created by fabricating an array (80 columns; 80 rows) of 1002F structures (250 µm [L] × 250 µm [W] × 70 µm [H]) on a 2 × 3 inch glass substrate which was then silanized as described above. After silanization, this 1002F mold was then used to fabricate a PDMS collection plate with wells. A thin layer (about 2 mm) of uncured PDMS was poured onto the mold and heated in an oven at 80 °C for 20 min, after which the assembly was taken out and the PDMS film was peeled off the mold. A PDMS ring (2 × 2 cm) was glued to the film to form a reservoir on the PDMS collection plate as described above. Before use, the collection-well plate was sterilized in 70% ethanol for 20 min followed by wash in phosphate buffered saline (PBS: 135 mM NaCl, 3.2 mM $KHPO_4$, 0.5 mM KH_2PO_4 and 1.3 mM KCl; pH = 7.4) ×5. Culture medium was added just before use.

7.2.7 Laser-based release of microstructures from the pallet array. A pulsed laser was used to release the pallets from the array as has been described in detail previously.[29] Briefly, a laser pulse (5 ns, 532 nm) from a Q-switched Nd:YAG laser (Minilite I, Continuum Electro-Optics Inc., Santa Clara, CA) was focused by a 40× microscope objective at the interface of the glass substrate and one of the pallets. The focused pulse led to formation of a plasma and cavitation bubble. The expansion of the cavitation bubble at the base of the pallet mechanically dislodged it in an upward direction.[30]

7.2.8 Cell plating and culture on the pallet array. HeLa, a human cervical carcinoma cell line; NIH 3T3, a murine fibroblast cell line; IA32, a mouse embryonic fibroblast cell line; A549, a human alveolar adenocarcinoma cell line, and HT1080, a human fibrosarcoma cell line, were used in the current studies. Both wild-type HeLa cells and a molecularly engineered HeLa cell line stably expressing a nuclear GFP fusion with the histone H1 protein were utilized. Cells on the array and those on pallets released from the array were cultured in conditioned media.[31] The base medium used was DMEM with 10% FBS, L-glutamine (584 mg/L), penicillin (100 units/mL) and streptomycin (100 µg/L). The arrays were sterilized by immersion in ethanol for 20 min and then allowed to dry in a sterile culture hood prior to use. Before use, the pallet array was placed in a sterile Petri dish (100 × 25 mm) that would eventually house the mated arrays. To enhance cell attachment and growth, the arrays were coated before use with fibronectin (5 µg/mL for pallet and 15 µg/mL for the printing array) in PBS by incubation in the fibronectin solution for 30 min at room temperature. The arrays were washed with sterile deionized water ×4 with a final rinse in media before use. To plate cells on the pallet array, a suspension of cells in 1 mL of media were added to the chamber formed by the PDMS ring and allowed to settle. For experiments to generate clonal colonies, the number of cells used was chosen to provide ≤1 cell per pallet as previously described.[31] Plated cells were cultured in a humidified, 5% CO_2 atmosphere at 37 °C.

7.2.9 Cell collection and culture after release. The pallet array was rinsed with fresh, pre-warmed culture media (37 °C) ×3 before the release procedure. After laser-based release, individual pallets with cells were collected directly onto a 1" × 3" glass and

PDMS chamber slide as previously reported.[31] The collected cells were maintained in freshly prepared conditioned media for expansion.

7.2.10 Cell viability assay. Cell viability on the arrays was determined by the ability of cells to uptake and convert the dye Calcein Red-Orange AM to its fluorescent product. This standard fluorescence-based viability assay was performed according to manufacturer protocol.

7.2.11 Lentiviral construct production, infection procedure and FACS. The vector containing the short hairpin RNA (shRNA) construct used to knockdown Coronin 1B and a GFP cassette as an infection marker was generated according to Cai, *et al* as was lentivirus production and infection.[32] Cells exposed to the lentivirus were suspended at 500,000 cells per ml in complete media. An aliquot was removed for plating on the pallet array with the remainder sorted by FACS as previously described.[33]

7.2.12 Immunocytochemical staining of cells. IA32 cells infected with lentivirus and plated on glass slides or present on the printing array were fixed with 4% paraformaldehyde in Krebs buffer for 10 min and permeabilized with 0.2% Triton X-100 in PBS. Anti-Coronin 1B antibody was incubated with fixed, permeabilized cells for 2 h at 1:200 in 3% BSA in PBS.[34] Cells were washed ×3 in PBS and incubated for 1 h with Cy5 secondary antibody at 1:250 and AlexaFluor568 dye conjugated phalloidin at 1:400 in 3% BSA in PBS. Cells were finally washed and imaged in PBS.

7.2.13 Western blotting. Western blotting was performed by standard techniques as follows. IA32 cells were lysed in RIPA buffer; protein was loaded onto polyacrylamide gels and transferred to PVDF membranes. Membranes were blocked with PBS and 3% non-fat milk (3% Milk/PBS) and incubated with specified primary

antibodies in 3% Milk/PBS overnight at 4°C. The immunoblots were washed in PBS and 0.2% Tween (PBS-T) and incubated for 2 h with HRP-conjugated secondary antibody in 3% Milk/PBS. Membranes were then washed with PBS-T and visualized with ECL substrate reagent (Pierce). Primary antibodies for Coronin 1B (1:500), GFP (1:1000) and GAPDH (1:5000-1:10000) were used as previously described.[34]

7.3 Results and Discussion

7.3.1 Array design and fabrication. The design employed the mating of two matching arrays of three-dimensional microstructures (Figure 7.1). A pallet array was composed of cuboid microstructures (Figures 7.1A and 7.4A).[28,35] A second or "printing" array consisted of square bases with a post projecting from the center of the base (Figures 7.1D and 7.4B). A two-step photolithography process utilizing the biocompatible photoresist 1002F was employed to create both arrays. For the pallet array, the initial photoresist layer was used to form the pallets while a second layer yielded an alignment structure used in array-array mating. For the printing array, the base elements were formed from an initial photoresist layer with the posts and the alignment structures fabricated as the second layer. Both arrays contained an identical number of elements positioned so that the centers of the pallets were axially aligned with the printing posts when the arrays were mated (Figures 7.1E). The printing posts served as a bridge between the elements of the two arrays when the pallet and printing arrays were mated. The individual pallets of the pallet array were of smaller area (150 × 150 μm) and greater height (120 μm) than the bases on the printing array (250 × 250 μm and 50 μm high). These dimensions were chosen to provide a stable virtual air wall (described in the Experimental Section) on each array while allowing the height of the printing base to be

minimized.[26] Minimization of the printing base height was desired in order to diminish polymer autofluorescence during imaging after immunocytochemical staining.[35] The dimensions of the printing posts atop each base on the printing array varied depending on the experiment (see below). The overall footprint of both arrays composed of 3000 elements was 1.5 × 1.5 cm. The lanes between the pallets and printing bases were coated with a perfluoroalkylsilane to form the virtual wall between the microstructures upon aqueous immersion.[28] When the two alignment structures were paired, the center of the post position was on average 17 ± 7 μm from the pallet center (n = 3 arrays, 20 sites analyzed/array) (Figures 7.5B and 7.3).

7.3.2 Colony printing. HeLa cells (2500 cells) were plated and cultured on an array containing 3000 pallets for 72 h to allow colonies to develop (Figure 7.5A). At that time, those pallets with colonies contained an average of 9 ± 3 cells per colony. A printing array possessing posts 60 μm on a side and 100 μm in height was then mated to the pallet array (Figure 7.5B) and the paired arrays were returned to culture. After 24 h, the paired arrays were separated; the cells were stained with a fluorescent viability dye, and examined microscopically (Figure 7.5C-F). When care was taken in mating and detaching the arrays to eliminate sliding of the microstructure surfaces across one another, cells were present on the printing array sites only when a corresponding colony was present on the pallet array. When an element on the pallet array possessed a colony, 87% ± 5% of the corresponding sites on the printing array also possessed a colony. Of the elements on the printing array that possessed cells, 35 ± 16% possessed cells on the posts alone, 12% ± 4% solely on the base, and 53% ± 19% on both post and base. This suggested that the site of initial attachment on the printing array was the post. To

determine whether the viability of cells on the mated arrays might be compromised due to the restricted access of nutrients, cells on both arrays were stained with the viability dye Calcein Red-Orange AM after array mating for 24 h. The cells on both arrays were fluorescent (100 ± 0%) suggesting that cell viability was not compromised over the 24-h period the arrays were mated.

7.3.3 Impact of post dimensions and cell type on printing efficiency. A series of experiments were conducted to assess whether the dimensions of the intervening post affected migration of cells from the pallet array to the printing array. In each of these experiments, HeLa cells (2500 cells/mL) were plated on the pallet array at ≤1 cell/pallet and then cultured for 72 h at which time the printing array was mated as described above. After an additional 24 h, the arrays were separated and analyzed for colony extension onto the printing array. The printing arrays possessed 100-μm tall posts with the post side or width varying between 30 – 250 μm. Only when the area of the top of the square post on the printing array was less than the area of the pallet on the pallet array were cells present on corresponding posts and bases on the printing array (Figure 7.6A). Smaller post diameters were more efficient at enabling transfer of cells, as demonstrated with the 30 μm post arrays which had on average 90% ± 6% of mated sites showing transfer of cells from the pallet array to the printing array.

A second series of experiments was then performed in which the post diameter was constant (30 μm on a side), while post height was varied between 20 – 120 μm (Figure 7.6B). The efficiency of cell transfer between the two arrays was greatest at the longer post lengths tested with a transfer rate of 0% ± 0% for the arrays with 20 μm posts and 91% ± 6% with 100 μm posts. When using the very short posts, the greatly decreased

fluid volume between the arrays was likely rapidly depleted of available nutrients and oxygen by the growing cells, thus an advantage in having a shorter distance to the printing array was not overcome by impaired cell migration and proliferation due to the nutrient-poor environment.

7.3.4 Accuracy of colony printing. The accuracy of colony printing was assessed by plating 130 wild-type HeLa cells on an array of 1296 pallets. After 72 h in culture, the pallet and printing arrays were mated and returned to culture. After 24 h, the two arrays were separated and maintained in culture for an additional 24 h. Cells on both arrays were stained with Calcein Red-Orange AM and identified by fluorescence and brightfield microscopy. In each of 3 experiments, 100 ± 0% of the colonies on the printing array were correlated with cell colonies present at that site on the original pallet array (225 sites analyzed/array, n = 3 arrays). To further evaluate the accuracy of colony printing and clonal maintenance, fluorescent HeLa cells stably transfected with GFP were mixed with wild-type HeLa cells at a ratio of 1:10 (total cell # = 2500) and plated on a pallet array (3000 pallets) such that most pallets contained ≤1 cell. The cells were cultured to form clonal colonies, and the arrays were mated, and then separated as described above. The separated pallet and printing arrays were imaged under fluorescence and brightfield microscopy. The pallet arrays were screened for regions possessing a single fluorescent colony with more than one adjacent non-fluorescent colony (Figure 7.5G-J). The corresponding elements on the printing array were then evaluated for the presence of a cell and its fluorescence phenotype. In every instance, the fluorescence status of the cells present on the printing array corresponded to the matching colony on the pallet array (n = 3 arrays, 8 regions analyzed/array). Furthermore, no colonies on either array were noted

to be a mixture of fluorescent and non-fluorescent cells. These data suggested that cells transferred to the printing array only by migration from the pallet array across the printing post and remained clonal.

7.3.5 Assessment of the printing efficiency for multiple different cell types. Using the optimized post dimensions of 30-μm diameter and 100-μm length, the efficiency of colony printing was evaluated for five different cell lines (HeLa, 3T3, A549, HT1080, and IA32). In four independent experiments, each cell type was plated on a pallet array at ≤1 cell/pallet and cultured for 72 h. The printing array was mated for 24 h and then the arrays were separated and analyzed. While there was some variability depending on cell type, all five cell types were efficiently transferred with printing rates between 78% and 92% (Figure 7.6C). To understand why the transfer efficiency was less than 100%, the flatness of the arrays was measured by profilometry. The pallet arrays with a single-photoresist layer possessed a height variability of ±5 μm across a 1.5-cm array. A printing array with 120 μm posts formed demonstrated a height variation of ±15 μm across the 1.5-cm array. When multiple arrays were screened, the surface height changes across the array varied and were concave, convex, or S-shaped. Thus, the mated arrays possessed vertical gaps that in some regions could be as high as 40 μm, much greater than the estimated minimal gap of 5 μm (the height of most adherent cells) for cells to efficiently bridge.[36] Improving the array flatness by careful photoresist placement as well as use of extremely flat glass for the array substrate would likely improve cell transfer efficiency.

7.3.6 Isolation of clonal cell lines exhibiting Coronin 1B knockdown. A paired-set of experiments was performed comparing the array printing method with the current

"gold-standard" of cloning by FACS and verification by western blotting. The experiment aimed to identify clones with stable shRNA-mediated knockdown of Coronin 1B, a member of a family of proteins critical for innate immune function implicated in a number of diseases.[37,38] Modulation of the expression levels of the coronin proteins through RNA interference (RNAi) is fundamental to understanding the biological roles of the coronins; however, heterogeneous silencing of protein expression by RNAi results in highly variable levels in the knockdown of the target protein.[39,40] To overcome this issue, cloning of a sub-population of stable knockdowns must be done, but the intensive effort that is required limits this approach to such a degree that cloning is in practice rarely performed.

In these experiments, IA32 cells were infected with the lentiviral vector encoding Coronin 1B shRNA and GFP, and then were split for FACS or plated on pallet arrays. After cell plating, the pallet and printing arrays were mated and then separated as described in previous paragraphs. Generally, cells remained adhered to the posts sidewalls and tops and did not occupy the bases of the printing arrays. This was likely a result of both reduced proliferation and migratory capacity seen in successful coronin-knockdown in the IA32 cells.[4,32,33,41] Pallets corresponding to printing array elements with cells that exhibited Coronin 1B knockdown (phalloidin^{+}/GFP^{+}/Coronin-1B^{-}) were released from the array (10 colonies/array, n = 3 arrays) with a Nd:YAG laser as previously described,[31] collected onto a glass substrate, and allowed to proliferate for 4 days (Figure 7.7). From the 30 pallets collected, 12 (40%) contained colonies that maintained GFP expression and Coronin 1B knockdown (Figure 7.7A,B), 10 colonies were identified as having Coronin 1B expression (Figure 7.7C,D), and cells on 8 pallets

failed to proliferate. Observation of Coronin 1B expression in some clones was likely a result of the known loss of protein knockdown over time that can occur in lentiviral-based shRNA infections.[39] Of the knockdowns that did not continue to proliferate after release and collection, the cells on 7 of the 8 pallets exhibited very intense GFP expression. It is likely that high infection dose and complete gene knockdown compromised the growth of these cells.

In parallel, IA32 cells (5×10^5) infected with the same lentivector were subjected to FACS at 4 days after infection. Single GFP^+ cells (384 cells) were deposited into individual wells of four 96-well plates. As is typical of these experiments, only a minority of wells (6%) produced a colony. After 4 weeks, the 23 colonies had reached a sufficient size to screen by western blot for protein knockdown. Only 5 of the 23 colonies were stably depleted of Coronin 1B, thus the overall success rate was 1.3% (5 $shRNA^+$/Coronin $1B^-$ cells in 384 sorted cells) despite the substantial time, labor, and FACS sorting costs. A comparison of these data with that obtained with the cell printing arrays reveal the improved efficiency of clonal cell line generation by use of the cell printing arrays (Table 7.1). Isolation of clonal cell lines by printing arrays is impressively more affordable than standard methods in terms of labor, reagent costs and instrumentation. Additionally, reduction in the experimentation time, required cell numbers and sample handling permitted improved efficiencies in clonal cell line generation with the printing arrays.

7.4 Conclusions

The printing array platform for sampling and identifying cell colonies can considerably reduce the time, manpower and reagent costs imposed by conventional

approaches for clonal selection by destructive assay. While demonstrated for screening Coronin 1B knockdown by RNAi, this platform is applicable to screening cells based on the expression of virtually any intracellular protein, thus its impact extends well beyond that of an shRNA screening tool. The miniaturized, highly-parallel method will be compatible with a wide range of molecular, but cell-destructive characterizations, for example protein concentration, post-translational modification such as phosphorylation or glycosylation, and expression of specific transcription factors. RNAi techniques, genetic engineering protocols, cell transformation procedures, and stem-cell studies are but a few instances where this method would greatly enhance biomedical research and biotechnology.

7.5 Tables and Figures

	FACS	Array
Time to identification (days)	47	11
Total man-hours	34	5
Sample size to establish clones (# cells)	5×10^5	3.9×10^3
Knockdown colonies / Sorted Cells (%)	1.3	40
Number knock down colonies obtained	5	12

Table 7.1 Comparison of Methods.

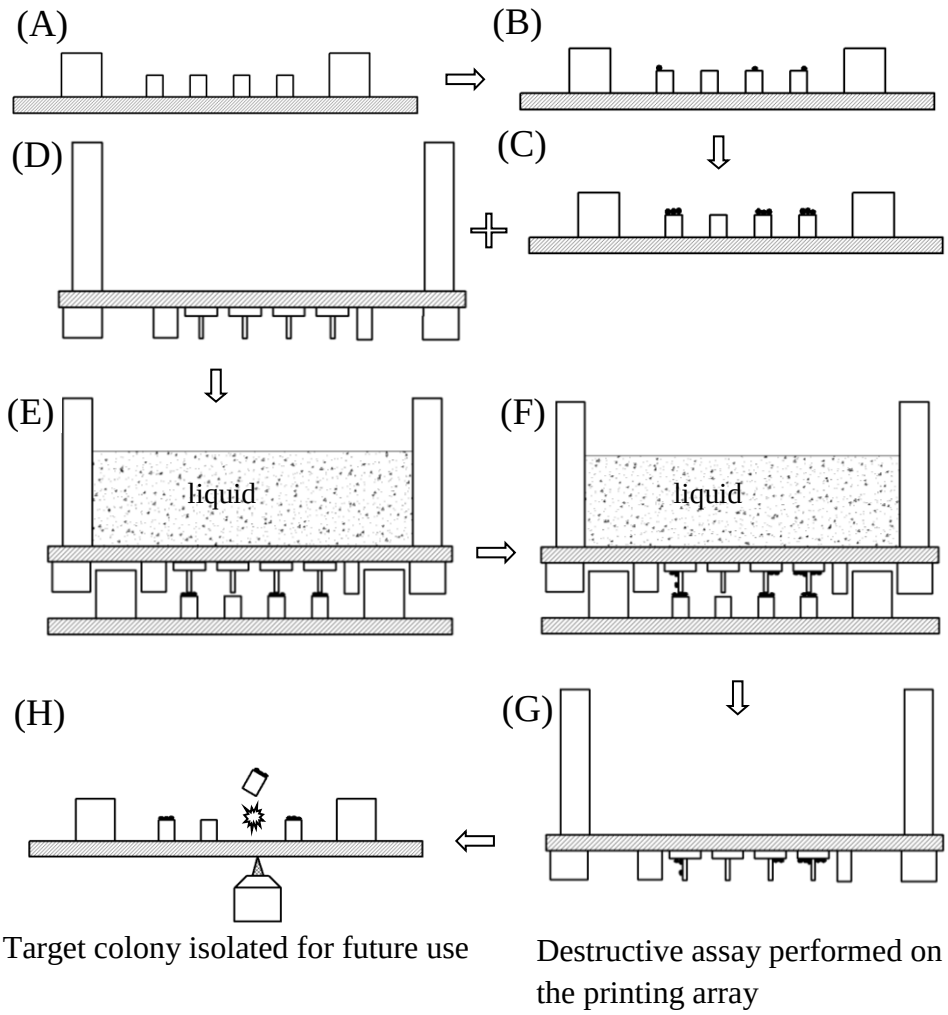

Figure 7.1 Schematic of cell printing and separation using the pallet and printing arrays. A) Cross sectional view of the pallet array. The larger squares at the edge of the array represent the alignment structures (schematic is not to scale). B) The pallet array with cultured single cells (small black circles). C) The cells on the pallet array have expanded into clonal colonies. D) Cross sectional view of the printing array which is below the substrate in this schematic. The rectangles at the edges of the array represent the alignment structures. Shown also is the fluid reservoir on the opposite side of the printing array substrate used to weight the array after mating. E) Cross sectional view of the mated arrays with liquid in the printing array reservoir. F) Cells are shown migrating along the posts upward to the printing array. G) The arrays are separated with the pallet array returned to culture and the printing array subjected to an assay for target identification. H) Target colony(s) are released and collected from the pallet array.

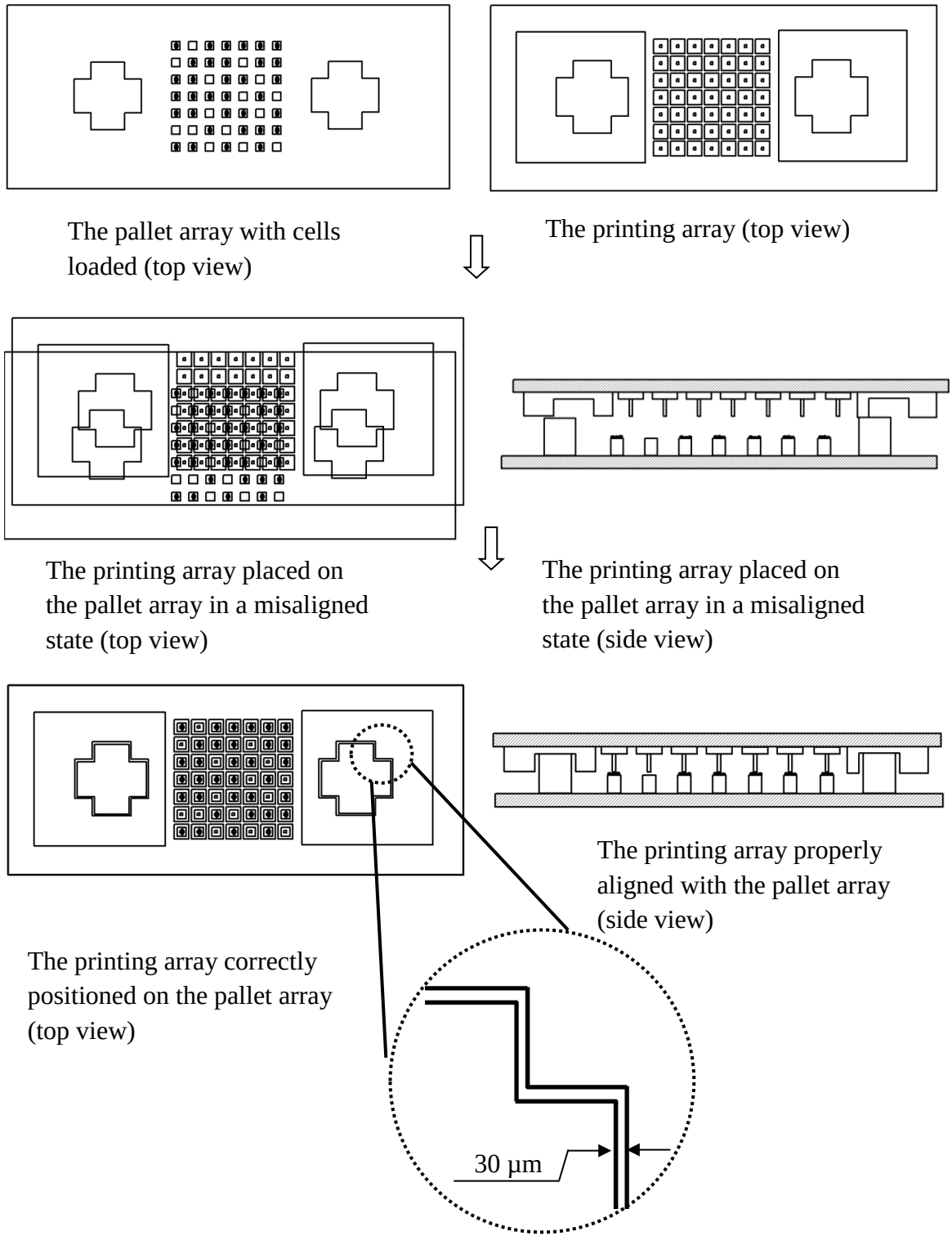

Figure 7.2 Schematic of array-array alignment procedure.

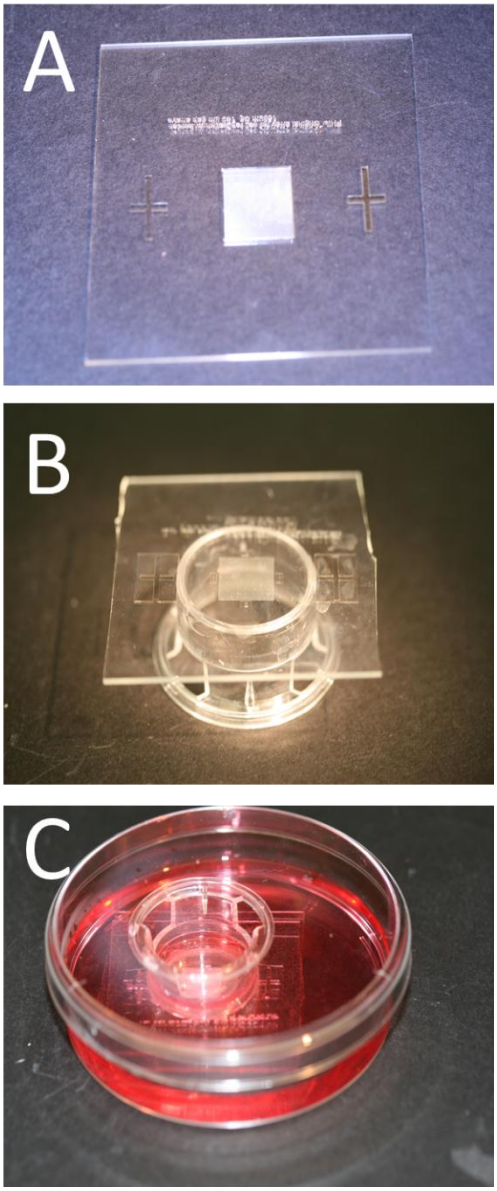

Figure 7.3 (A) Original pallet array with alignment markers. Array shown measures 1×1 cm and contains 1296 individual pallets. The cross-shaped alignment markers are seen on the right and left of the central pallet array (B) 1×1 cm printing array with alignment marker grooves to either side of the array. The array is facing upward while a Transwell® chamber has been attached to the backside of the printing array. (C) The mated arrays placed in a Petri dish during cell transfer. The Transwell® chamber is on the top surface and filled with media to press the two arrays together. The pallet array is the bottom-most array seated in the base of the Petri dish. Media is added to cover both arrays.

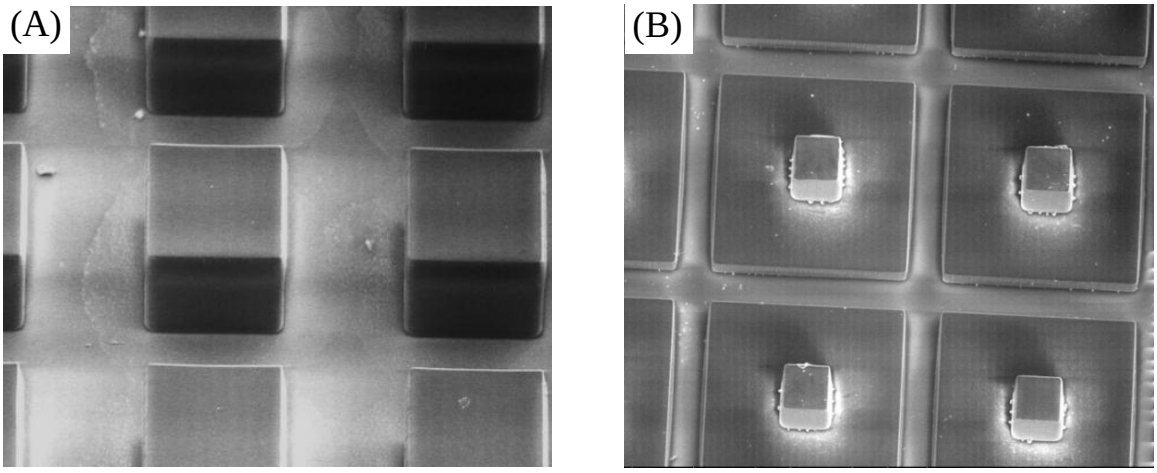

Figure 7.4 Scanning electron micrographs of the arrays. A) The pallet array. The individual pallets are 150 µm (L) × 150 µm (W) × 120 µm (H) with a 150 µm inter-pallet gap. B) The printing array. The base is 250 µm (L) × 250 µm (W) × 50 µm (H) with a 50 µm inter-pallet gap. The post dimensions are 60 (L) × 60 (W) × 100 (H) µm.

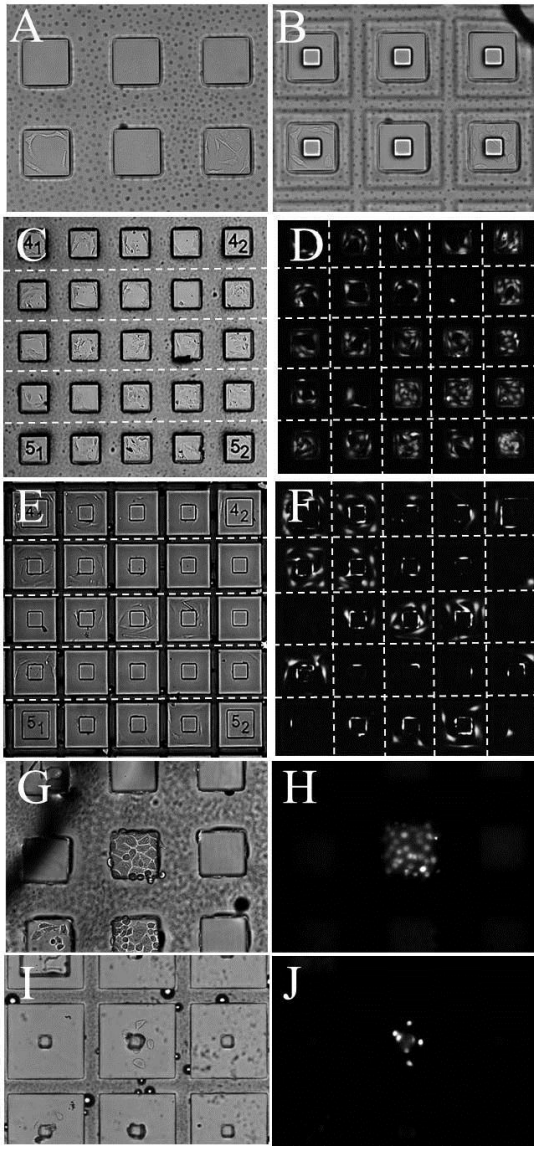

Figure 7.5 Culture and printing of cells. A) Brightfield image of a small region of a pallet array with colonies of HeLa cells after 72 h in culture. B) Brightfield image of the pallet array mated with a printing array with 60-µm-wide posts. The focal plane is at the contact plane of the posts with the pallet array. C-F) Brightfield and fluorescence images of cells stained with the viability dye calcein red-orange present on corresponding regions of the pallet array (C,D) and the printing array (E,F) after the arrays have been mated for 24 h and then separated. Cells can be seen on the pallets of both arrays as well as along the posts. G-J) Localization of GFP-expressing and wild-type colonies on the arrays. Shown are brightfield and fluorescence images of corresponding regions of pallet and printing arrays with replicated colonies from a mixture of wild-type HeLa cells and cells expressing a nuclear GFP fusion protein. In G and H, 3 colonies are seen only one of which is composed of cells expressing GFP. In I and J, the replicated colonies are seen to be composed of the same phenotypes. Note that the cells from the colony in the lower center pallet are on the post and have not yet spread to the printing base.

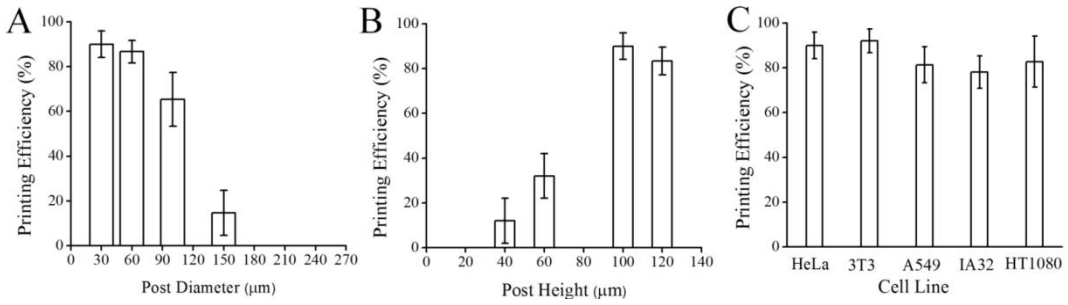

Figure 7.6 Histogram plots of the printing efficiency as various parameters are modified. A) Printing efficiency *vs.* post diameter for HeLa cells after printing arrays with posts of 100 μm height had been mated for 24 h. B) Printing efficiency *vs.* post height for HeLa cells after printing arrays of posts 30 μm diameter had been mated for 24 h. C) Printing efficiency *vs.* cell type after the arrays had been mated for 24 h.

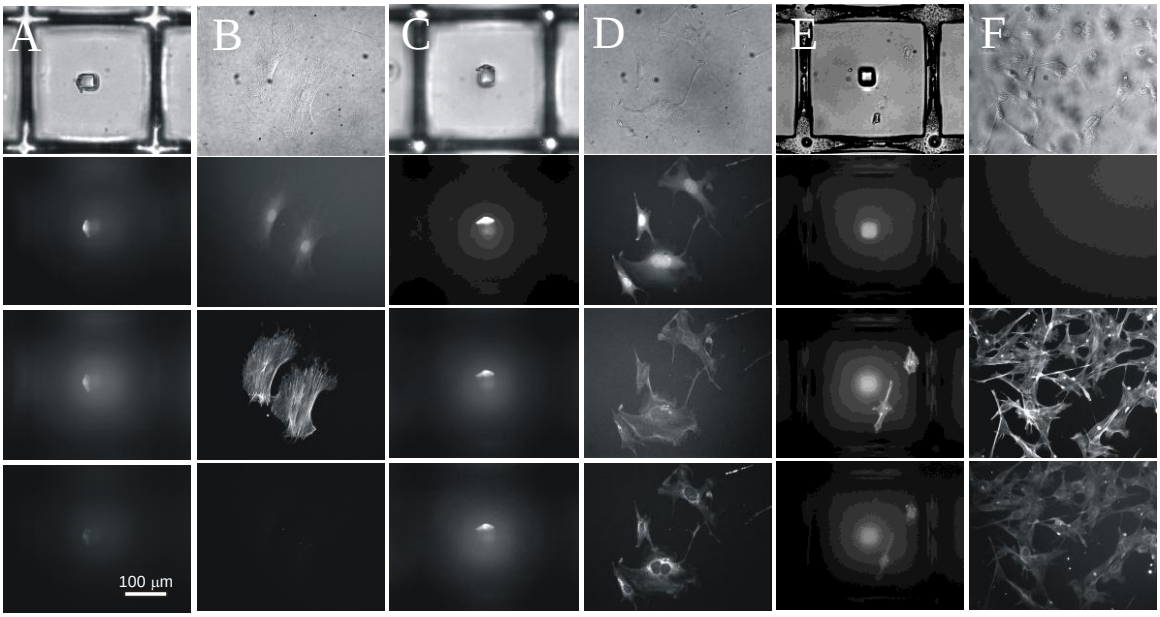

Figure 7.7 Isolation of Coronin 1B knockdown in IA32 clones. Each column contains in descending order: brightfield image, fluorescence image for GFP expression, fluorescence image of phalloidin-stained actin, and fluorescence image for Coronin 1B. A) Images of a successful knockdown of Coronin 1B in IA32 cells (GFP^+/Coronin $1B^-$) replicated onto printing array, and B) corresponding cells isolated and cultured. C) Images of IA32 cells expressing GFP and expressing Coronin 1B replicated onto cell printing array, and D) corresponding cells isolated and cultured. E) Images of IA32 cells lacking GFP expression and lacking Coronin 1B knockdown replicated onto cell printing array, and F) corresponding cells isolated and cultured.

7.6 References

1. Giepmans BN, Adams SR, Ellisman MH, Tsien RY. The fluorescent toolbox for assessing protein location and function. *Science*. 2006;312(5771):217-224.

2. Givan AL. Flow Cytometry First Principles (2nd ed). New York: Wiley-Liss; 2001.

3. Shapiro HM. The evolution of cytometers. *Cytometry*. 2004;58A(1):13-20.

4. Vitriol EA, Uetrecht AC, Shen F, Jacobson K, Bear JE. Enhanced EGFP-chromophore-assisted laser inactivation using deficient cells rescued with functional EGFP-fusion proteins. *Proceedings of the National Academy of Sciences of the United States of America*. 2007;104:6702-6707.

5. Sambrook J, Fritsch EF, Maniatis T. Molecular Cloning (3rd ed). Plainview, NY: Cold Spring Harbor Laboratory Press; 2001.

6. Freshney RI. Culture of Animal Cells. New York: Wiley-Liss; 2000.

7. Walter G, Bussow K, Lueking A, Glokler J. High-throughput protein arrays: prospects for molecular diagnostics. *Trends in Molecular Medicine*. 2002;8:250-253.

8. Smith JH, Madan D, Salhaney J, Engelstein M. Automation and robotics for genetic analysis. *Current Protocols in Human Genetics*. 2001;Appendix 2(Appendix 2E).

9. Uber DC, Jaklevic JM, Theil EH, Lishanskaya A, McNeely MR. Application of robotics and image processing to automated colony picking and arraying. *Biotechniques*. 1991;11:642-647.

10. Huber R, Palmen TG, Ryk N, et al. Replication methods and tools in high-throughput cultivation processes- recognizing potential variations of growth and product formation by on-line monitoring. *BMC Biotechniques*. 2010;10:22-32.

11. Ashton RS, Peltier J, Fasano CA, et al. High-throughput screening of gene function in stem cells using clonal microarrays. *Stem Cells*. 2007;25:2928-2935.

12. Charnley M, Textor M, Khademhosseini A, Lutolf M. Integration column: microwell arrays for mammalian cell culture. *Integrative Biology*. 2009;1:625-634.

13. Lindstrom S, Andersson-Svahn H. Overview of single-cell analyses: microdevices and applications. *Lab on a Chip*. 2010;10:3363-3372.

14. Lindstrom S, Andersson-Svahn H. Miniaturization of biological assays - overview on microwell devices for single-cell analyses. *Biochimica Biophysics Acta*. 2011;1810:308-316.

15. Sims CE, Allbritton NL. Microfabricated Devices for Cell Sorting. In: Gomez F, ed. Biological Applications of Microfluidics. Indianapolis: Wiley; 2008:29-64.

16. Holmes D, Gawad S. The application of microfluidics in biology. *Methods in Molecular Biology*. 2010;583:55-80.

17. Lecault V, VanInsberghe M, Sekulovic S, et al. High-throughput analysis of single hematopoietic stem cell proliferation in microfluidic cell culture arrays. *Nature Methods*. 2011;8:581-586.

18. Barbulovic-Nad I, Au SH, Wheeler AR. A microfluidic platform for complete mammalian cell culture. *Lab on a Chip*. 2010;10:1536-1542.

19. Hufnagel H, Huebner A, Gulch C, Guse K, Abell C, Hollfelder F. An integrated cell culture lab on a chip: modular microdevices for cultivation of mammalian cells and delivery into microfluidic microdroplets. *Lab on a Chip*. 2009;9:1576-1582.

20. Ma D, Chen H, Li Z, He Q. Thermomodulated cell culture/harvest in polydimethylsiloxane microchannels with poly(N-isopropylacrylamide)-grafted surface. *Biomicrofluidics*. 2010;4:044107(044101-044108).

21. Tekin H, Anaya M, Brigham MD, Nauman C, Langer R, Khademhosseini A. Stimuli-responsive microwells for formation and retrieval of cell aggregates. *Lab on a Chip*. 2010;10:2411-2418.

22. Lee JY, Jones C, Zern MA, Revzin A. Analysis of local tissue-specific gene expression in cellular micropatterns. *Analytical Chemistry*. 2006;78:8305-8312.

23. Villa-Diaz LG, Torisawa Y, Uchida T, et al. Microfluidic culture of single human embryonic stem cell colonies. *Lab on a Chip*. 2009;9:1749-1755.

24. Xu W, Herman A, Phillips C, Pai JH, Sims CE, Allbritton NL. Selection and separation of viable cells based on a cell-lethal assay. *Analytical Chemistry*. 2011;83(1):278-283.

25. Wei X, Sims C, Allbritton N. Microcup Arrays for the Efficient Isolation and Cloning of Cells. *Analytical Chemistry*. 2010;82(8):3161-3167.

26. Wang Y, Bachman M, Sims CE, Li GP, Allbritton NL. Stability of virtual air walls on micropallet arrays. *Analytical Chemistry*. 2007;79:7104-7109.

27. Wang Y, Sims CE, Marc P, Bachman M, Li GP, Allbritton NL. Micropatterning of living cells on a heterogeneously wetted surface. *Langmuir*. 2006;22:8257-8262.

28. Wang Y, Young G, Aoto P, et al. Broadening cell selection criteria with micropallet arrays of adherent cells. *Cytometry A*. 2007;71:866-874.

29. Salazar GT, Wang Y, Sims CE, Bachman M, Li GP, Allbritton NL. Characterization of the laser-based release of micropallets from arrays. *Journal of Biomedical Optics*. 2008;13(3):034007.

30. Quinto-Su PA, Salazar GT, Sims CE, Allbritton NL, Venugopalan V. Mechanism of pulsed laser microbeam release of SU-8 2100 polymer micropallets for the collection and separation of adherent cells. *Analytical Chemistry*. 2008;80:4675-4679.

31. Wang Y, Young G, Bachman M, Sims CE, Li GP, Allbritton NL. Collection and expansion of single cells and colonies released from a micropallet array. *Analytical Chemistry*. 2007;79:2359-2366.

32. Cai L, Marshall TW, Uetrecht AC, Schafer DA, Bear JE. Coronin 1B coordinates Arp2/3 complex and cofilin activities at the leading edge. *Cell*. 2007;128(5):915-929.

33. Wu C, Asokan SB, Berginski ME, et al. Arp2/3 is critical for lamellipodia and response to extracellular matrix cues but is dispensable for chemotaxis. *Cell*. 2012;148(5):973-987.

34. Cai L, Holoweckyj N, Schaller MD, Bear JE. Phosphorylation of coronin 1B by protein kinase C regulates interaction with Arp2/3 and cell motility. *Journal of Biological Chemistry*. 2005;280(36):31913-31923.

35. Pai JH, Wang Y, Salazar GT, et al. Photoresist with low fluorescence for bioanalytical applications. *Analytical Chemistry*. 2007;79(22):8774-8780.

36. Alberts B, Johnson A, Lewis J, Raff M, Roberts K, Walter P eds. Molecular Biology of the Cell. New York: Garland Science; 2002.

37. Roadcap DW, Clemen CS, Bear JE. The role of mammalian coronins in development and disease. *Subcellular Biochemistry*. 2008;48:124-135.

38. Chan KT, Creed SJ, Bear JE. Unraveling the enigma: progress towards understanding the coronin family of actin regulators. *Trends in Cell Biology*. 2011;21(8):481-488.

39. Petrocca F, Lieberman J. Promise and challenge of RNA interference-based therapy for cancer. *Journal of Clinical Oncology*. 2011;29:747-754.

40. Shegokar R, Al Shaal L, Mishra PR. SiRNA delivery: challenges and role of carrier systems. *Pharmazie*. 2011;66:313-318.

41. Miller MJ, Safrina O, Parker I, Cahalan MD. Imaging the single cell dynamics of CD4+ T cell activation by dendritic cells in lymph nodes. *Journal of Experimenal Medicine*. 2004;200(7):847-856.